ISSN 2395 - 4221
Volume **1** Issue **3** 2019

Additive Manufacturing Journal

The international journal for research & development on Additive Manufacturing & 3D Printing Technologies

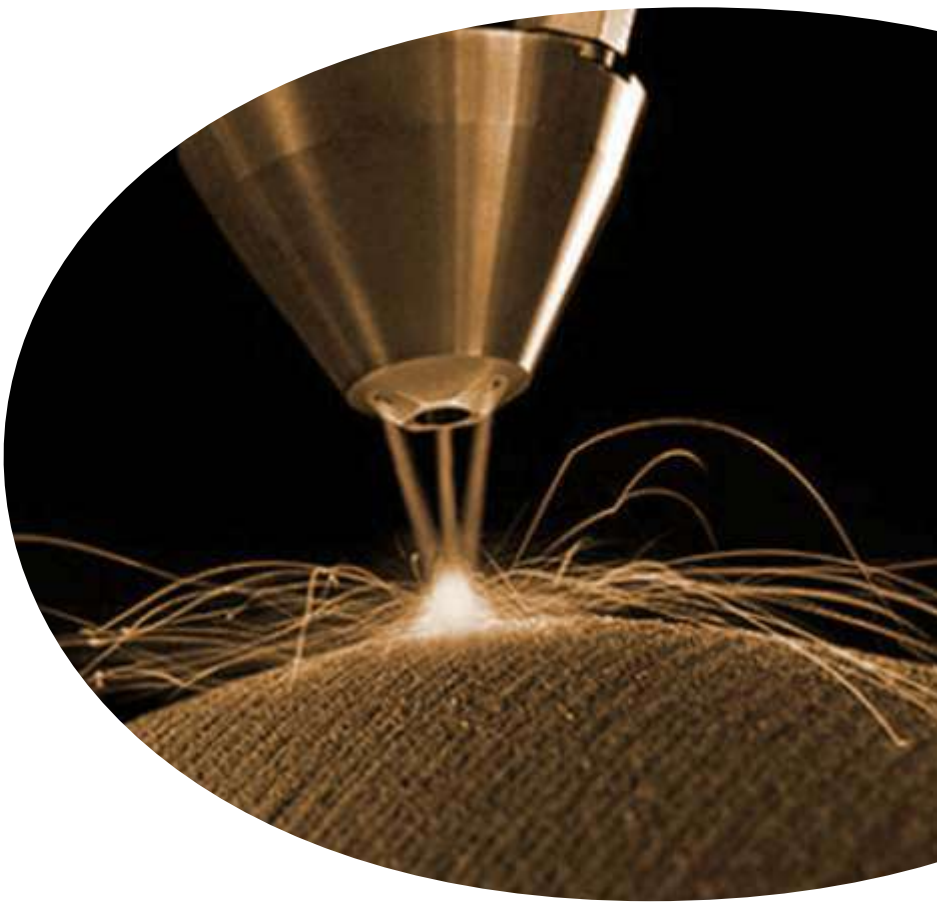

www.amsi.org.in

Additive Manufacturing Journal

ISSN 2395 - 4221

Mission Statement :
Additive Manufacturing Journal provides our Researchers, academic & industrialists with useful information regarding research & development of additive manufacturing & 3D printing Technologies. A Peer review process ensures the content's quality and relevance.

About Additive Manufacturing Journal
Additive Manufacturing Society of India (AMSI) is a professional body with the objective to promote 3D printing & Additive Manufacturing Technologies. AMSI helps the design, research and development organizations, manufacturing professionals and academics in 3D Printing, Additive Manufacturing and allied technologies.
AMSI is the publisher of International Journal on Additive Manufacturing technologies. The journal is dedicated to 3D printing and Additive Manufacturing technologies and peer reviewed by experts. The journal aims to benefit the researchers and authors in emerging 3D printing and additive manufacturing technology.

This journal is also available online at :
journal Information
issuu.com/amsiindia/docs/am_journal
Online journal content available worldwide at :
www.issuu.com

Volume 1 Issue 3 2019
ISSN 2395 -4221

Additive Manufacturing Journal

The international journal for research & development on Additive Manufacturing & 3D Printing Technologies

Contents

Editorial

Dear readers it is my great pleasure to invite you and read the third issue of the 'Additive Manufacturing Journal'. Additive Manufacturing Journal is comprised of high quality, peer reviewed conference papers presented during the 9th International Conference on "3D Printing and Additive Manufacturing Technologies- AM 2019", held on 6-7th September 2019 at The Lalit Ashok, Bangalore, India. The journal consists of high quality, peer reviewed technical papers from various scientists, research scholars an industry professionals. I hope the research work featured in this journal will be helpful to the readers to further enhance 3D Printing and Additive manufacturing research work.

Dr. L. Jyothish Kumar
Managing Editor
Additive Manufacturing Journal

Application Of Computational Fluid Dynamics In Developing Process Parameters For Additive Manufacturing

David Sonders
Vice President of Support & Services
Flow Science Inc.
Santa Fe, USA
dsves@flow3d.com

Pareekshith Allu
Senior CFD Engineer, Sales Marketing
Flow Science Inc
Santa Fe, USA
paree@flow3d.com

Anurag Chandorkar
General Manager
Flow Science Software Pvt. Ltd.
Pune, India
anurag@flow3d.com

Ruendy Castillo
Civil Engineering Student
University of New Mexico
USA
rcastillo134@unm.edu

***Abstract*—Several numerical studies were conducted to demonstrate practical use of computational fluid dynamics (CFD) in developing optimum process parameters such as laser/electron beam power, scan speed, powder compaction and hatch spacing for selective electron beam melting and laser powder bed fusion (LPBF) processes. The CFD models (provided by *FLOW-3D®*) solve fundamental conservation equations and the detailed physics involved such as laser/electron beam-powder interaction, melt pool dynamics, phase change and solidification. The first case study is a benchmark, that validates model results against the melt pool dimensions provided by National Institute of Standards and Technology (NIST) for different combinations of laser parameters for an IN625 flat metal substrate. The next study compares keyhole related porosity defects predicted by the CFD models for various laser power and scan speed combinations to experimental results. The study shows the laser beam irradiating primarily on the front keyhole wall produces a stable keyhole, resulting in minimal porosity formation. Next, the effect of laser parameters, powder packing density and particle size distribution on balling defects are studied. It is found that high scan speeds and a powder size distribution skewed towards larger size particles can potentially cause melt pool to break into islands (balling) of molten metal, adversely affecting the surface quality. The last study uses solidification rate and temperature gradients predicted by the CFD models to assess solidification morphology and grain size for single layer scan tracks LPBF processes. Such high-fidelity multi-physics simulations provide insights into additive manufacturing processes at the micro and meso-scales.**

Keywords— CFD simulations, laser keyhole welding, FLOW-3D, melt pool dynamics, balling defects

I. Introduction

Metal additive manufacturing (AM) processes such as laser powder bed fusion (LPBF) and selective electron beam melting (SEBM) can produce parts with complex geometries that can significantly reduce part weight and metal scrap while meeting all the design requirements. The challenge with these processes is in optimizing the process parameters such as laser power, scan speed, hatch spacing, powder size distribution and compaction. These process parameters affect the melt pool dynamics which in turn affects the quality of the part. Computational fluid dynamics (CFD) modelling can help researchers understand the effects of process parameters on underlying physical phenomena such as melt pool dynamics, phase change and solidification. These numerical models, which are based on a rigorous solution of the conservation equations of mass, momentum and energy, can provide useful insights such as fluid convection in the melt pool, formation of keyholes, temperature gradients and solidification rates. Current work presents four case studies from industry and academia that highlight the use of CFD and numerical models in understanding the effects of process parameters as discussed.

II. Case Study 1

During the metal AM process, the shape and size of the melt pool and the resulting thermal gradients have an impact on the microstructure and the structural properties of the final part. Understanding the dynamics of the flow in the melt pool and predicting the correct dimensions of the melt pool is thus the key to deeper understanding of the process. The first case study focuses on predicting the melt pool dimensions i.e. depth, width and length of the melt pool and compares CFD results with the experimental data provided by National Institute of Standards and Technology (NIST).

A. Experiment

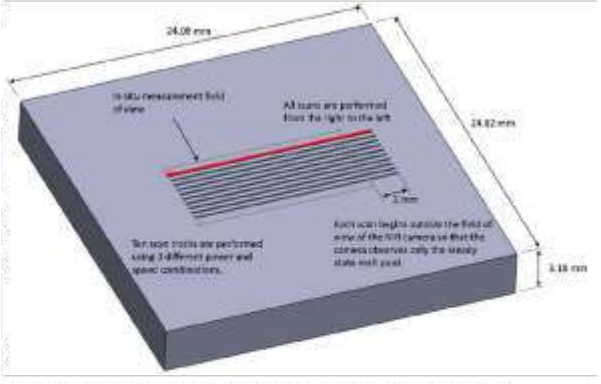

Fig. 1. Schematic of IN625 substrate, and nominal positions of scan tracks.

The experiment consists of laser powder bed fusion (LPBF) with single scan tracks on bare metal substrates (no powder) of nickel-based superalloy IN625. Three different power and speed combinations are performed with multiple replications of each. The laser used is a continuous-wave (CW) ytterbium fiber (Yb:fiber) laser, with a wavelength of 1070 nm. In-situ measurements of the melt pool length are performed. Fig. 1 presents an illustration of the substrate, and the series of 10 scan tracks. Each track is 14 mm long with hatch spacing of 0.5 mm. The tracks begin 2 mm outside of the field of view of the camera as the in-situ melt pool length measurements were limited to steady state. The length of the melt pool is measured as the distance between the leading edge and the trailing edge of the melt pool, each of which are defined by the solidus temperature. The scan tracks were then cross-sectioned perpendicular to the laser track at the center position. The cross-sections were then polished and etched in order to measure melt pool width and depth. NIST conducted these experiments on two machines, first one referred to as Additive Manufacturing Metrology Testbed (AMMT) and second one as Commercial Build Machine (CBM). For this case study results from AMMT were used as the melt pool depth and width were reported only for AMMT.

TABLE I. PARAMETERS FOR THE EXPERIMENTS WITH AMMT

Case	Laser power (W)	Scan speed (mm/s)	Replicatio ns	Laser spot size (D4σ) diameter
A	137.9	400	3	170 μm
B	179.2	800	3	170 μm
C	179.2	1200	4	170 μm

B. CFD model

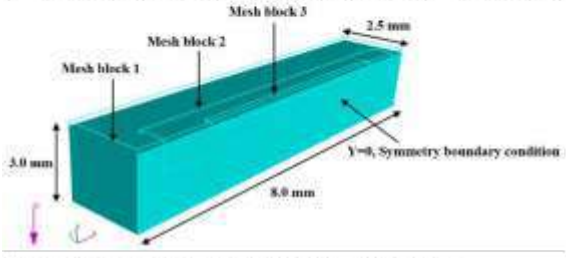

Fig. 2. Schematic showing the geometry for the CFD model

In the CFD model (using ***FLOW-3D®*** software), as per the experimental data three simulations (for Case A, B and C) were setup, each for a different combination of laser power and scan speed. The CFD models simulated single scan track for each case. ***FLOW-3D®*** incorporates a proprietary volume-of-fluid method (TruVOF) that accurately tracks the evolution of liquid metal-air interface as the laser beam irradiates the substrate. Energy from the laser beam is applied on the substrate using a gaussian heat flux distribution over the laser spot diameter. Following is the list of physical models included in the simulation

- Molten metal flow is assumed to be Newtonian, laminar and incompressible.
- A Gaussian distribution for the laser beam power is utilized.
- Evaporation induced recoil pressure that controls the amount of heat and mass flux from the melt pool into the void is implemented using the Clausius-Clapeyron equation.
- Radiation heat transfer from plasma/vapor to the part
- Surface tension induced Marangoni convection is also accounted for.

C. Results and discussion

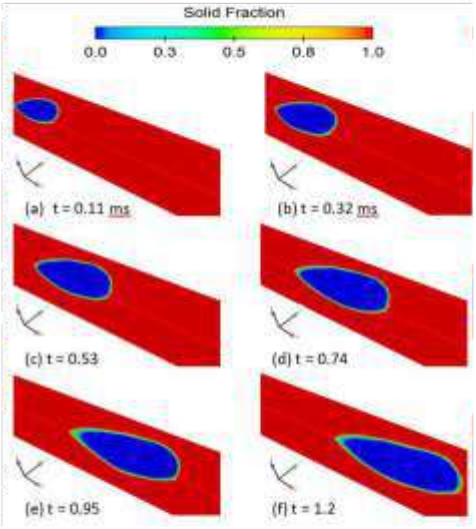

Fig. 3. Melt pool evolution for Case A

Evolution of the melt pool depth, width and length as a function of time can be seen in Fig. 3. for Case A. Similar patterns are seen for case B and C as well. As can be seen in Fig. 3, for the process parameters used for this case study, the depth of the melt pool is shallow as a result no laser keyhole formation is observed. Due to the absence of laser keyhole, laser reflections of the melt pool surface do not play an important role in deciding the dynamics of the melt pool. For all the cases used for this study, the dimensions of the melt pool are primarily controlled by laser power, scan speed, heat transfer and phase change.

TABLE II. COMPARISON OF NIST EXPERIMENTAL AND CFD RESULTS

	Depth (μm)		Width (μm)		Length (μm)	
Case	*Experiment*	*CFD*	*Experiment*	*CFD*	*Experiment*	*CFD*
A	42.50	47.50	147.90	152.00	380.00	304.00
B	36.00	37.62	123.50	136.00	359.00	356.00
C	29.60	25.96	106.00	120.52	370.00	320.00

Table II summarises the results for all three cases. From the table we can conclude that the predicted dimensions of the melt pool are in good agreement with the experimental data.

III. CASE STUDY 2

Keyhole-induced porosity is a major cause of defects in metal AM as well as in laser welding process. Such defects lead to weakening of the structural properties, and thus it is of importance to understand the mechanism of keyhole and keyhole-induced porosity formation [9]. In this case study, researchers from General Motors, USA and Shanghai Jiao Tong University, PR China developed 3D CFD models using

FLOW-3D® to outline the formation of porosity in laser keyhole welding [3]. Void or porosity formation typically takes three steps: a) bubble formation in the melt pool due to collapsing keyholes, b) bubbles floating to the rear molten pool due to convection, and c) bubbles being captured by an advancing solidification front. These processes result in porosity. With better control of process parameters, it is possible to interfere with any of the three steps and so, keyhole-induced porosity can potentially be mitigated. It is observed that high laser welding speeds and large angles of beam inclination, help in creating a quiescent rear molten pool thus stabilizing the keyhole and decreasing the rate of bubble formation.

A. Experiment

Fig. 4 shows the schematic of the remote laser lap welding process of two AA5182 metal plates. The laser beam is an IPG 6kW continuum wave fiber laser system, and two galvo mirrors are utilized to direct the laser beam at specific angles of inclination on to the metal plates.

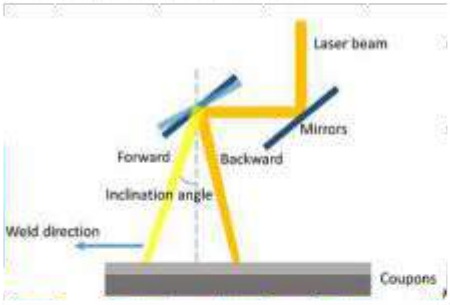

Fig. 4. Schematic of remote laser lap welding process on AA5182 1 mm + 2 mm plates

The 1mm plate is stacked on top of the 2mm plate and the welding is performed with beam's focus plane on the top surface. A beam spot size of 0.6mm is used and a total distance of 25mm is laser welded. The laser scanning speed and beam inclination angle are varied independently and parametrically to evaluate the effects of each parameter on the formation of porosity.

B. CFD model

The physics implemented in the ***FLOW-3D®*** models include laser-material interaction and energy absorption, phase change, recoil pressure, fluid flow, solidification evolution, heat and mass transfer. Multiple laser reflections are calculated based on the incident beam angle and local normal to the metal surface, and simultaneously Fresnel absorption is applied to account for the dependency of heat input into the metal region based on the angle of incidence and other laser and material dependent coefficients.

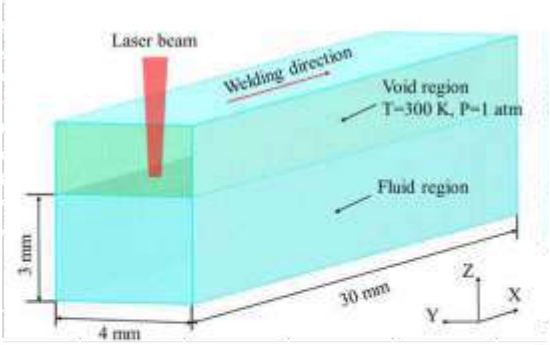

Fig. 5. Illustration of the mesh and computational domain used in the simulation

Fig. 5 showcases the mesh used in the computational simulation and indicates the relevant fluid and void regions. The numerical procedure involves the solution of mass, momentum and energy conservation equations using the ***FLOW-3D®*** software. Additionally, the free surface is tracked using the TruVOF method.

C. Results and discussions

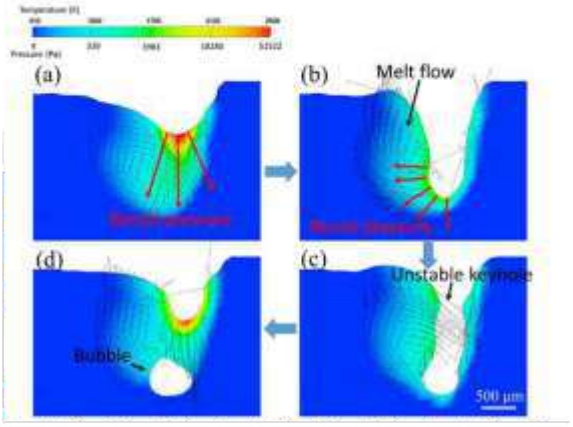

Fig. 6. Process of bubble formation due to keyhole collapsing (P = 2.5 kW, v = 3 m/min): (a) 0.2340 s; (b) 0.2345 s; (c) 0.2350 s; and (d) 0.2355 s.

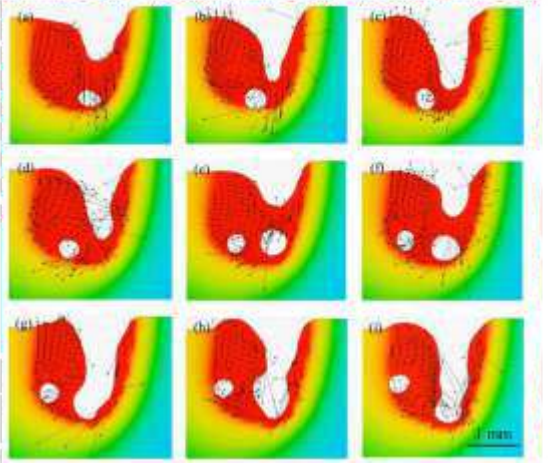

Fig. 7. Process of bubble formation due to keyhole collapsing (P = 2.5 kW, v = 3 m/min): Time at (a) 0.2340 s, Time at (i) 0.2380 s, Time step from (a) to (i) 0.0005 s

In Fig. 7 (a)-(e), the mechanism behind keyhole-induced porosity is shown. As the laser beam shines on the melt pool surface at 0.234 seconds, it causes the melt pool to depress due to evaporation induced recoil pressure. This melt pool depression along with surface tension induced Marangoni convection causes the re-circulation in the rear molten pool, which leads to the rear keyhole wall collapsing on the front keyhole wall, and results in bubbles trapped in the melt pool.

However, not all bubbles in the melt pool result in porosity. Only when a bubble is captured by the advancing solidification front as seen in Fig. 7 (a)-(e) does the trapped bubble become a void. Another bubble that is formed in Fig. 7 (e) goes on to recombine with the free surface of the melt pool and thus, avoids becoming captured by the advancing solidification front. Next, a parametric study on process parameters is implemented to understand their influence on keyhole induced porosity.

TABLE III. WELDING PROCESS PARAMETERS

	Laser Power (kW)	Welding speed (m/min)	Beam inclination angle (°)
Effect of welding speed	2.5	3.0	0
	5.0	10.0	0
	6.0	12.0	0
Effect of beam inclination angle	2.5	3.0	-15
	2.5	3.0	0
	2.5	3.0	15
	3.0	3.0	30
	3.0	3.0	45

In Table III, the laser welding speed is increased from 3m/min to 12m/min while also increasing the laser power to keep the depth of penetration the same. Accordingly, in Fig. 8, it is seen that simulations predict a decrease in the formation of porosity, which is also corroborated by the experimental results in Fig. 9.

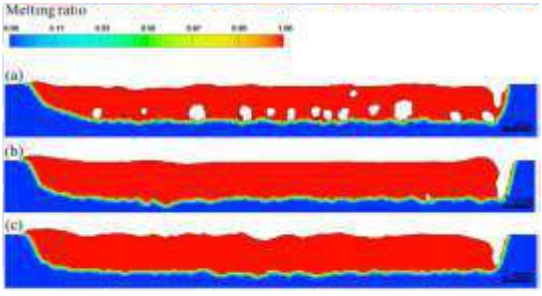

Fig. 8. Distribution of porosity in longitudinal welding sections from simulations with following sets of parameters: (a) P = 2.5 kW, v = 3 m/min; (b) P = 5.0 kW, v = 10 m/min; and (c) P = 6.0 kW, v = 12 m/min

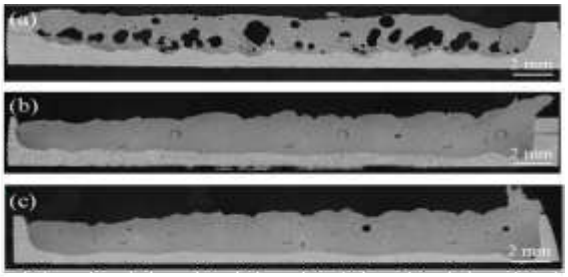

Fig. 9. Distribution of porosity in longitudinal welding sections from experiments with following sets of parameters: (a) P = 2.5 kW, v = 3 m/min; (b) P = 5.0 kW, v = 10 m/min; and (c) P = 6.0 kW, v = 12 m/min.

A look at the process simulations helps discern the reason for high powers and welding speeds being beneficial to the welding joint. It is seen in Fig. 10 that at high speeds and powers, the width of the keyhole opening at the top is greater, thus preventing the collapse of the rear keyhole wall onto the front.

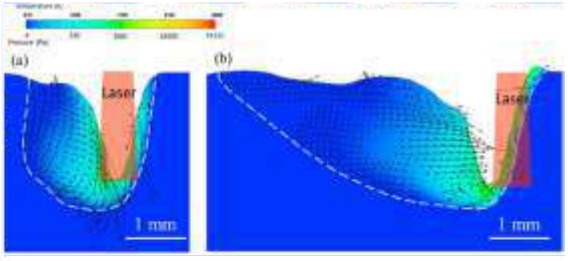

Fig. 10. Predicted velocity fields and temperature distribution in the molten pools, and laser's position relative to keyhole surface for: (a) P = 2.5 kW, v = 3 m/min and (b)P = 6 kW, v = 12 m/min

Additionally, a large fluctuation in keyhole depth is observed for the low speed and low power case, although the depth of penetration of the laser beam is the same. This change in depth is a likely indication of keyhole collapsing due to the violent nature of melt pool dynamics in the rear keyhole wall. This can be attributed to the laser beam shining on both the front and rear keyhole-walls causing turbulent melt pool dynamics in the rear molten pool. It is also seen in Fig. 10 that at large speeds and powers, the melt pool behind the keyhole is elongated, and this is beneficial for the bubbles to escape before getting trapped by advancing solidification fronts. The laser beam also predominantly shines on the front keyhole wall, thus minimizing turbulence in the larger rear molten pool.

Next, the role of laser beam inclination angles on laser welding is studied. Since the optics in remote laser welding are far from the workpiece as compared to conventional laser welding, the inclination angle can influence melt pool dynamics. As listed in Table III, the angles of inclination are varied between -15°, 0°, 15°, 30°, and 45°.

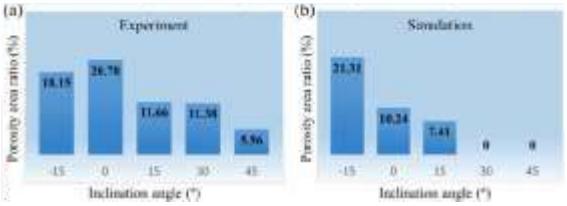

Fig. 11. Pore area percentage at different inclination angle: (a) experiment results and (b) simulation results.

Fig. 11. plots the pore area percentages in both experiments and simulations. It is seen that porosity is suppressed with an increase of inclination angle as seen in both experiments and simulations. The experiments show a larger pore area percentage compared to simulations, which can be attributed to the laser beam focal plane being shifted away from the top surface of the weld plates, when the angle of inclination changes. The simulations, on the other hand, make the approximation that the laser beam focal plane is always at the top surface of the weld plates. Nevertheless, the trends predicted are in good agreement.

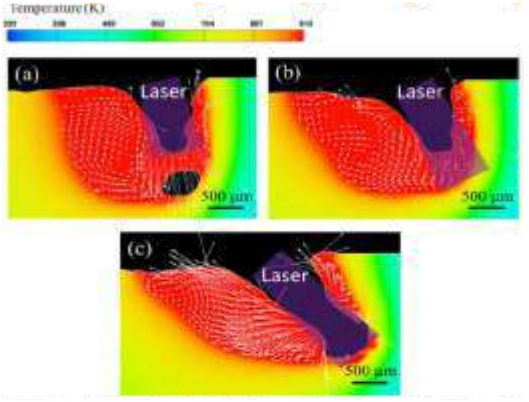

Fig. 12. Calculated velocity fields and temperature distribution in the molten pools for different inclination angles and laser powers: (a) 2.5 kW, 3 m/min and 15°; (b) 3 kW, 3 m/min and 30°; and (c) 3 kW, 3 m/min and 45°.

To understand why larger beam angles of inclination show a reduction in porosity, it is worth investigating the melt pool dynamics as shown in Fig. 12. At a 15° angle of inclination, there is intense re-circulation observed in the rear molten pool, and the keyhole collapsing with bubble formation is seen. Two vortices are observed at a 30° angle of inclination, which arise due to recoil pressure and surface tension forces, and this causes the rear wall to be less steep compared to the 15° angle of inclination rear motel pool wall. Finally, at 45°, the rear molten pool now has laminar flow going away from the rear keyhole wall due to gravity and recoil pressure becoming more aligned, thus driving the flow downward and backward. Once again, a more stable rear molten pool eventually leads to mitigation of porosity.

IV. Case Study 3

Process parameters such as laser scan speed, laser power, packing density and particle size distribution have a direct impact on the melt pool dynamics in a laser powder bed fusion process. The highly transient nature of the melt pool affects the final surface quality of the solidified melt region. This case study conducted by researchers from Ohio state university uses CFD models to perform qualitative study of the process parameters on the balling defect for LPBF processes in Inconel® 718 [6].

A. CFD model

In addition to the physical models used in case studies 1 and 2, this case study uses discrete element method (DEM) to model the metal powder particles. The DEM model is capable of modelling (powder) particle-particle interaction and the different powder particle distributions for varying particle size.

B. Results and discussion

As illustrated in Fig. 13, balling defects occur when the molten pool becomes discontinuous and breaks into separated islands of molten metal. Such defects can be attributed to void formations in the melt pool, which eventually break the melt pool into separate regions as seen in Fig. 13(a) – 13(f).

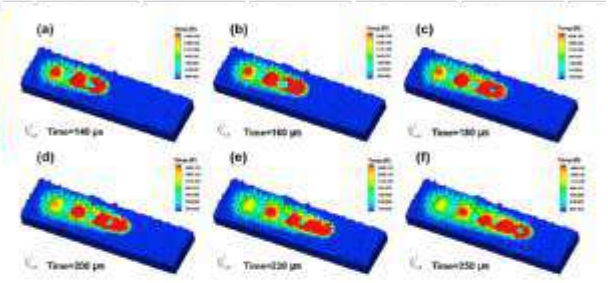

Fig. 13. Evolution of molten pool profile illustrating the formation of balling defect.

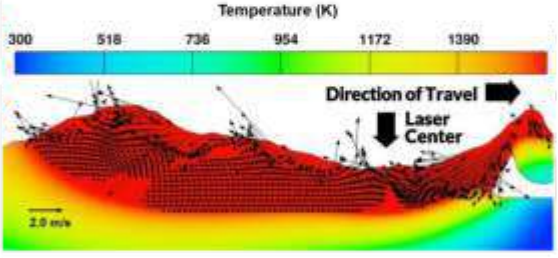

Fig. 14. 2D view of the melt pool showing the formation of "hump" due to Marangoni effect. (Scanning speed = 1.1 m/s, laser power = 200W, and powder packing density = 38%.).

The thermal gradients in the melt pool produce gradients in surface tension which then induces Marangoni flow in the direction opposite to the laser scan. As the Marangoni effect pushes molten metal to the rear end of the melt pool, a distinctive hump is formed. With increasing length-to-width ratio of the melt pool, Rayleigh Taylor instabilities set in and cause the melt pool to break down into tiny islands of molten metal which then solidify to adversely affect the surface quality [7].

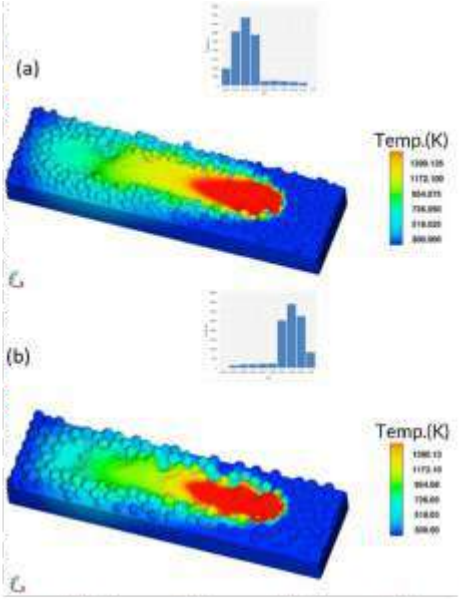

Fig. 15. Molten pool profile for (a) Particle size distribution with higher percentage of smaller particles (b) Particle size distribution with higher percentage of larger particles

The effect of particle size distribution on the balling defect can be seen in Fig. 15. For both results shown in Fig 15 (a) and (b) the particle size varies between same minimum to maximum diameter. Both have the same process parameters i.e. laser power and scan speed. But for simulation with particle size distribution skewed towards larger particle size (Fig. 15 b) we see that the molten pool surface is less smooth and has more corrugated edge as compared to the results in Fig. 15 (a) which has particle distribution with larger percentage of smaller particles. This can be attributed to the fact that with same laser power scan speed larger particles tend to show partial melting as compared to smaller particles.

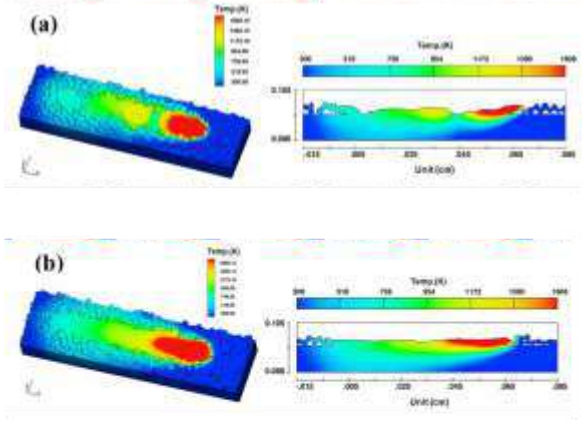

Fig. 16. Molten pool profile for (a) Laser scan speed of 2.3 m/s (b) Laser scan speed of 1.1 m/s. All other conditions, i.e. laser power = 200W, power packing density = 38% are same

Fig. 16 illustrates that at higher scan speeds length to width ratio of the melt pool can become high enough to cause the melt pool to break up and cause balling defects.

V. Case Study 4

The microstructure evolution in laser powder bed fusion processes is investigated using fluid flow and heat transfer models built in ***FLOW-3D®***. Solidification parameters, particularly solidification rate and temperature gradients that are calculated from temperature fields are used to assess solidification morphology and grain size for LPBF of Inconel® 718 using existing theoretical models. The numerical models are validated by calibrating the dimensions of the melt pool for two partially overlapping laser scan tracks, and it can be seen below in Fig. 17 that the cross-sectional dimensions compare well between experiments and simulations.

Solidification parameters at the molten pool side edge and the molten pool trailing end are calculated. These locations correspond to the maximums and minimums of solidification parameters, and by using existing analytical models for welding and cladding processes, it is calculated that columnar dendrite is the dominant morphology in IN718 made by LPBF. The primary dendrite arm spacing (PDAS) is another important microstructure parameter and the dendrite size was estimated to be between 1.32 and 1.87 µm. The calculated solidification morphology and PDAS are consistent with experimentally observed results. The reader is invited to refer to the cited journal article for more information on the methodology and results. The reader is invited to refer to the cited journal article [7] for more information on the methodology and results.

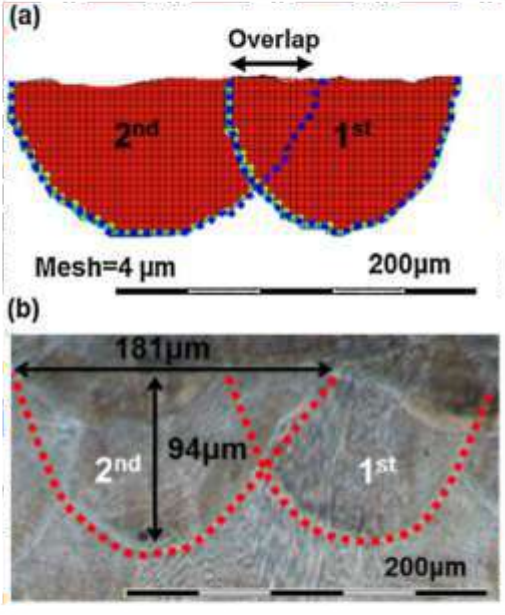

Conclusion

This study demonstrates that the CFD models based on solving fundamental equations of mass, momentum and energy coupled with the laser models can be successfully used to improve the understanding of the metal and heat flow dynamics during metal AM processes. These high-fidelity CFD models can help researchers and engineers develop optimum process parameters for metal AM processes there by limiting the need to carry out expensive experimental trials.

REFERENCES

[1] L.J. Zhang, J.X. Zhang, A. Gumenyuk, M. Rethmeier, S.J. Na, Numerical simulation of full penetration laser welding of thick steel plate with high power high brightness laser, Journal of Materials Processing Technology, Volume 214, Issue 8, 2014.

[2] Flow Science, Inc., 2017. FLOW 3D® User Manual V11.2.

[3] Ruiqi Lin, Hui-ping Wang, Fenggui Lu, Joshua Solomon, Blair E. Carlson, Numerical study of keyhole dynamics and keyhole-induced porosity formation in remote laser welding of Al alloys, International Journal of Heat and Mass Transfer, Volume 108, Part A, 2017.

[4] Wu, Yu-Che & San, Cheng-Hung & Chang, Chih-Hsiang & Lin, Huey-Jiuan & Marwan, Raed & Baba, Shuhei & Hwang, Weng-Sing. (2017). Numerical modeling of melt-pool behavior in selective laser melting with random powder distribution and experimental validation. Journal of Materials Processing Technology. 254. 10.1016/j.jmatprotec.2017.11.032.

[5] Mesoscopic simulation of heat transfer and fluid flow in laser powder bed additive manufacturing." Lee, Y. S., and W. Zhang. Proceedings of the Annual International Solid Freeform Fabrication Symposium, Austin, TX, USA. 2015.

[6] Lee, Yousub & Zhang, W. (2016). Modelling of heat transfer, fluid flow and solidification microstructure of nickel-base superalloy fabricated by laser powder bed fusion. Additive Manufacturing. 12. 178-188. 10.1016/j.addma.2016.05.003.

[7] Wentao Yan, Wenjun Ge, Yn Qian, Stephen Lin, Bin Zhou, Wing Kam Liu, Feng Lin, Gregory J. Wagner, Multi-physics modelling of single/multiple-track defect mechanisms in electron beam selective melting, Acta Materialia, Volume 134, 2017, Pages 324-333, ISSN 1359-6454.

[8] Pareekshith Allu, CFD simulations for laser welding of Al alloys, Lasers in Manufacturing Conference, 201

FULL PAPER SUBMISSION FOR 9TH INTERNATIONAL CONFERENCE ON ADDITIVE MANUFACTURING TECHNOLOGIES - AM 2019 (AMSI)

IN-SITU LASER REMELTING (LASER POLISHING) OF TOP SURFACE OF Cobalt Chrome (CoCr) SAMPLE BY Selective Laser Melting (SLM) PROCESS

Abhishek Kumar[1*], C. S. Kumar [1], A. K. Nath[1]

[1]Mechanical Engineering Department, Indian Institute of Technology Kharagpur, India

*Corresponding author: abhishek.mech.iit@gmail.com

Abstract: Additive manufacturing is a part of Direct Digital Manufacturing (Major part of Fourth Industrial Revolution) process which is an automated fabrication process based on the layer by layer mass customized additive manufacturing process. The major drawback of this process is that it gives high surface roughness. So Polishing is done to reduce surface roughness. Conventional polishing is contact processes thus have many limitations. So to overcome these limitations, Laser polishing operation is done which is a contactless polishing process. Laser polishing involves melting a thin layer of the substrate, with surface tension causing the material to flow from peaks to valleys. In laser polishing, the material is not removed but is relocated as a molten pool. Polished surface mainly depended on the surface material, initial topography and laser beam density. The energy density delivered to the workpiece plays a major role in the thermal cycle, fluid dynamics, microstructure and consequent surface profile, and is controlled by changing the input power and scanning speed. In this experiment, In-situ laser surface remelting was done that is laser surface remelting done on the same machine (EOS M 270) in which sample was built, thus reducing production time and cost (Cost Effective Process). Cobalt-chrome or cobalt-chromium (CoCr) is a metal alloy of cobalt and chromium. Cobalt-chrome has a very high specific strength and is commonly used in gas turbines, dental implants, and orthopedic implants. The experiment was performed in different process parameter that is varying Scanning speed, Hatching distance and Hatching direction, no. of powder layer remelted. Thus we got improvement in surface roughness from around average initial surface roughness of 14 - 15 microns to 1.02 micron, thus 92% improvement of surface roughness in both longitudinal (Along with scan speed) and transverse direction (Direction perpendicular to scan speed).

Keywords: Additive Manufacturing, Laser Polishing/Remelting, Selective Laser Melting, Surface Roughness, Cost Effective process

1. Introduction

1.1. Additive Manufacturing

Orientated on the geometry only, manufacturing technology, in general, is divided into three fundamental clusters [1]:

1. Subtractive manufacturing technology,
2. Formative manufacturing technology, and
3. Additive manufacturing technology.

Additive manufacturing creates the desired shape by adding material, preferably by staggering contoured layers on top of each other. Therefore, it is also called layer (or layered) technology. The principle of layer technology is based on the fact that any object, at least theoretically, can be sliced into layers and rebuilt using these layers, regardless of the complexity of its geometry.

Additive manufacturing (AM) is an automated fabrication process based on layer technology. AM integrates two main sub-processes: the physical making of every single layer and the joining of subsequent layers in sequence to form the part. Both processes are done simultaneously. The AM build process just requires the 3D data of the part, commonly called the virtual product model. It is a characteristic of AM that not only the geometry but the

material properties of the part as well are generated during the build process.

In general, AM deals with adding material instead of its removal. First, a computer-aided design (CAD) file of the desired part needs to be created or designed. This CAD file can be completely designed by a designer, or it can be created by scanning an object. Subsequently, the CAD file will be converted into layers with specific thickness, usually ranging from 20 to 100 μm [2], using supporting software such as Autofab (Materialise, Louvain, Belgium). Finally, an AM machine will fabricate the part layer by layer [3]. All AM machines need a source of energy to fabricate the cross-section of each layer. There are a variety of energy sources, including those based on laser, electron beam, and ultrasonic [4].

Different types of materials are used in the AM techniques, including powder, wire, and sheet. Although powder-bed-based methods are only capable of using powder [5], the flow-based methods can utilize either powder or wire [6,7]. The sheet is the only type of material used in sheet lamination techniques.

1.2 Post-manufacturing Processing

After fabrication by AM techniques, post-processing tasks are usually required to produce desired functionality and form. Post-processing techniques are being used to enhance AM fabricated parts or to overcome AM limitations. These include support removal, surface texture improvements, aesthetic improvements, and property enhancements using thermal techniques. Post processing plays an important role in price marketing, and therefore, competitive companies may neglect post-processing to reduce costs.

These include natural supports (i.e., materials that surround the part during fabrication process) and synthetic supports (i.e., rigid extra structures that connect the main part to the substrate to support and restrain the main part) removal. [3, 6]. AM parts may have undesirable surface texture features that need to be removed. These include stair-steps, powder adhesion, fill patterns from built material, and witness marks from support removal. Because of the discrete layer-based approach, every AM part inherits the staircase effect on the surface. The staircase effect between the consecutive layers impairs the physical surface quality of AM objects. The deviation introduced by the staircase effect is measured with the cusp height, which is defined as the maximum distance from the manufactured part's surface perpendicular to the model surface [7]. Thermal processes enhance the properties of the final AM parts [9]. Traditional heat treatment is a common thermal technique to relieve residual stresses and form the desired microstructure. Grinding and polishing techniques are widely used to reduce the roughness of surfaces. In this experiment, Laser polishing that is laser surface remelting is mainly focused.

2. Laser Surface Remelting (Laser Polishing):

Grinding and polishing techniques are widely used to reduce the roughness of surfaces and thus enhancing the surface related property. A new method to attain such high-quality surfaces is polishing with laser radiation. In principle, there are three different process variants.

2,1 Types of Laser Polishing:

There is three types of laser polishing process (Broad classification) as mention below:

a) Polishing by Large-Area Ablation

b) Polishing by Localized Ablation

c) Polishing by Remelting – Metals

In this experiment, Laser polishing by remelting was done.

Polishing by Remelting – Metals: A thin surface layer is molten and the surface tension leads to a material flow from the peaks to the valleys. No material is removed but reallocated while molten. It is a new method for the automatic polishing of 3D surfaces. For metals for the process variant polishing by remelting, two sub-variants exist macro polishing and micro polishing.[8]

2,2 Mechanism of Laser Surface Remelting (Laser Polishing)

Laser polishing involves melting a thin layer of the substrate, with surface tension causing the material to flow from peaks to valleys. In laser polishing, the material is not removed, but is relocated as a molten pool. Polished surface mainly depended on the surface material, initial topography, and laser beam density. The laser beam melts a microscopic layer on the surface, which re-solidifies under shielding gas protective conditions, resulting in a smoother surface. The polishing mechanism is based on the fusion of a microlayer of material due to the action of the laser beam. Melt pool dynamics significantly influence the surface profile. The energy density delivered to the workpiece plays a major role in the thermal cycle, fluid dynamics, microstructure, and consequent surface profile, and is controlled by changing the input power and scanning speed.[9]

The surface roughness of the laser polished region significantly depends on the melt pool velocity, which itself is influenced by the laser power and speed. Increase in input energy results in increased melt pool velocity, which subsequently generates periodic striation patterns in the laser polished surface and should be avoided. A laser polished zone with good surface profile and roughness can be achieved by restricting the melt pool convection to a minimum. Low melt pool velocity helps achieve wider laser polished track width. Increase in melt pool velocity

increases the melt pool depth without a significant increase in melt pool width, which is not ideal for laser polishing.

Laser-polishing process is based on the melting of a microscopic layer and a fast re-solidifying of the melted material. The affected layer has to be deep enough to melt the roughness peaks, but it must not be deeper than the valleys. Therefore, the energy of the laser beam must be carefully controlled to melt just a microscopic layer.[10]

3. Experiment

In situ laser polishing is done on CoCr sample by varying scan speed and no. of pass. Surface roughness and residual stress analysis were done. Laser radiation is absorbed on the surface; the energy is converted to heat and the surface layer is melted very quickly. Subsequently, the heat is dissipated into bulk material and the surface layer re-solidifies.

3.1 Material

Cobalt-chrome or cobalt-chromium (CoCr) is a metal alloy of cobalt and chromium. Cobalt-chrome has a very high specific strength and is commonly used in gas turbines, dental implants, and orthopedic implants. Cobalt-chrome-molybdenum alloys are widely used in orthopedic implants. The alloy has a much higher tolerance in the human body that cobalt or nickel, and thus, much less toxicity. CCM is a low carbon, wrought version of ASTM F75 cast alloy.

3.2 Process

In this experiment, Laser surface remelting of CoCr samples were performed in the same machine where the sample was built. For this process, the bulk part of the sample was built in a standard EOS process parameter. On the top surface, process parameter: Scan Speed, Hatching distance and Hatching direction was changed. Also, three sets of the sample was made in which on the first set of sample (A); a single exposure (No powder layer recoated at last layer) was given. In the second set (B), one layer thickness of 80 microns of powder was spread by recoater blade and then single exposure of specified process parameter was given. In the third sample (C), two layer thickness of 80 microns of powder was spread by recoater blade and then single exposure of specified process parameter was given.

In surface roughness analysis, Average surface roughness (Longitudinal) mean that surface roughness is measured perpendicular to the direction of scan direction of the laser beam that is the breadth of the sample while average surface roughness (Transverse) mean that surface roughness is measured along the direction of scan direction of the laser beam that is the length of the sample.

3.3 Observation

Initial process parameter table shows parameters set before doing the experiment and final observation table shows output surface roughness value. Sample built in EOS M 270 is shown below.

Fig 1 Sample with parameter chart

Initial Process Parameter Chart

Sample name	Power (W)	Speed (mm/sec)	X	Y	Hatch distance	Power/speed (J/mm)	Power/Speed*Hatch distance) J/mm²	6000*P / (S *H.D.)
EPS080X	195	800	1	0	0.08	0.24	3.05	38281.25
EPS080Y	195	800	0	1	0.08	0.24	3.05	38281.25
EPS081X	195	800	1	0	0.04	0.24	6.09	36562.50
EPS081Y	195	800	0	1	0.04	0.24	6.09	36562.50
EPS082X	195	800	1	0	0.02	0.24	12.18	73125.00
EPS082Y	195	800	0	1	0.02	0.24	12.18	73125.00
EPS180X	195	1600	1	0	0.08	0.12	1.52	9140.62
EPS180Y	195	1600	0	1	0.08	0.12	1.52	9140.62
EPS181X	195	1600	1	0	0.04	0.12	3.05	18281.25
EPS181Y	195	1600	0	1	0.04	0.12	3.05	18281.25
EPS182X	195	1600	1	0	0.02	0.12	6.09	36562.50
EPS182Y	195	1600	0	1	0.02	0.12	6.09	36562.50
EPS280X	195	3200	1	0	0.08	0.06	0.76	4570.31
EPS280Y	195	3200	0	1	0.08	0.06	0.76	4570.31
EPS281X	195	3200	1	0	0.04	0.06	1.52	9140.62
EPS281Y	195	3200	0	1	0.04	0.06	1.52	9140.62
EPS282X	195	3200	1	0	0.02	0.06	3.05	18281.25
EPS282Y	195	3200	0	1	0.02	0.06	3.05	18281.25

Table 1. Observation Table (Initial Process Parameter)

Final Process Parameter Chart

Sr No.	Sample Name	Sample Set	Scan Speed	Hatching Distance (mm)	Hatching Direction	Average Surface Roughness (um) (Longitudinal)	Average Surface Roughness (um) (Transverse)
1	EPS0H0X	A	800	0.08	X	2.14	1.03
2	EPS0H0X	B	800	0.08	X	2.91	1.08
3	EPS0H0X	C	800	0.08	X	5.27	1.69
4	EPS0H0Y	A	800	0.08	Y	1.83	3.58
5	EPS0H0Y	B	800	0.08	Y	5.27	6.33
6	EPS0H0Y	C	800	0.08	Y	7.39	12.05
7	EPS0H1X	A	800	0.04	X	3.73	2.01
8	EPS0H1X	B	800	0.04	X	6.52	4.33
9	EPS0H1X	C	800	0.04	X	10.83	7.47
10	EPS0H1Y	A	800	0.04	Y	1.02	1.84
11	EPS0H1Y	B	800	0.04	Y	1.50	2.83
12	EPS0H1Y	C	800	0.04	Y	1.41	4.93
13	EPS0H2X	A	800	0.02	X	2.01	1.48
14	EPS0H2X	B	800	0.02	X	4.08	4.03
15	EPS0H2X	C	800	0.02	X	8.24	6.12
16	EPS0H2Y	A	800	0.02	Y	3.74	5.68
17	EPS0H2Y	B	800	0.02	Y	6.90	17.35
18	EPS0H2Y	C	800	0.02	Y	Too rough	Too rough
19	EPS1H0X	A	1600	0.08	X	7.35	3.33
20	EPS1H0X	B	1600	0.08	X	9.02	5.22
21	EPS1H0X	C	1600	0.08	X	8.80	7.64
22	EPS1H0Y	A	1600	0.08	Y	3.58	4.19
23	EPS1H0Y	B	1600	0.08	Y	6.96	9.92
24	EPS1H0Y	C	1600	0.08	Y	13.35	12.30
25	EPS1H1X	A	1600	0.04	X	2.35	1.81
26	EPS1H1X	B	1600	0.04	X	5.81	4.14
27	EPS1H1X	C	1600	0.04	X	10.30	6.96
28	EPS1H1Y	A	1600	0.04	Y	4.14	5.13
29	EPS1H1Y	B	1600	0.04	Y	4.02	7.91
30	EPS1H1Y	C	1600	0.04	Y	4.26	7.31
31	EPS1H2X	A	1600	0.02	X	3.07	2.90
32	EPS1H2X	B	1600	0.02	X	11.65	12.51
33	EPS1H2X	C	1600	0.02	X	15.22	5.85
34	EPS1H2Y	A	1600	0.02	Y	2.15	2.02

35	FPS1H2Y	B	1600	0.02	Y	1.27	3.15
36	FPS1H2Y	C	1600	0.02	Y	5.73	6.47
37	FPS2H0X	A	3200	0.08	X	5.28	4.05
38	FPS2H0X	B	3200	0.08	X	11.63	9.24
39	FPS2H0X	C	3200	0.08	X	14.02	12.56
40	FPS2H0Y	A	3200	0.08	Y	3.20	5.16
41	FPS2H0Y	B	3200	0.08	Y	16.60	15.16
42	FPS2H0Y	C	3200	0.08	Y	17.70	16.53
43	FPS2H1X	A	3200	0.04	X	5.86	3.54
44	FPS2H1X	B	3200	0.04	X	9.22	8.34
45	FPS2H1X	C	3200	0.04	X	11.78	10.19
46	FPS2H1Y	A	3200	0.04	Y	2.90	4.61
47	FPS2H1Y	B	3200	0.04	Y	Too rough	Too rough
48	FPS2H1Y	C	3200	0.04	Y	Too rough	Too rough
49	FPS2H2X	A	3200	0.02	X	4.11	5.10
50	FPS2H2X	B	3200	0.02	X	8.58	8.34
51	FPS2H2X	C	3200	0.02	X	14.50	12.09
52	FPS2H2Y	A	3200	0.02	Y	4.82	5.60
53	FPS2H2Y	B	3200	0.02	Y	8.62	9.76
54	FPS2H2Y	C	3200	0.02	Y	14.64	12.35

Table 2. Observation Table (Surface Roughness)

4. Result and Conclusion

The result is shown in tabular format.

FPS0H0X (A)	1.03	Lowest Surface Roughness/Best Surface Finish in transverse direction
FPS0H0X (B)	1.08	Lower Surface Roughness/ Better Surface Finish in transverse direction
FPS0H2X (A)	1.43	Low Surface Roughness/ Good Surface Finish in transverse direction
FPS0H1Y (A)	1.02	Lowest Surface Roughness/Best Surface Finish in longitudinal direction
FPS1H2Y (B)	1.27	Lower Surface Roughness/ Better Surface Finish in longitudinal direction
FPS0H1Y (C)	1.43	Low Surface Roughness/ Good Surface Finish in longitudinal direction

Thus, it can be concluded that there was a 94% reduction in surface roughness by laser surface remelting in the same machine (EOS M 270) in which the sample was built. Minimum surface roughness obtained by measuring it with Taylor and Hobson contact profilometer was 1.03 micron. SEM image of the sample is shown to feature laser polishing operation.

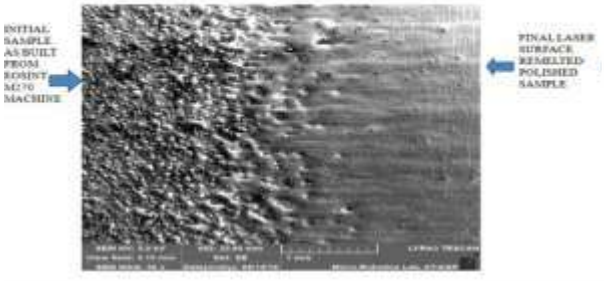

Fig 2. SEM Image of best sample

SEM image analysis shows an improvement in surface roughness due to metal peak remelted down to valley giving a smooth surface.

Thus, in this experiment, In-situ laser surface remelting was done which is cost effective and faster post-processing process. Future works include residual stress simulation and optimization of laser polishing surface energy by mathematical modeling of the geometry of surface roughness and applying various optimization tools.

Acknowledgment

Thanks to lab staff and senior for successfully conducting the experiment at Laser processing lab and direct digital manufacturing lab at IIT Kharagpur.

References

1. Burns, 93, AMT, 14
2. Ravari, M. K., M. Kadkhodaei and A. Ghaei (2015). A Microplane constitutive model for shape memory alloys considering tension-compression asymmetry. Smart Materials and Structures 24(7): 075016.
3. Gibson, I., D. W. Rosen and B. Stucker (2010). Additive Manufacturing Technologies, Springer, New York.
4. Mici, J., B. Rothenberg, E. Brisson, S. Wicks and D. M. Stubbs (2015). Optomechanical performance of 3D-printed mirrors with embedded cooling channels and substructures. SPIE Optical Engineering+ Applications, International Society for Optics and Photonics, 957306-957306.
5. Baufeld, B., E. Brandl and O. Van der Biest (2011). Wire-based additive layer manufacturing: Comparison of microstructure and mechanical properties of Ti–6Al–4V components fabricated by laser- beam deposition and shaped metal deposition. Journal of Materials Processing Technology, 211(6): 1146–1158.
6. Andani, M. T., N. S. Moghaddam, C. Haberland, D. Dean, M. J. Miller and M. Elahinia (2014). Metals for bone implants. Part 1. Powder metallurgy and implant rendering. Acta biomaterialia 10(10): 4058–4070
7. Moghaddam, N. S., M. T. Andani, A. Amerinatanzi, C. Haberland, S. Huff, M. Miller, M. Elahinia and D. Dean (2016a). Metals for bone implants: Safety, design, and efficacy. Biomanufacturing Reviews, 1(1)
8. Polishing with laser radiation by E. Willenborg pp. 196–203
9. A. Lamikiz, J. A. Sánchez, L. N. López de Lacalle, and J. L. Arana, "Laser polishing of parts built up by selective laser sintering," *Int. J. Mach. Tools Manuf.*, vol. 47, no. 12–13, pp. 2040–2050, 2007.
10. S. Marimuthu, A. Triantaphyllou, M. Antar, D. Wimpenny, H. Morton, and M. Beard, "Laser polishing of selective laser melted components," *Int. J. Mach. Tools Manuf.*, vol. 95, pp. 97–104, 2015

Volume 1 - Number 3 - 2019 - 3-10

A novel method to generate mesh support for printability and minimize distortions within fabricated part

Gaurav Kumar Sharma, Jasvinder Singh, Vishnu Vardhan Reddy, Anoop Kishor
Dassault Systemes, Bangalore, India
{GauravA.SHARMA, Jasvinder.SINGH, VishnuVardhan.REDDY, Anoop.KISHOR}@3ds.com

Abstract *- Various lattice and mesh supports are being widely used in additive manufacturing to minimize the wastage of the support materials and energy consumption. It is often easy to remove these supporting structures from the part by applying small shear force. However, existing methods to generate these structures still suffer from various limitations. These methods may not generate stable configuration of support structures standing firm against the build platform especially for the supporting zones with small area (point support, edge support). Such small sized zones may need to carry large weight depending on the number of layers to be built above them or moment of force generated by the re-coater or side-weight of already built layers. This develops high stress on the supports anchoring these zones. As a result, the part may not be printable after printing certain number of layers on such zones. Even if part could be printed for certain materials, there is a large distortion in the support, leading to high distortion or large spring-back within the fabricated part after removal of supports. We propose a new method that generates the skeleton of the supports in the vicinity of the small-sized zone needing support. Such skeletons are generated by rolling the maximal disc on the boundary of small-sized zones needing support. Using this approach, the number of support skeletons increases proportionally with the increase in sharp features within the support zones. As a result, there are always exists sufficient number of supports to neutralize the high stress. These support skeletons are further skinned using the sphere or disc of appropriate dimension in order to minimize the deformation within these supports.*

Index Terms *–Lattice Supports, Mesh Supports, Additive Manufacturing, Stable, Distortion*

I. Introduction

The additive manufacturing process has been developed to build what you see in design. Unlike subtractive manufacturing, additive manufacturing can save expensive materials by adding what is required across the layers. The process of layering allows the designer to customize and fabricate the complex structures. However, the layered manufacturing comes with limitation of providing the support to the substrate similar to the supports required in construction of building and bridges. The difference in the supports used in construction of building, bridges etc is that additive manufacturing builds the supports on the fly during the process of layering and joining the adjacent layers of the part to be manufactured. The role of support is to resist the deformation caused by the gravity during the fabrication of the components. They also act as bridge supporting two unconnected regions which gets attached in successive layers. Another role of support is to balance the part during printing so that it remains securely attached to the build platform during the manufacturing process.

There has been lot of work done in generation of support using Fused Deposition Modeling (FDM) because of the easy accessibility and testing using FDM process. However, support building for metal printing to realize the topologically optimized structures have not gained much attention unlike FDM. The supports in metal printing play an additional role that affects the quality of printed objects. In metal printing (SLS, SLM), these supports behaves like a heat conductor, while the metal powder acts as an insulator. Thus, the supports being heat conductor defines the rate of fusion across the mounted successive layers and determines the build up any residual stress after fabrication. The residual stress within metals affects the mechanical properties of the product. If the residual stress is higher that yield stress, the part would undergoes plastic deformation on applying load. If the residual stress is higher than the ultimate stress, it would lead to crack or fracture within the part. Another important aspect in the metal printing is the deviation in the geometric dimensioning and tolerance of the final manufactured product, which, if not respected, would lead to rejection of the parts. These deviations can arise due to the residual strain arising due to uneven cooling of the melt pool or spring back caused by the supports. During the process of building part, the supports get deformed due to its own weight, forces generated by re-coater or weight of the buildup material. As a result, the supported zones of the part get displaced from its original position at the time of removal of these supports.

The focus of this paper is to address issues in the overhang regions (or support zones) of the part having small area. Such zones needing support are often supported in the way other overhanging areas are supported. As a result supports defined under such zones may get large deformation due to small area, large load, etc, which might not even result in large distortion within the fabricated part but also may affect printability process itself. The following considerations should be taken while generating supports on such zones.

1. Sufficient number of supports should anchor the zones with small area to resist the forces or the moment arising due to the re-coater at every successive layer.

The supports under zones with sharp features may undergo high stress due to the weight of the printed material or any imbalance in moment arising due to the shift in center of gravity of part during the fabrication process. As a result, the lattice structures may even run into the risk of buckling depending on the slenderness ratio and type of material used for support. This demands the skinning of mesh supports to improve its aspect ratio.

2. The maximum deformation allowed at these supports needs to be controlled to avoid spring back within fabricated part after manufacturing in order to respect the geometric dimensioning and tolerance of the part.

This paper develops a new method to generate supports for small-sized zones needing support. The method rolls the maximal disc on the boundary of the zone, which generates the locus of center of disc contained by the part and build tray. The line joining the center of the disc of the foot-points on maximal disc forms the skeleton of the support. The method automatically generated large envelop based on the sharp feature of such zones. The resulting skeleton of the supports are skinned with appropriate size of the sphere or disc using minkowski operator in order to minimize the deformation of the supports during the build process.

II. Literature Survey

Most of the methods developed for generating support mainly focus on minimization of the amount of material for supports, minimizing its print time and ease of removal of the supports during post-processing. Another complimentary view is to replace the need of support by either optimizing the part orientation or changing the design features such that they need minimal or no support.

The simplest kind of support is the volume support generated over the overhang area. Such supports are very useful for metal printing (SLS, SLM) to conduct heat resulting in minimizing residual stress, but it produces a lot of sacrificial waste and they are difficult to be removed from narrow and deeper zones. The natural approach is to optimize these support structures geometry. Strano et.al. [1] used an optimization algorithm to develop graded cellular supports where the gradation is controlled according to the robustness of support required, thus, providing significant amount of material saving. Hussein et.al. [2] investigated the cellular supports for metallic part based on SLM. Their preliminary investigations suggest the high distortion of the parts due to high thermal gradients present in the phase transition process. However, they recommended the use of the lattices structures like diamond and gyroid as suitable supports to reduce the build time and material. As the volume fraction of the material in lattice support is reduced, these supports are difficult to be fabricated within SLM for a given laser resolution. Vidhya and Anand[3] applied the unit-cell approach to generate the supports. These unit cells are stacked together using Dijkstra's shortest path algorithm [4] to minimize the support volumes. Their approach shows significant amount of material saving compared to the solid support, along with advantages of providing good accessibility to remove the supports. They have described their approach using truncated octahedrons and rhombic dodecahedrons. Various tree-like support structures [5, 6] have been developed for FDM to save filament materials. Dumas et al.[7] considered the stability of the part during the build process. They developed the bridge scaffoldings supported by pillars at the extremities, which are more strong and stable in comparison to the tree supports. Another way to generate support structures is to use different material, which can be dissolved or sacrificed in other ways. Various methods supporting FDM [8, 9, 10] and SLM [11, 12] have been developed. These methods are not yet matured for any practical usage in metal printing and need lot of investigation for finding the type of material that can be used as support corresponding to the different metals.

III. Methodology

The method starts with identification of the small-sized overhang area on the part in step 1 based on the deviation in normal across its adjacent faces. Using these small sized zones of the part and the build tray, the topological skeleton of the supports are constructed in step 2. Various shapes are embedded over these skeletons in step 3 in order to satisfy various possible loading conditions and thermal distortions. The number of skeletons and thickness of the skin over these skeletons can be adaptively refined or regenerated on the fly by the user.

1. *Identification of Candidate Support Zones*: The overhang regions or support zones on a part having small-sized area are identified by the steep change in normal across its neighborhood points. For example, figure 1 and 2 shows small-sized point and edge support, where the maximum possible deviation in normal of faces incident on the point and edge respectively is quite large.

The input to the method is mesh representation of the given CAD model. It is represented using graph structure [13] to stores the topological information.

$$S = (V, E, F)$$

where F is set of faces, each face is bounded by set of edges E and each edge is bounded by the set of vertices V.

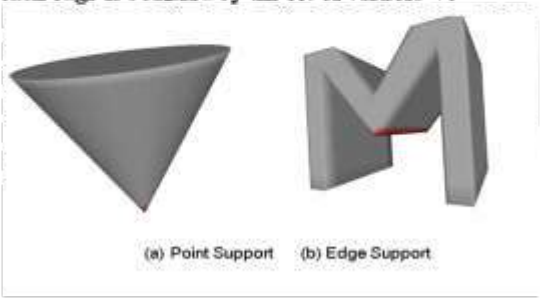

Figure 1: Support zones marked in red

The zones needing support Z are defined as the subset of the original mesh representation S. The procedure to identify such smalls-zed zones is as follows:

Procedure:

- Find the mesh elements $s \subset S$ needing support based on the orientation of each face i.e. normal n to each face shown be down-facing with respect to the build direction or dot product $(n, z)<0$.

- Find the mesh elements corresponding to the small-sized zone $Z \subset s$ such that the deviation in the normal across the neighborhood faces is beyond certain threshold limit. If the normal deviation is beyond the threshold value across the neighborhood faces incident on a vertex and vertex is locally minima, it would be called as *point support*. If the normal deviation is beyond the threshold value across the neighborhood faces incident on an edge and edges is locally minima, it is called as *edge support*. Similarly, the normal deviation across a face is beyond threshold, it would be *surface type support zone*.

2. Construction of Topological Skeleton of the supports:

(a) Any point $P \in Z$, the normal is defined by using the normal of the corresponding face for the *surface type support zone*. The normal is undefined for *point or edge support*, which is evaluated by the linear combination of the normal at the faces incident on corresponding point or edge.

Figure 2 shows a point P on the edge support. If the normal at the face incident on point P are respectively n_1 and n_2, then the normal at P is $n_p = s.n_1+(1-s).n_2$, $0<=s<=1$. Thus, in general, normal at any point P shared by faces $F_1, F_2, F_3...F_N$ having corresponding normal as $n_1, n_2....n_N$ is evaluated as follows:

$$n_p = s_1.n_1+s_2.n_2+s_3.n_3.....s_N.n_N$$

where $0<= s_1, s_2, s_3...s_N<=1$ and $s_1+s_2+s_3...+s_N=1$.

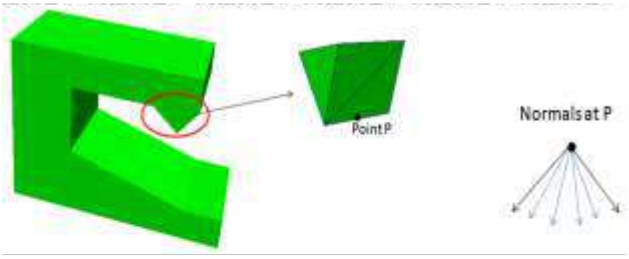

Figure 2 (a) Support Zones with steep change in normal (b) Set of all possible normal at P

(b) For a given normal n_p, the maximal disc is evaluated tangential to the normal and contained by the part or Build tray. Figure (a) shows the evolution of the maximal disc, (b) shows the maximal disc, the line joining the foot-points (point of contact) and center forms the skeleton.

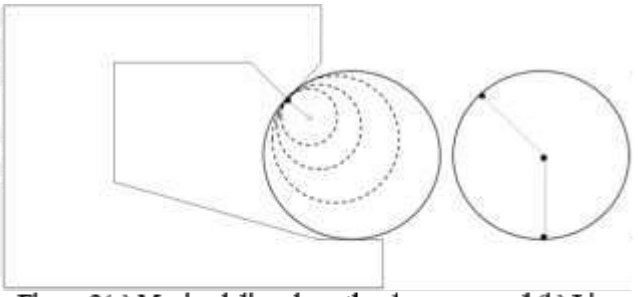

Figure 3(a) Maximal disc along the chosen normal (b) Line joining the foot-points and center form the skeleton of the support.

The step (b) is repeated for all possible normal at point P to form a set of skeletons of support as shown in figure 4.

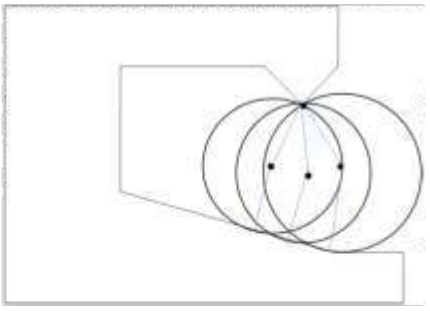

Figure 4 Set of skeleton for the support using the locus of maximal disc

If the set of such skeletons T is represented using poly-lines written as T = (C, P, Q), where C is center of disc, P is point of contact on the support zone and Q is the point contact with either part or build tray.

3. Embedding the support elements over the skeleton of the support:

- The support skeletons T are embedded with sphere or disc or any other self-supporting unit cell to generate the skin of support. This is achieved by using minkowski operator. If the sphere M of radius r is used to skin the support, where the choice of radius r is user-driven based on the loading condition and type of the material used, the support geometry is represented as follows:

$$T \oplus M = \{t + m | t \in T, m \in M\}$$

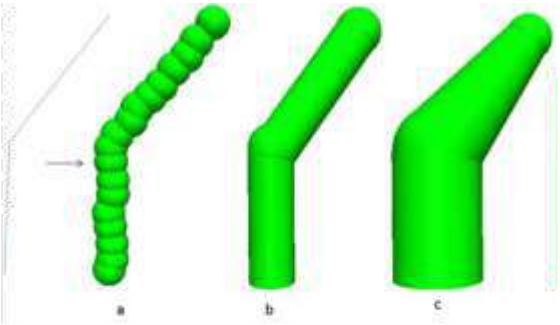

Figure 5 Skinning of the support skeleton using sphere in discrete set of points separated by radius of sphere in (a) cylindrical disc of fixed radius in (b) cylindrical disc of variable radius in (c)

The skeleton of the support is embedded with self-supporting unit cells i.e. sphere and disc as shown in figure 5 (a) and (b). The radius of the disc is varied from high to low along the direction of build to achieve gradient in size in figure 5 (c).

IV. RESULTS

Figure 6 shows the supports generated using proposed method highlighted using red boundary. The numbers of supports elements generated for sharp feature in 6(a) depends on the deviation in normal rather than the area of supported zone. Thus, high stress on such zones dues to small area gets neutralized by these supported elements minimizing the deformation of the supports. Other regions needing support use simple ray-casting method for generating support. Similarly figure 6(b) shows the support zone having well-defined normal but higher deviation across adjacent points on these zones. Such zones would automatically get supported by elements forming an upward umbrella with an intermediate branching. Such intermediate branching would save lot of material compared to the set of erected vertical supports.

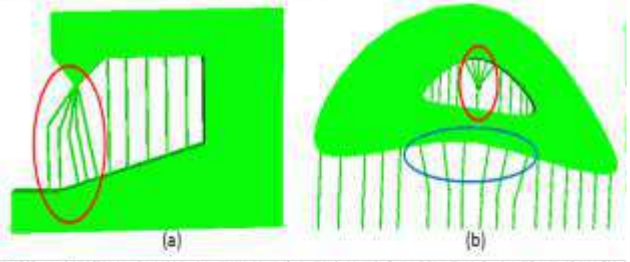

Figure 6 Supports generated by proposed method are bordered in red. The support in (a) anchors as an inverted umbrella while it anchors as upward umbrella in (b).

V. Discussion and Conclusion:

This method is useful for small-sized zones having sharp features or large curvature. In other overhang regions, this method would be computationally expensive to be used because each skeleton of supports needs expensive computation of maximal disc. Hence, other overhang zones use simple ray casting method to generate support skeleton. As shown in figure 6(b) region bordered by blue generates supports using developed method, which could have been simply supported using ray-casting method itself. It is to be noted that not all support skeletons constructed using maximal disc could be used as support. The set of lines joining foot-point and center of disc, which are not self-supporting, have to be filtered out from support skeletons.

The developed method shows how to generate more supports required in the overhang regions with the sharp features in order to neutralize the possible high stress in such area and minimize support deformation. However, supports emanating from smooth surface associated with high curvature would get branch out in the middle; thus, saving material that would otherwise have been consumed in extending all supports to the bottom. In addition, this method allows the user to adaptively grade the thickness of support by appropriately skinning the support skeletons to keep deformations under limit in order to respect the geometric dimensioning and tolerance of fabricated part.

References

[1] Strano, Giorgio, et al. "A new approach to the design and optimisation of support structures in additive manufacturing." The International Journal of Advanced Manufacturing Technology 66.9-12 (2013): 1247-1254.

[2] Hussein, Ahmed, et al. "Preliminary investigation on cellular support structures using SLM process." Innovative Developments in Virtual and Physical Prototyping: Taylor & Francis Group: London, UK (2011): 609-612.

[3] Vaidya, Rohan, and Sam Anand. "Optimum support structure generation for additive manufacturing using unit cell structures and support removal constraint." Procedia Manufacturing 5 (2016): 1043-1059.

[4] Dijkstra, Edsger W. "A note on two problems in connexion with graphs." Numerische mathematik 1.1 (1959): 269-271.

[5] Vanek, Juraj, Jorge A. Garcia Galicia, and Bedrich Benes. "Clever support: Efficient support structure generation for digital fabrication." Computer graphics forum. Vol. 33. No. 5. 2014.

[6] Schmidt, Ryan, and Nobuyuki Umetani. "Branching support structures for 3D printing." ACM SIGGRAPH 2014 Studio. ACM, 2014.

[7] Dumas, Jérémie, Jean Hergel, and Sylvain Lefebvre. "Bridging the gap: automated steady scaffoldings for 3D printing." ACM Transactions on Graphics (TOG) 33.4 (2014): 98.

[8] Domonoky, BonsaiBrain. Support—Full Disclosure 2016. Available online: http://ifeelbeta.de/index.php/support/support-full-disclosure (accessed on 30 November 2019).

[9] Hopkins, P.E.; Priedeman, W.R., Jr.; Bye, J.F. Support Material for Digital Manufacturing Systems. U.S. Patent 8,246,888 B2, 21 August 2009.

[10] Ni, F.; Wang, G.; Zhao, H. Fabrication of water-soluble poly(vinyl alcohol)-based composites with improved thermal behavior for potential three-dimensional printing application. J. Appl. Polym. Sci. 2017, 134.

[11] Mumtaz, K.A.; Vora, P.; Hopkinson, N. A Method to Eliminate Anchors/Supports from Directly Laser Melted Metal Powder Bed Processes. In Proceedings of the Solid Freeform Fabrication Symposium, Austin, TX, USA, 8–10 August 2011; pp. 55–64.

[12] Lefky, C.S.; Zneker, B.; Wright, D.; Nassar, A.R.; Simpson, T.W.; Hildreth, O.J. Dissolvable Supports in Powder Bed Fusion-Printed Stainless Steel. 3D Print. Addit. Manuf. 2017, 4, 3–11.

[13] Cheng, Siu-Wing, Tamal K. Dey, and Jonathan Shewchuk. Delaunay Mesh Generation. CRC Press, 2012.

Comparative Study on Additive Manufacturing Technologies from Stereolithography to Continuous Liquid Interface Production – A Review

Ribin Varghese Pazhamannil and Dr. Govindan P

***Abstract*—Additive Manufacturing is a technology capable of producing complex geometries which are difficult to generate via conventional subtractive machining processes. They build the part geometry layer by layer directly from the CAD model. Traditional additive manufacturing processes include Stereolithography (SLA), Selective Laser Sintering (SLS), Fused Deposition Modelling (FDM) etc. whose major limitations are large time consumption and weak overall structure due to its layer by layer making. A game changing technology was developed by CARBON3D in the year 2014 where the use of layer by layer manufacturing was eliminated by Continuous Liquid Interface Production (CLIP). CLIP is achieved with the use of oxygen permeable window which creates a dead zone where photopolymerization is inhibited between the window and the polymerizing part. This paper presents a comparative study of AM technologies from Stereolithography to CLIP. This article concentrates on the research done in the area of Continuous Liquid Interface Production.**

***Index Terms*—Additive manufacturing, continuous liquid interface production, dead zone thickness, oxygen permeable window, stereolithography, selective laser sintering, material jetting, binder jetting, direct energy deposition, fused deposition modelling, laminated object manufacturing, photopolymerization**

I. Introduction

Additive Manufacturing is a technique of manufacturing parts layer by layer directly from the CAD model. It has got the capability of making complex geometries which are otherwise difficult or impossible to create using conventional subtractive machining or forming processes. It has created an impact in all industry sectors including aerospace, construction, medical and military [1,2]. Additive manufacturing has got a variety of applications which includes do-it yourself, tissue engineering, low density high strength materials, energy, molecular visualization, micro fluidics etc. [3] The ASTM F42 technical committee defines additive manufacturing (AM) as the "process of joining materials to make objects from three-dimensional (3D) model data, usually layer upon layer, as opposed to subtractive manufacturing methodologies" [4]. It is also known as rapid prototyping, rapid manufacturing, layer manufacturing, additive fabrication, additive processes, direct digital manufacturing and solid freeform fabrication.

Ribin Varghese Pazhamannil (e-mail: ribinvarghese92@gmail.com)
Corresponding author: Dr. Govindan P (e-mail: govindanformegeek@gmail.com)

The main challenges faced by designers and production engineers are to meet the customer demands which are way ahead of the production rate. This should be solved to be successful over competitors. Additive manufacturing uses an efficient technique of building complex architectures in short design and production cycle time at low cost due to absence of tooling needs [5,6]. Currently, the applications are shifting to- wards end product manufacturing which demands accurate dimensions, good mechanical properties etc. This requires determination of relationships between process parameters and end-use properties. The working principle of AM gives several advantages like near-net-shape capabilities, superior design, geometrical flexibility, multi-material fabrication, reduced tooling and fixturing, short cycle time, instant local production at a global scale and material, energy and cost efficiency [7].

Although several rapid prototyping techniques exist, all employ the same basic five step process [8,9]. The steps involved are:

- Create a CAD model of the required design.
- Convert the CAD model to STL format.
- Slice the STL file into layers according to our requirements.
- Construct the model one layer atop another.
- Clean and finish the model.

Since 1980s, AM processes have been investigated and they include Stereolithography (SLA), Selective Laser Sintering (SLS), Material Jetting (MJ), Binder Jetting (BJ), Direct Energy Deposition (DED), Fused Deposition Modelling (FDM) and Laminated Object Manufacturing (LOM) [10-16]. The materials used in all these processes include photo-curable resin, polyamide, wax, ABS, polycarbonate, metal/ceramic/polymer powders, adhesive coated sheets etc. The various types of AM technologies, its merits and demerits are discussed in the next section.

II. Types of Additive Manufacturing Technologies

A. Fused Deposition Modelling (FDM):

The FDM process was invented and patented by Scott Crump in 1988. FDM is a filament extrusion-based process which incorporates materials science, extrusion process, CAD system, and the computer numerical control to fabricate 3D

parts directly from a CAD model. In the basic FDM process, filament is drawn into a liquefier head, where the filament is heated to a semi liquid state and then extruded through a nozzle to fill each layer of the part onto a temperature-controlled platform. The computer-controlled head moves in X–Y plane while the platform moves in the Z-direction as required by the selected layer thickness [17]. The principle of operation is material extrusion. The materials used are thermoplastic filaments typically ABS, Nylon, PLA, PC, Composites, Nano fillers etc. Advantages of FDM includes low cost, simplicity, low maintenance etc. Limitations include void creation, low accuracy etc. One of the major causes of part inaccuracy in FDM is the shrinkage which does not

occur in a uniform manner along the different axis [18]. Schematic of the fused deposition modelling process is shown in the below figure 1.

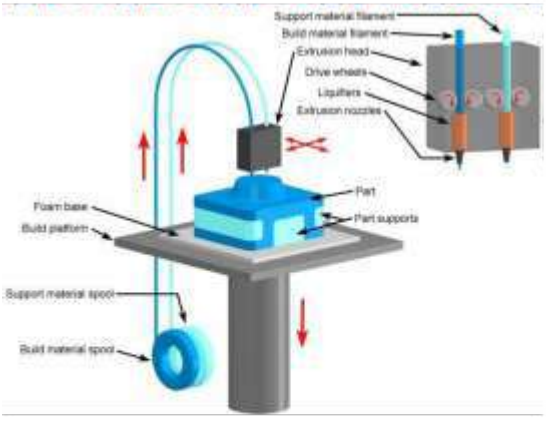

Fig. 1. Fused Deposition Modelling

B. Stereolithography (SLA):

Stereolithography involves the curing or solidification of a liquid photosensitive polymer through the use of an irradiation light source, which supplies the energy that is needed to induce a chemical reaction bonding large numbers of small molecules and forming a highly cross-linked polymer [19]. The process can be divided into two namely top down and bottom up processes. The principle of operation is vat photopolymerization [20-23]. When curing is done with a laser it is known as vector scanning stereolithography and when cured with a projector (DLP) it is known as projection stereolithography. The materials which can be used are liquid photopolymers (acrylic or epoxy based). Main advantage is its high accuracy. Disadvantages include expensive, requires significant support structures etc. In top down process, the platform moves downward after each layer of liquid resin is cured. In bottom up process, the build platform lifts the part being cured from the pool resin after each layer. SLA was the first rapid prototyping technology developed. Stereolithographic process is shown in the following figure 2.

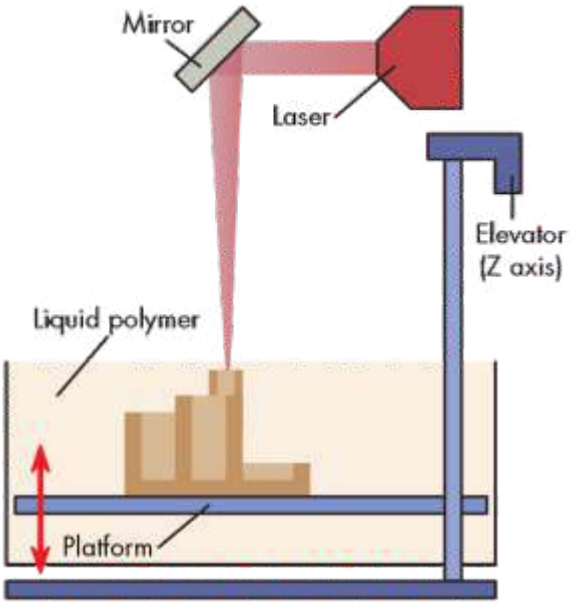

Fig. 2. Stereolithographic Process

C. Laminated Object Manufacturing (LOM):

Helisys introduced the LOM technique which creates parts using a unique additive process. A layer of material with an adhesive coating on one side is placed on a platform with adhesive side down. A heated roller passes over the material and sticks the material to the platform. A laser beam then traces the outline of one slice of the part and cutting through the layer of the material. The laser beam then cross hatches the material that does not form part of the cross section again cutting through the layer. The platform is then lowered one layer thickness, another layer of material is stuck onto the previous layer and the procedure is repeated with the next cross section slice of the part. When all cross-section slices have been added, the solid block of material is removed from the platform. The crosshatched areas of the block are then broken away from the final part [24-27]. This process uses the principle of sheet lamination. Materials used are polymer composites, ceramics, paper, metal filled tapes etc. Advantages include high speed and low cost. Disadvantages are the requirement of post-processing depending on the material and limited availability of materials. The process is shown in figure 3.

D. Selective Laser Sintering (SLS):

SLS uses the same geometry as SLA, except that SLS uses a CO_2 laser to sinter or fuse a powder layer rather than solidify liquid photo-polymer. The SLS process deposits powdered material layer by layer on a platform. The CO_2 laser beam is used to heat a cross-section of one slice of the part. Once the laser beam heats the powder, the influenced particles are sintered or fused together. Another layer of powder is then

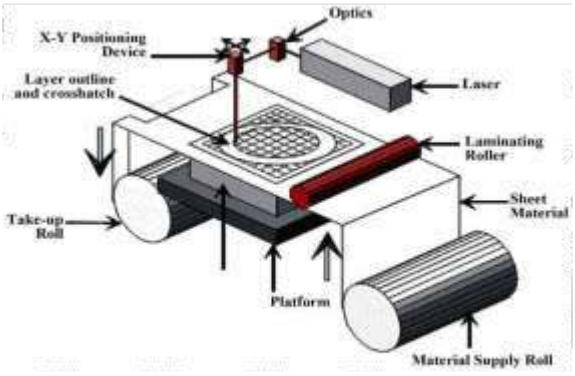

Fig. 3. Laminated Object Manufacturing

deposited on top of the first layer using a roller mechanism and another slice of the part is sintered onto the sintered material in the previous slice. The layer thickness of SLS is between 0.080 - 0.500 mm. The un-sintered power in each layer can work as a support structure for the part. Finally, when the part is built, the un-sintered material can be easily brushed off [28-30]. Materials which can be used are Stainless steel, Titanium, Aluminium, Cobalt Chrome, Steel, Plastic etc. Large range of material options and no support structure requirements are the main popularities of this process. Limitations include high power usage, size limitations, powder grain size issues, effects surface finish etc. SLS is shown below in figure 4.

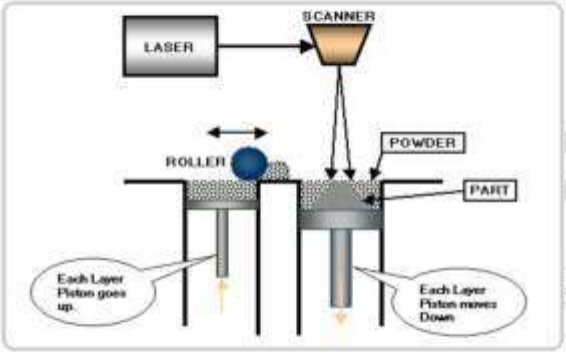

Fig. 4. Selective Laser Sintering

E. Material Jetting (MJ):

Material jetting is capable of creating objects in a similar manner as that of a two dimensional ink jet printer. Material is jetted onto the build platform using either continuous or Drop on Demand (DOD). Material is jetted onto the build surface where it solidifies and the model is built layer by layer. Material is deposited from a nozzle which moves horizontally across the build platform. Machines vary in complexity and in their methods of controlling the deposition of material. The material layers are then cured or hardening using ultraviolet (UV) light [31,32]. As material are deposited in drops, the number of materials available to be used are also limited. Commonly used materials are polymers. Precision, production of complex structures, fast and efficient are the major advantages where as high maintenance is its drawback. The process is shown below in figure 5.

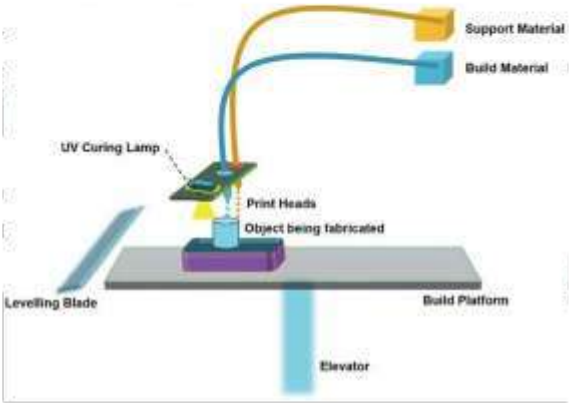

Fig. 5. Material Jetting

F. Binder Jetting (BJ):

Each layer begins with a thin distribution of powdered material over the surface of powder bed. A binder material selectively joins the particles where the object is formed. The bed is then lowered by a fixed distance. Powder is then deposited and spread evenly across the bed with a roller mechanism, and a second layer is built. This is repeated until the entire model is fabricated. The completed object is embedded inside unprocessed powders and is extracted by brushing away the loose powders [33,34]. Here powder base and liquid binders are used. The powder is spread evenly and the binder glues to the desired shape. Materials commonly used include gypsum, sand, metal, ceramic, polymers etc. Mechanical properties are weak and powder form only can be used. But the process is fast, simple and relatively cheap.
Binder jetting process is shown in figure 6.

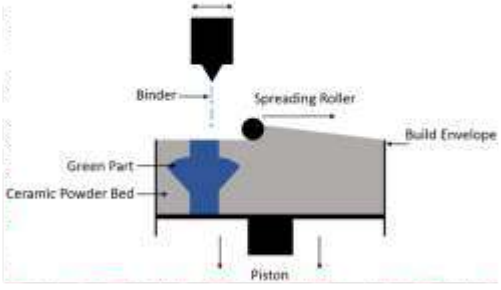

Fig. 6. Binder Jetting

G. Direct Energy Deposition (DED):

Direct energy deposition is a major subset of currently available AM processes, in which a high-energy density heat source, such as a laser, electron beam, or arc is used to create a melt pool into which metal powder or wire is injected. Several processes like Laser Engineered Net Shaping (LENS), Directed Light Fabrication (DLF), Direct Metal Deposition (DMD) are included in this type [35,36]. A nozzle combined with a multi-axis arm deposits melted material onto a specified surface. The nozzle can move in multiple directions and is not fixed to a specific axis. Materials which can be used include Cobalt, Chrome, Titanium, Polymers, Ceramics. Flexibility is its main advantage. It can be used for repair of structures. Limited material use and post processing may be required for this process [37]. The process is explained below in figure 7.

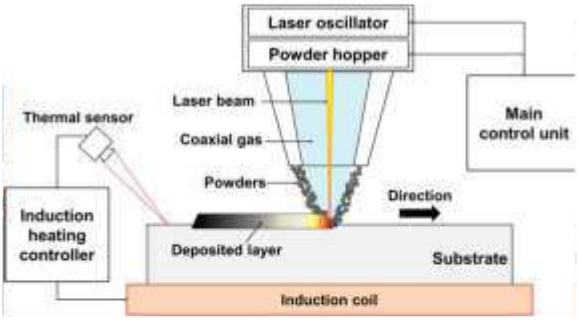

Fig. 7. Direct Energy Deposition

Additive manufacturing techniques can be classified based on the state of material used to make final 3D products. It is well explained in the table I [38-52].

The progress of the technology development in the area of additive manufacturing has been amazing thereby improving industrial applications. AM is capable of producing low volume high variety complex products when compared to subtractive machining. AM techniques also offer customised product development especially in medical areas. We have been discussing the various technologies available under AM. All those processes were based on layer by layer manufacturing where the individual merits and demerits have already discussed. The main drawbacks of AM technologies discussed above are mainly large time consumption and weak overall structure [53]. It lacks the critical information such as process repeatability and consistency of manufactured products [54,55].

III. Continuous Liquid Interface Production

In 2014, a game changing advancement in this area was developed by Carbon3D where the use of layer by layer manufacturing which was used for past 35 years were avoided [56]. The technology was titled 'Continuous Liquid Interface Production'. CLIP is based on the principle of photopolymerization. It is actually growing objects from a pool of resin. Controlled usage of light and oxygen helps to produce parts continuously from the resin. Light is used to cure resin and oxygen acts as the inhibiting agent [57]. Important parts of CLIP include:

- imaging unit
- oxygen permeable window
- build platform

Each of these is shown in figure 8.

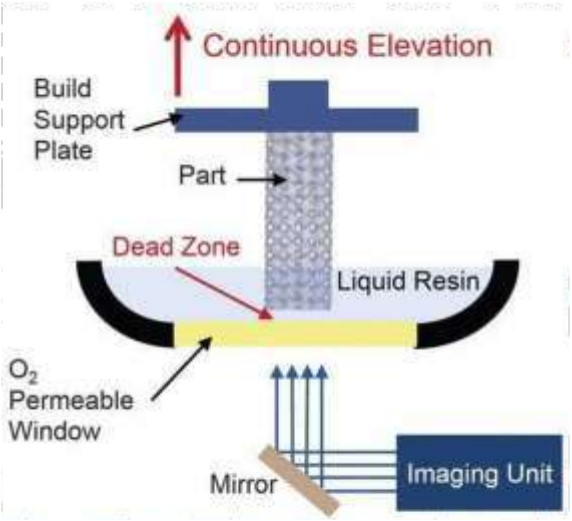

Fig. 8. Parts of CLIP

Instead of printing parts layer by layer as in conventional AM techniques, CLIP uses light to cure resin and oxygen as an inhibiting agent to print continuously. CLIP is made possible with the oxygen permeable window below the UV image projection plane. Photopolymerization is inhibited between the window and the part thereby creating dead zone. Maintenance of dead zone thickness is the key for successful application of CLIP as dead zone created helps in continuous production of parts. The build platform is first lowered into the resin pool and is lifted gradually as the object is being cured. The projector projects the series of cross-sectional images relative to the object being created and the oxygen acts as the inhibiting agent thereby creating a dead zone.

The working of CLIP is shown in figure 9.

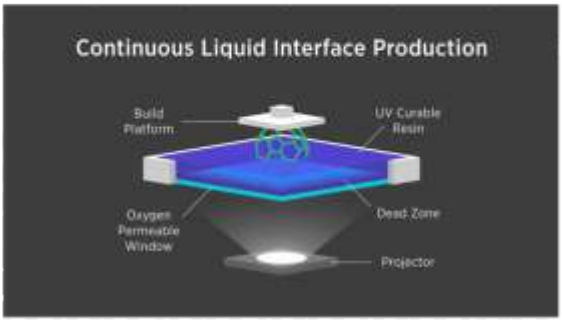

Fig. 9. Working of CLIP

TABLE I
COMPARISON OF AM PROCESSES BASED ON STATE OF STARTING MATERIAL

State of Starting Material	Process	Material Preparation	Layer Creation	Materials
Liquid	SLA	Liquid resin in a vat	Laser/ Digital light projector	UV curable resin, ceramic suspension
	MJ	Liquid polymer in jet	Ink-jet printing	Polymers
Filament/ Paste	FDM	Filament melted in nozzle	Continuous extrusion and deposition	Thermoplastics, waxes
Solid sheet	LOM	Laser cutting	Feeding & binding of sheets with adhesives	Plastic, paper, metal
Powder	SLS	Powder in bed	Laser scanning	Thermoplastics, waxes, metal powder, ceramic powder
	BJ	Powder in bed	Drop on demand binder printing	Polymer, metal, ceramics and other powders
	DED	Powder injection through nozzle	On-demand powder injection & melted by laser	Metal

Above the dead zone, the curing part is continuously drawn out of the resin bath, thereby creating suction forces necessary to renew reactive resin. The first CLIP developed used an amorphous fluoropolymer window (Teflon AF 2400) with excellent oxygen permeability, UV transparency, and chemical inertness. Now, researches are going on in developing oxygen permeable windows and new membranes which can potentially improve the productivity of the process.

Dead zone thickness mainly depends on three control parameters namely photon flux (Φ_0), photo- initiator absorption coefficient (α_{PI}) and resin curing dosage (D_{e0}) and the relation is shown in equation 1.

$$Dead\ zone\ thickness = C\left(\frac{\Phi 0 \alpha PI}{De0}\right)^{-0.5} \quad (1)$$

Where C is the proportionality constant.

The dead zone is created by oxygen permeation through the window. When pure oxygen is used below the gas-permeable window, the dead zone thickness increases (twice as compared to air). If nitrogen is used, the dead zone vanishes, resulting in adhesion of the cured resin to the window.

Above the dead zone, photopolymerization takes place at a certain cured thickness, which depends on Φ_0 α_{PI} /D_{e0} together with the exposure time (t) and the resin absorption coefficient (α) and is explained in equation 2.

$$Cured\ thickness = \frac{1}{\alpha} ln\left(\frac{\Phi 0 \alpha PI}{De0}\right) \quad (2)$$

Note that α is the inverse of the characteristic optical absorption height (h_A) of the resin. From the expressions of dead zone thickness and cured thickness, a simple relationship between print speed, h_A (i.e., resolution) and $\Phi_0\alpha_{PI}$ /D_{e0} is derived:

$$\frac{Speed}{h_A} \propto \frac{\Phi 0 \alpha PI}{De0} \quad (3)$$

Print speed for CLIP is limited by resin cure rates and viscosity and not by stepwise layer formation. For a given h_A, speed can be increased by increasing Φ_0 or α_{PI} or by using a resin with lower D_{e0}. Dead zone thickness decreases as speed increases and will become too thin for the production to be stable. For CLIP, the empirically determined minimum thickness is 20 to 30 μm. Dead zone thickness below this may lead to window adhesion related defects. Once the minimum dead zone thickness is reached, the speed of production can be increased only by increasing the h_A value of the resin [57].

Comparison of CLIP with other AM techniques can be understood from the table II [58-65].

A. Researches Undergone in the Area of Continuous Liquid Interface Production

In 2014, Joseph M DeSimone et al. [57] introduced a new additive manufacturing technology where traditional layer by layer manufacturing is replaced by continuous generation of polymeric parts with feature resolution below 100 micrometers. Dead zone created using oxygen permeable window is the key for the continuous production. Several control parameters affecting the speed of production is studied. This work shows that complex geometries can be drawn out of the resin pool at rates of hundreds of millimeters per hour which can be improved further by proper investigation.

Rima Januszlewicza et al. investigated the mechanical properties of CLIP fabricated parts using the optimized printing parameters to explore bulk properties as a function of slice thickness and build orientation [66]. These parts have im- proved surface finish without sacrificing build time as well as isotropic mechanical properties enabling fabrication of large overhangs, as in the case of the open book

TABLE II
COMPARISON OF CLIP AND OTHER AM TECHNIQUES

CLIP	OTHER AM TECHNIQUES
Speed is 25-100 times faster	Slower than CLIP
Continuous Production	Layer by layer
High quality products	Low quality products
Fabrication of overhangs without support	Needs support
Dead zone is maintained	No dead zone is created
Photopolymerization with controlled oxygen inhibition	SLA uses photopolymerization but considers oxygen as an enemy
Less stair-casing effect	More stair-casing effect
Not suitable for metal manufacturing	SLS, DED can be used for metal manufacturing

benchmark. The ability to additively manufacture parts that are layerless and monolithic using CLIP is a key step for AM to move out of the realm of rapid prototyping and into manufacturing.

Ashley R Johnson et al. [67] demonstrated the ability to use CLIP to rapidly generate microneedles of any geometry and composition in 2016. The work showed that CLIP is the fastest and most versatile microneedle prototyping scheme to date. These microneedles can puncture skin painlessly and can enable transdermal delivery of medica- tions that are difficult using traditional ones. Materials like polyacrylic acid, trimethy- lolpropane triacrylate, polycaprolactone etc. were used to manufacture microneedles which took only less than 10 minutes per patch.

In 2017, Judah Balli et al. conducted a study to learn the challenges and oppor- tunities of the new technology CLIP developed by Carbon3D. They address various materials that can be used to produce parts required like RPU, FPU, EPU, CE, UMA, EPX etc. Their properties are also been investigated. Obviously its speed is the biggest opportunity. The challenges stated are build envelope and pot life of resins [68].

Prathmesh Chopade [56] studied the advancements in the additive manufacturing area and comparison between various technologies is done. The new technology CLIP proves to be best among all in terms of time and mechanical properties. Various applications of this technology is also explored.

Andrew T Miller et al. studied the deformation and fatigue of tough 3D printed elastomer scaffolds processed by fused de- position modeling and continuous liquid interface production. They examined the effects of architecture on the mechanical behavior of elastomeric polyurethanes. Comparison of two AM techniques namely FDM and CLIP based on structure property relationship is done. Architecture had an impact on the tensile fatigue of the solids produced via different AM techniques. Elastomeric PU's found to be tolerant of architectures and notches. Limitation of the work includes one type of cross hatch orientation and limited number of architectures and notches [69].

In 2018, Dilan Ezgi Duzgun & Krzysztof Nadolny [70] explained the use of CLIP in rapid prototyping and comparison of SLA and CLIP is shown. Surface comparison with CLIP and other AM techniques is done. Surface topology of the parts produced via CLIP seemed to be far better when compared to other AM processes. Reduction of stair-casing effect is observed which is otherwise seen in layer by layer approach. Experiments are done by varying the slicing thickness and surface topology is studied.

The study done by Davis J McGregor et al. [71] in 2018 presents design, production and mechanical property testing of hexagonal lattice parts made using CLIP. They tested 84 parts over four different designs and in three polymer materials. The parts had relative density ranging from 0.06 to 0.23 and feature sizes as small as 0.35 mm. Experiment revealed that wall lengths deviate from design target by up to 3% and wall thickness by up to 9%. Compression testing allowed measurement of part modulus and strength which was close to desired value. This is the largest study on the accuracy and performance of AM lattice parts and the first made using CLIP. Wenxiong Lin et al. investigated the use of track etched membrane (TEM) as oxygen permeable window and showed that it will enhance continuous liquid interface production. TEMs were made from polyethylene terephthalate by irradiat- ing with accelerated heavy ions. CLIP process is demonstrated with printing speed of 800 mm/hr in pure oxygen which matches with the theoretically predicted maximum printing speed. Maximum printing speed of 470 mm/hr is obtained even using air. Oxygen permeability of the fabricated PET TEM is one order of magnitude larger than Teflon AF 2400 films [72].

Continuous researches are being done in the volumetric ad- ditive manufacturing technology area developing new methods for producing parts continuously rather than layer by layer conventional technique. This will help in rapid development of end use products with prescribed properties. Materials that can be used should be explored and improved for industrial applications.

IV. Applications

The developments in the area of additive manufacturing has led to broader applications. AM is suitable for production of low volume and high complex geometry products. But the latest technology CLIP can be used for high volume production also as its speed is much faster than conventional AM techniques and it takes only few minutes for production. The mechanical properties of the products are also improved due to continuous production and can be utilized for end use products development. Major applications of AM include:

1) Aerospace: Aerospace components have complex geometries which are difficult to manufacture using subtractive machining process. They also use advanced materials for the products. So AM technology is best suited for its production. Fabrication of complex components for satellites, helicopters and jet engines was done using AM [73-78]. AM techniques are also used to repair aircraft engine parts such as compressors, turbine and combustor castings, blades etc. [79-85]. Another aerospace application is the building of wind tunnel testing models for aircraft, missiles, airfoils etc. [86]
2) Automobile: Product development according to the market needs is a must to survive in automotive sector. AM technology helps in developing components of new products in short time and low cost. AM processes have been used to make small quantities of structural and functional parts such as engine exhausts, gear box components, drive shafts and breaking systems. These use high complex structures which are otherwise difficult to manufacture. Manufactoring functional components for racing cars is another application [87-92]. Engine parts were made using lattice structures to reduce weight and improve mechanical properties [93,94].
3) Biomedical: Researches in the area of AM as well as in biomaterials have improved the application of AM in medical field. Customized product delivery is possible with the help of additive manufacturing. Orthopedic implants, complex tissue scaffolds, artificial organs, medical devices, biologic chips etc. are the major applications [95-101].

The potential applications of the technology CLIP is not yet explored as it is a recent development. Although metal manufacturing is not possible via CLIP, it has a wide range of applications due to its speed and improved mechanical properties. Medical sector can be improved as CLIP is capable of printing customized implants in few minutes. A recent application of CLIP is the announcement of alphaedge4D shoes for athletes by Adidas. This is the first shoe to come with Adidas' new 4D midsole. Adidas claims that the new 4D midsole is designed to deliver the most intuitive energy return on running shoes [102-104]. In addition, it also adds breathable cushioning for runners. More applications can be developed out of this new technology for its continuous production.

V. Conclusions

The various types of additive manufacturing techniques are discussed in detail starting from layer by layer Stereolithographic process to Continuous Liquid Interface Production. The use of AM techniques are discussed and its applications in aerospace, automotive, biomedical etc. are explored. Although advantages and limitations of each type is explained, AM techniques can be mainly divided into layer by layer manufacturing and volumetric manufacturing. CLIP uses light and oxygen in a controlled manner to create parts continuously out of the resin pool. This process have improved the surface finish without sacrificing build time and mechanical properties. There are two broad categories of the materials available from Carbon3D, prototyping resins, and engineering resins. While the prototyping resin is used for the cosmetic models and the engineering resins are used for the practical applications. This review on AM technologies show that CLIP is superior to conventional AM processes available. There are numerous challenges in this new technology. The scope of research in the area of Continuous Liquid Interface Production is very high as it is the latest technology and has the capacity to produce objects continuously. Volumetric additive manufacturing techniques are gaining importance and novel methods are developed recently namely tomographic reconstruction and dual wavelength volumetric polymerization. Size of build envelope, limitation of using only one resin, metal manufacturing etc. are the major challenges that needs to be resolved. But undoubtedly it can be said that technology developments and researches in the Additive Manufacturing area are in the right pace for creating a brighter future.

References

[1] M. Upadhyay, T. Sivarupan, and M. E. Mansori, "3D printing for rapid sand casting—A review," Journal of Manufacturing Processes, vol. 29, pp. 211–220, 2017.

[2] P. Konarzicki, "A Review of Fused Deposition Modeling Process Models," in 1st Renewable Energy Sources-Research and Business. Wroclaw, Poland: Springer, pp. 241-247, 2016.

[3] Ford et al., "Additive manufacturing and sustainability: an exploratory study of the advantages and challenges," Journal of Cleaner Production, vol. 137, pp. 1573–1587, 2016.

[4] "F2792-10 standard terminology for additive manufacturing technologies," ASTM. ASTM.

[5] O. A. Mohamed, S. H. Masood, and J. L. Bhowmik, "Optimization of fused deposition modeling process parameters: a review of current research and future prospects," Advances in Manufacturing, vol. 3, no. 1, 2015.

[6] C. C. Kai, L. K. Fai, and L. Chu-Sing, "Rapid prototyping: principles and applications in manufacturing," World Scientific Publishing Co., Inc, 2003.

[7] Zhai et al., "Additive manufacturing: making imagination the major limitation," Jom, vol. 66, no. 5, pp. 808–816, 2014.

[8] S. H. Masood, "Advances in fused deposition modeling," Swinburne University of Technology, 2014.

[9] K. V. Wong and A. Hernandez, A review of additive manufacturing. ISRN Mechanical Engineering, 2012.

[10] Kruth et al., "Progress in additive manufacturing and rapid prototyping," Cirp Annals, vol. 47, no. 2, pp. 525–540, 1998.

[11] P. F. Jacobs, "Rapid prototyping & manufacturing: fundamentals of stereolithography," Society of Manufacturing Engineers, 1992.

[12] O. A. Mohamed, S. H. Masood, and J. L. Bhowmik, "Optimization of fused deposition modeling process parameters: a review of current research and future prospects," vol. 3, no. 1, 2015.

[13] Gibson et al., "Material properties and fabrication parameters in selective laser sintering process," Rapid prototyping journal, pp. 129–136, 1997.

[14] Park et al., "Characterization of the laminated object manufacturing (LOM) process," Rapid Prototyping Journal, vol. 6, no. 1,

pp. 56–50, 2000.

[15] Thompson et al., "An overview of Direct Laser Deposition for additive manufacturing; Part I: Transport phenomena, modeling and diagnostics," Additive Manufacturing, vol. 8, pp. 36–62, 2015.

[16] Chen et al., "Process parameters optimization for improving surface quality and manufacturing accuracy of binder jetting additive manufacturing process," Rapid Prototyping Journal, vol. 22, no. 5, pp. 527–538, 2016.

[17] Nithin Sajan et al., "An investigation on circularity error of components processed on Fused Deposition Modeling," Materials Today: Proceedings, vol. 5, 2018, pp. 1327–1334.

[18] Habibur Rahamn et al., "Investigation on the Scale Factor applicable to ABS based FDM Additive Manufacturing," Materials Today: Proceedings, vol. 5, 1640-1648, 2018.

[19] K. Chockalingam, N. Jawahar, K. N. Ramanathan, and P. Banerjee, "Optimization of stereolithography process parameters for part strength using design of experiments," The International Journal of Advanced Manufacturing Technology, vol. 29, no. 1, pp. 2–79, 2006.

[20] Bartolo P. J., "Stereolithography: materials, processes and applications," Springer Science & Business Media, 2011.

[21] F. P. Melchels, J. Feijen, and D. W. Grijpma, "A review on stereolithography and its applications in biomedical engineering," Biomaterials, vol. 31, no. 24, pp. 6121–6130, 2010.

[22] C. Zhou, H. Ye, and F. Zhang, "A novel low-cost stereolithography process based on vector scanning and mask projection for high- accuracy, high-speed, high- throughput, and large-area fabrication," Journal of Computing and Information Science in Engineering, vol. 15, no. 1, p. 011003, 2015.

[23] Chartrain et al., "A review on fabricating tissue scaffolds using vat photopolymerization," Acta biomaterialia, 2018.

[24] Feygin et al., "Laminated object manufacturing (LOM): a simpler process," International Solid Freeform Fabrication Symposium 1991.

[25] Park et al., "Characterization of the laminated object manufacturing (LOM) process," Rapid Prototyping Journal, vol. 6, no. 1, pp. 36–50, 2000.

[26] Weisensel et al., "Laminated object manufacturing (LOM) of SiSiC composites," Advanced Engineering Materials, vol. 6, no. 11, 899-03, 2004.

[27] Paul B.K. et al., "Effect of layer thickness and orientation angle on surface roughness in laminated object manufacturing," Journal of manufacturing processes, pp. 94–101, 2001.

[28] J. J. Beaman, J. W. Barlow, D. L. Bourell, R. H. Crawford, H. L. Marcus, and K. P. McAlea, "Solid freeform fabrication: a new direction in manufacturing.", Eds. Norwell, MA: Kluwer Academic Publishers, 1997, pp. 25–49.

[29] Fischer et al., "Highly precise pulsed selective laser sintering of metallic powders," Laser Physics Letters, vol. 2, no. 1, p. 48, 2004.

[30] Antonov et al., "Fabrication of polymer scaffolds for tissue engineering using surface selective laser sintering," Laser Physics, vol. 16, no. 5, pp. 774–787, 2006.

[31] Y. L. Yap, C. Wang, S. L. Sing, V. Dikshit, W. Y. Yeong, and J. Wei, "Material jetting additive manufacturing: an experimental study using designed metrological benchmarks," Precision, vol. 50, pp. 275–285, 2017.

[32] Lee et al., "Fundamentals and applications of 3D printing for novel materials," Applied Materials Today, vol. 7, pp. 120–133, 2017.

[33] S. Meteyer, X. Xu, N. Perry, and Y. F. Zhao, "Energy and material flow analysis of binder-jetting additive manufacturing processes," Procedia CIRP 2014, vol. 15.

[34] Bai Y et al., "Binder jetting additive manufacturing with a particle-free metal ink as a binder precursor," Materials & Design, vol. 147, pp. 146–156, 2018.

[35] Heigel et al., "Thermo-mechanical model development and validation of directed energy deposition additive manufacturing of Ti–6Al–4V," Additive manufacturing, vol. 5, pp. 9–19, 2015.

[36] Heigel et al., "Measurement of forced surface convection in directed energy deposition additive manufacturing," Journal of Engineering Manufacture vol. 230, 2016, pp. 1295–1308.

[37] Mitchell et al., "Additive manufacturing-A review of 4D printing and future applications," Additive Manufacturing, 2018.

[38] Allen Brady et al., "Stereolithography of ceramic suspensions," Rapid Prototyping Journal, vol. 3, no. 2, pp. 61–65, 1997.

[39] Griffith et al., "Freeform fabrication of ceramics via stereolithography," Journal of the American Ceramic Society, vol. 79, no. 10, pp. 2601–2608, 1996.

[40] Tan K. H et al., "Selective laser sintering of biocompatible polymers for applications in tissue engineering," Bio-medical materials and engineering, pp. 113– 124, 2005.

[41] C. K. Chua, K. F. Leong, and C. S. Lim, "Rapid prototyping: principles and applications (with companion CD-ROM)," World Scientific Publishing Company, 2010.

[42] A. Bellini and S. Güçeri, "Mechanical characterization of parts fabricated using fused deposition modeling," Rapid Prototyping Journal, vol. 9, no. 4, pp. 252–264, 2003.

[43] Hutmacher et al., "Mechanical properties and cell cultural response of polycaprolactone scaffolds designed and fabricated via fused deposition modeling," Journal of Biomedical Materials Research: An Official Journal of The Society for Biomaterials, The Japanese Society for Biomaterials, and The Australian Society for Biomaterials and the Korean Society for Biomaterials, vol. 55, no. 2, pp. 203–216, 2001.

[44] Campbell et al., "Additive manufacturing: rapid prototyping comes of age," Rapid prototyping journal, vol. 18, no. 4, pp. 255–258, 2012.

[45] Bellini et al., "New developments in fused deposition modeling of ceramics," Rapid Prototyping Journal, vol. 11, no. 4, pp. 214–220, 2005.

[46] Phan et al., "Selective laser sintering: applications and technological capabilities," Proceedings of the Institution of Mechanical Engineers, Part B: Journal of Engineering Manufacture, vol. 213, 1999, pp. 435–449.

[47] Murr et al., "Characterization of titanium aluminide alloy components fabricated by additive manufacturing using electron beam melting," Acta materialia, vol. 58, no. 5, pp. 1887–1894, 2010.

[48] Hofmeister and Griffith, "Solidification in direct metal deposition by LENS processing," Jom, vol. 53, no. 9, pp. 30–34, 2001.

[49] Dimitrov et al., "Advances in three dimensional printing–state of the art and future perspectives," Rapid Prototyping Journal, vol. 12, no. 3, pp. 136–147, 2006.

[50] Kruth et al., "Consolidation phenomena in laser and powder-bed based layered manufacturing," CIRP annals, vol. 56, no. 2, pp. 730–759, 2007.

[51] J. Park, M. J. Tari, and H. T. Hahn, "Characterization of the laminated object manufacturing (LOM) process," Rapid Prototyping Journal, vol. 6, no. 1, pp. 36–50, 2000.

[52] Y. Bai and C. B. Williams, "An exploration of binder jetting of copper," Rapid Prototyping Journal, vol. 21, no. 2, pp. 177–185, 2015.

[53] M. Shishkin, T. Didier, G. K. Lau, and A. J. Qureshi, "Fast deviation simulation for fused deposition modeling process," Procedia CIRP, vol. 43, 2016.

[54] Zhang Y et al., "3D FEA simulations of fused deposition modeling process," in ASME 2006 International Manufacturing Science and Engineering Conference, pp. 1121–1128.

[55] Y. M. Huang, J. Mazumder, and A. Donmez, "Additive Manufacturing: Current State, Future Potential, Gaps and Needs, and Recommendations," ASME J. of Manufacturing Sci. and Eng, vol. 137, no. 1, p. 014001, 2015.

[56] Prathamesh Chopade, "Advancements in Additive Manufacturing – CLIP, SLS and 3D printing Technology," International Journal for Engineering Applications and Technology, ISSN 2321.

[57] J. R. Tumbleston, D. Shirvanyants et al., "Continuous liquid interface production of 3D objects," Science, vol. 347, no. 6228, pp. 1349–1352, 2015.

[58] L. Chumier, S. Guessasma, S. Belhabib, G. D. Valle, and

Leandin, D., & Leroy R., "Material extrusion of plant biopolymers: opportunities & challenges for 3D printing," Additive Manufacturing, vol. 21., 2017.

[59] K. J. Hodder, J. A. Nychka, and R. J. Chalaturnyk, Process limitations of 3D printing model rock, 2018, vol. 3, no. 3.

[60] G. A. Adam and D. Zimmer, "On design for additive manufacturing: evaluating geometrical limitations.," Rapid Prototyping Journal, vol. 21, no. 6, pp. 662–670, 2015.

[61] T. D. Ngo, A. Kashani, G. Imbalzano, K. T. Nguyen, and D. Hui, "Additive manufacturing (3D printing): A review of materials, methods, applications and challenges," Composites Part B: Engineering, vol. 143, pp. 172–196, 2018.

[62] Y. Rao, R. Miren, and S. Reckinger, "Limitations of additive manufacturing on microfluidic heat exchanger components," Journal of Manufacturing Science and Engineering, vol. 137, no. 3, p. 034504, 2015.

[63] D. L. Bourell, T. J. Watt, D. K. Leigh, and B. Fulcher, "Performance limitations in polymer laser sintering," Physics Procedia, vol. 56, pp. 147–156, 2014.

[64] S. E. Zeltmann, N. Gupta, N. G. Tsoutsos, M. Maniatakos, J. Rajendran, and R. Karri, "Manufacturing and security challenges in 3D printing," Jom, vol. 68, no. 7, pp. 1872–1881, 2016.

[65] K. P. Cooper, "Layered manufacturing: challenges and opportunities," MRS Online Proceedings Library Archive, 2002.

[66] Janusziewicz et al., "Layerless fabrication with continuous liquid interface production," Proceedings of the National Academy of Sciences, vol. 113, pp. 11 703–11 708, 2016.

[67] Johnson et al., "Single-step fabrication of computationally designed microneedles by continuous liquid interface production," PLoS One, vol. 11, no. 9, p. 0162518, 2016.

[68] J. Batal, S. Kumpaty, and V. Aneventer, "Continuous Liquid Interface Production of 3D Objects: An Unconventional Technology and its Challenges and Opportunities," American Society of Mechanical Engineers, 2017.

[69] A. T. Miller, D. L. Safranski, C. Wood, R. B. Guldberg, and K. Gall, "Deformation and fatigue of tough 3D printed elastomer scaffolds processed by fused deposition modeling and continuous liquid interface production," Journal of the mechanical behavior of biomedical materials, pp. 1–13, 2017.

[70] D. E. Ditzgha and K. Nadolny, "Continuous liquid interface production (CLIP) method for rapid prototyping," Journal of Mechanical and Energy Engineering, vol. 2, no. 1, pp. 5–12, 2018.

[71] D. J. McGregor, S. Tawfick, and W. P. King, "Mechanical properties of hexagonal lattice structures fabricated using continuous liquid interface production additive manufacturing," Additive Manufacturing, vol. 25, pp. 10–18, 2019.

[72] W. Lin, H. Liu, H. Huang, J. Huang, K. Ruan, Z. Lin, and Y. Ge, "Enhanced continuous liquid interface production with track-etched membrane," Rapid Prototyping Journal, vol. 25, no. 1, pp. 117–125, 2019.

[73] A. A. Antonysamy, "Microstructure, texture and mechanical property evolution during additive manufacturing of Ti6Al4V alloy for aerospace applications," Doctoral dissertation, The University of Manchester, 2012.

[74] S. C. Joshi and A. A. Sheikh, "3D printing in aerospace and its long- term sustainability," Virtual and Physical Prototyping, vol. 10, no. 4, pp. 175–185, 2015.

[75] L. Nickels, "AM and aerospace: an ideal combination," Metal Powder Report, vol. 70, no. 6, pp. 300–303, 2015.

[76] R. Liu, Z. Wang, T. Sparks, F. Liou, and J. Newkirk, "Aerospace applications of laser additive manufacturing. Woodhead Publishing, 2017.

[77] V. K. Vashishtha, R. Makade, and N. Mehla, "Advancement of rapid prototyping in aerospace industry-a review," International Journal of Engineering Science and Technology, vol. 3, no. 3, pp. 2486–2493, 2011.

[78] L. J. Kumar and C. K. Nair, "Current trends of additive manufacturing in the aerospace industry," Singapore: Springer, 2017.

[79] R. P. Mudge and N. R. Wald, "Laser engineered net shaping advances additive manufacturing and repair," WELDING JOURNAL-NEW YORK-, vol. 86, no. 1, p. 44, 2007.

[80] M. Hedges and N. Calder, "Near net shape rapid manufacture and repair by LENS," Rapid Prototyping, 12(4), 1, 2006.

[81] J. M. Wilson, C. Piya, Y. C. Shin, F. Zhao, and K. Ramani, "Remanufacturing of turbine blades by laser direct deposition with its energy and environmental impact analysis," Journal of Cleaner Production, vol. 80, pp. 170–178, 2014.

[82] K. H. Richter, S. Orban, and S. Nowotny, "Laser cladding of the titanium alloy Ti6242 to restore damaged blades," International Congress on Applications of Lasers & Electro-optics, Vol.1396, No. 1, 2004.

[83] L. Ren, A. P. Padalia, J. Ruan, T. Sparks, and F. W. Liou, "Three dimensional die repair using a hybrid manufacturing system," 2008.

[84] G. Bi and A. Gasser, "Restoration of nickel-base turbine blade knife- edges with controlled laser aided additive manufacturing," Physics Procedia, vol. 12, pp. 402–409, 2011.

[85] A. Gasser, G. Backes, I. Kelbassa, A. Weisheit, and K. Wissenbach, "Laser Additive Manufacturing: Laser Metal Deposition (LMD) and Selective Laser Melting (SLM) in Turbo-Engine Applications," Laser Technik Journal, vol. 7, no. 2, pp. 58–63, 2010.

[86] S. Dansheasand, R. Adelnia, and S. Aghanajafi, "Design and production of wind tunnel testing models with selective laser sintering technology using glass- reinforced Nylon," Trans Tech Publications, vol. 532, 2006.

[87] T. Vilaro, S. Abed, and W. Kaupp, "Direct manufacturing of technical parts using selective laser melting: example of automotive application," Proceedings of 12th European Forum on Rapid Prototyping, 2008.

[88] G. Tromans, "Automotive applications. Rapid manufacturing: an industrial revolution for the digital age," John Wiley & Sons, 2006.

[89] Snelling D et al., "Lightweight metal cellular structures fabricated via 3D printing of sand cast molds," Advanced Engineering Materials, vol. 17, no. 7, pp. 923–932, 2015.

[90] Prakash K S et al., "Additive Manufacturing Techniques in Manufacturing- An Overview," Materials Today: proceedings Vol. 5, 3873-3882, 2018.

[91] I. Campbell, D. Bourell, and I. Gibson, "Additive manufacturing: rapid prototyping comes of age," Rapid Prototyping Journal, vol. 18, no. 4, pp. 255–258, 2012.

[92] V. Juechter, M. M. Franke, T. Merenda, A. Stich, C. Körner, and R. F. Singer, "Additive manufacturing of Ti-45Al-4Nb-C by selective electron beam melting for automotive applications," Additive Manufacturing, vol. 22, pp. 118–126, 2018.

[93] S. K. Moon, Y. E. Tan, J. Hwang, and Y. J. Yoon, "Application of 3D printing technology for designing light-weight unmanned aerial vehicle wing structures," International Journal of Precision Engineering and Manufacturing-Green Technology, vol. 1, no. 3, pp. 223–228, 2014.

[94] B. P. Conner, G. P. Manogharan, A. N. Martof, L. M. Rodomsky, and Rodomsky C. M., D. C. Jordan, and J. W. Limperos, "Making sense of 3- D printing: Creating a map of additive manufacturing products and services," Additive Manufacturing, vol. 1, no. 64, p. 76, 2014.

[95] S. Bose, S. Vahabzadeh, and A. Bandyopadhyay, "Bone tissue engineering using 3D printing," Materials today, vol. 16, no. 12, pp. 496–504, 2013.

[96] F. P. Melchels, J. Feijen, and D. W. Grijpma, "A review on stereolithography and its applications in biomedical engineering," Biomaterials, vol. 31, no. 24, pp. 6121–6130, 2010.

[97] H. N. Chia and B. M. Wu, "Recent advances in 3D printing of biomaterials," Journal of biological, vol. 9, no. 1, p. 4, 2015.

[98] F. P. Melchels, M. A. Domingos, T. J. Klein, J. Malda, P. J. Bartolo, and D. W. Hutmacher, "Additive manufacturing of tissues and organs," Progress in polymer science, vol. 37, no. 8, 1079-1104, 2012.

[99] S. L. Sing, J. An, W. Y. Yeong, and F. E. Wiria, "Laser and electron beam powder-bed additive manufacturing of metallic implants: A review on processes, materials and designs," Journal of Orthopaedic

Research, vol. 34, no. 3, pp. 369–385, 2016.

[100] Murr L E et al., "Next generation orthopaedic implants by additive manufacturing using electron beam melting," International journal of biomaterials," 2012.

[101] S. Sumedhya, N. Vij, P. Chaturvedi, S. Tiwari, B. Arora, and Y. K. Modi, "Medical applications of additive manufacturing," International Journal of Scientific Progress and Research, vol. 12, no. 1, pp. 11–17, 2015.

[102] Sun H, "Researches on Application Fields of 3D Printing Technology in Product Design and Production," 3rd International Conference on Arts, Design and Contemporary Education, Atlantis Press, 5 2017.

[103] [Online]. Available: https://www.adidas.com.sg/ultraedge-4d-shoes/ AQ0742.html

[104] C. J. . Mahoney, U.S. Patent Application, vol. 29, no. 604, 2018.

Ribin Varghese Pazhanavanil, Research Scholar, Government College of Engineering Kannur

Dr. Govindan P, Assistant Professor, Government College of Engineering Kannur

Appraisal of metallurgical and mechanical properties of polyamide 12 reinforced with *x* wt% of glass fiber by FDM process

R.Soundararajan[a*], J.Jayasuryaa[b], T.Mithulpranav[b], R.Jayasurya[b],

[a] Associate Professor, Department of Mechanical Engg, Sri Krishna college of Engg and Tech, Coimbatore, India.*
[b] UG Student, Department of Mechanical Engineering, Sri Krishna college of Engg & Tech, Coimbatore, India

*Corresponding author E-Mail ID: soundararajan.mtech@gmail.com, Mobile: 9894534879

ABSTRACT

The primary objective of this examination is to build up an arrangement of new polyamide blends with inventive properties. The composite blends of polyamide 12 (PA12) reinforced with 10, 20 and 30 wt% of glass fiber (GF) were prepared and delivered in a form of wire in a filament extruder machine and taken for the further process. Standard Tensile strength specimens were created by melting and compounding techniques, and they were smoothly printed by means of a commercial processing method of fused deposition model (FDM) by three dimensional (3D) printer. The printed sample outcome indicates that incorporation of filler stacking with equally distributed particles and higher weight percentage (30 wt%) of glass fiber has influenced in higher mechanical properties of virgin PA12 and lower weight percentage (10 wt% and 20 wt%) gives moderate mechanical properties for the same. These composites were found to perform well with FDM method as it lays the groundwork for the next stages of progression in automobile applications.

Keywords: Polyamide 6, Glass fiber, FDM, SEM analysis, Mechanical properties.

1. INTRODUCTION

Additive Manufacturing (AM) technologies have turned into a new standard in design because of product geometric, creation and customization conceivable outcomes. It is yet another imaginative progress rolled out possible by the improvement from simple to advanced structures. Additive manufacturing utilizes information from 3D object scanners that is later converted to a stereolithography (STL) file or the drawing made in the CAD software is approximated by triangles and sliced containing the information of each layer that will be printed [1]. There are various types of AM processes which are available in the market for Industrial Needs. They are classified into binder jetting, material jetting, direct energy deposition, sheet laminations, material extrusion, powder bed fusion, and vat polymerization [2-3]. Those innovations have been developing quickly, changing the application potential outcomes and abilities as far as time, quality, plan and execution [4]. AM make it feasible to construct a substantial scope of models or practical segments with complex geometries those can't or difficult to made by ordinary techniques. [5-6]. Among the various rapid prototyping techniques, including Stereo lithography (SLA), Selective Laser Sintering (SLS) [7], Laminated Object Manufacturing (LOM) [8], the Fused Deposition Modeling (FDM) [9] technique is the trendiest one, although

already existing last three decades. Right now, FDM is the method, demonstrating the higher potential for product fabrication, with the capacity to contend with ordinary polymer processing methods [10]. The computer model is sliced into layers, and the information from the model is used to build a part by using continuous filament feedstock which will be enabled by FDM with remote manufacturing capabilities [11-12]. The applications of polymer composites for different engineering components are gaining popularity in the industries. These polymer composites are reasonable swap for traditional materials because of high strength and stiffness. In order to enhance the mechanical properties, different thermoplastic polymer blends can be reinforced by different types of fibrous material [13]. The polyamide 12 (PA12/Nylon12) is extreme, having high rigidity, flexible and luster. They are wrinkle proof and highly resistant to abrasion and chemicals [14]. It is widely used, because of its excellent all-round properties, easy moulding and manufacturing. Traditionally PA12 is an exceptionally stable polymer and not promptly debased in the environmental condition. Thus, natural contamination from manufactured plastics has been perceived as a vast issue, to dodge this it has been reused [15]. In order to reduce the consumptions of the polymer, natural or synthetic fibers are incorporated in the matrix. The reinforcement of fibers in the matrix has increased the mechanical properties of 3D printed polymer composites parts [16]. Carbon fiber or glass fiber reinforced thermoplastic laminates in matrices such as polyetherimide (PEI), polyetheretherketone (PEEK) and polyphenylene sulphide (PPS) have already been used extensively in the aerospace sector due to their excellent mechanical properties, heat stability and low flammability [17]. In the recent decades, natural fibers as an alternative reinforcement in polymer composites have pulled in the consideration of numerous analysts and researchers because of their preferences over traditional glass and carbon fibers. [18]. Natural fibers may play an important role in developing biodegradable composites to resolve the current ecological, environmental problems but compared to natural fibers, glass fiber has improved the mechanical properties of the virgin polymer [19].

In light of the writing audit, it was inferred that incorporation of the fiber particles in the polyamide have lessened the volume of utilization of the polyamide and amazingly improved the mechanical properties of the virgin polyamide. Surprisingly only a few researches have concentrated on carrying out the experiments on mechanical properties of polymer composites filament processed through FDM. But there is no thorough study on the specified ones. Based on the detailed literature survey, after identifying the research gaps the following three different compositions of glass fiber percentage (10%, 20% and 30%) with PA12 on FDM process were prepared and the metallurgical and mechanical properties of these composition were appraised.

2. EXPERIMENTAL SETUP

2.1 Materials and methods

The PA12 is semi crystalline polyamide which is most ordinarily known as nylon 12 or polylaurolactam. PA12 filaments are extreme, shows high tensile properties, elongation and luster. PA12 has the density of 1.01 g/cm^3, melting point of range 178-180°C and it can protect heat upto150°C. PA12 having poor biodegradability to the environment that is the reason behind recycle of polymer. Glass fiber has generally tantamount mechanical properties compared to other fibers. It has density of 2.58 g/cm^3 and no true melting point but softens up to 1200 °C, where it starts to degrade. Despite the fact that not as rigid as carbon fiber, it is considerably less expensive and essentially less brittle when utilized in composites. For present study blend of different compositions of PA12 and GF in granules form has been selected as target material for investigation because of their all-round material properties and melt processing capabilities.

2.2 Extrusion of the material

The primary process before extrusion of material is to dry the material at 90°C for a minimum of 6 hours. This is done by placing the desired weight percentage of granulates into the "Heraeus Instruments" in warmed atmosphere. The preheated material is extruded using the 3Devo-NEXT Filament Extruder is shown in Fig 1, at extrusion temperature of 175°C, nozzle diameter of 1.75mm and length of 10m. The four set of experiments were carried out to extract the filaments such as virgin PA12, incorporation of 10%, 20% and 30% glass fiber with PA12 respectively.

2.3 Fused deposition modeling

Tensile test specimens of ISO 523-4/1B/5 has been modeled with the help of SolidWorks software and saved as ". stl" format. This file is then imported into "slic3r" and the G-codes are generated. The generated G-codes are uploaded to the kühling and kühling HT500.2-3D printer is shown in Fig 2. Four different combination of prepared filament are feed into the 3D printer in order to produce the tensile specimens at extrusion temperature 215°C, fill angle 45°, bed temperature of 60°C, and layer height of 0.3mm and filament diameter of 1.75mm. The printed specimens were taken for testing.

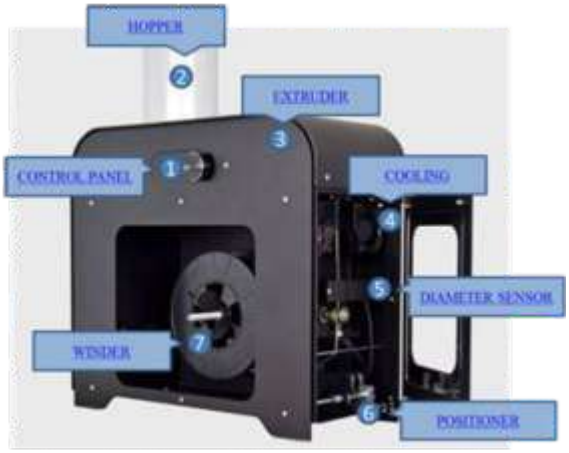

Fig 1. Filament Extruder

Fig 2. 3D Printer (FDM)

2.4 Testing of the specimen

The tensile properties of the 3D printed specimens were tested according to ISO 523-4/1B/5 standard in Instron 5584 universal testing machine (Fig 3). The specimens were loaded with a speed of 5 mm/min. The important parameters such as maximum load, elongation at break were noted for pure polymer and three different compositions of polymer and glass fiber. The tested specimens are shown in Fig 4. With the help of these values tensile strength, elongation at break and Young's modulus has been calculated for the same and shown in table 1. To ensure the fibers distribution in the matrix SEM analysis (Philips XL 30ESEM) was taken a portion of the same specimen.

Fig 3.Instron 5584 universal testing machine

Fig 4. Tensile tested specimens

Table 1. Measurement of mechanical properties of PA 12 with Glass Fibers

Samples/Responses	Tensile strength (MPa)	Elongation at break (%)	Young's modulus (MPa)
PA 12	23.37	20.8	1385
PA 12+10wt%GF	28.04	10.1	2056
PA 12+20wt%GF	36.03	6.3	2948
PA 12+30wt%GF	40.56	4.7	4026

3. RESULT AND DISCUSSION

3.1 SEM analysis

The micrography of the sample PA12 with10 wt%GF, PA12 with 20 wt%GF and PA12 with 30 wt%GF was taken by using SEM analyzer for the 100x magnifications were shown in the Fig 5(a-c). From SEM analysis, it is inferred that glass fiber were present and uniformly dispersed over the polymer matrix of all three compositions because of composites filament were prepared through extruder and it was printed by FDM machine under optimal parametric condition. Fig 5(a-b) reveals that wide and average distribution of glass fiber content in the polymer matrix due to lower weight percentage addition of (10wt% and 20wt%) reinforcement respectively. Fig 5(c) depicts that high dense and homogeneous distribution of glass fiber content in the polymer matrix due to 30wt% reinforcement of glass fiber. The micrography of 30wt% glass fiber reinforced polymer reveals that more amount of particles were distributed over the polymer matrix, it results in improvement of strength. During this SEM observation absence of reinforcement argumentation was observed.

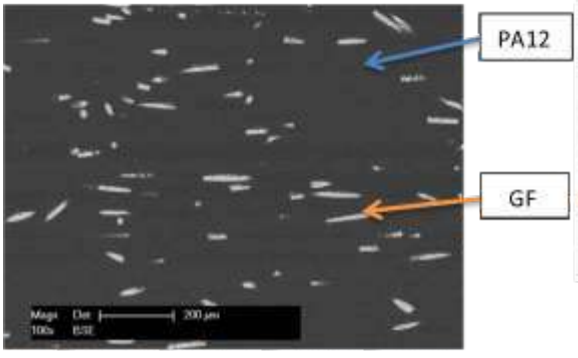

Fig 5(a). SEM for PA12 with10 wt%GF

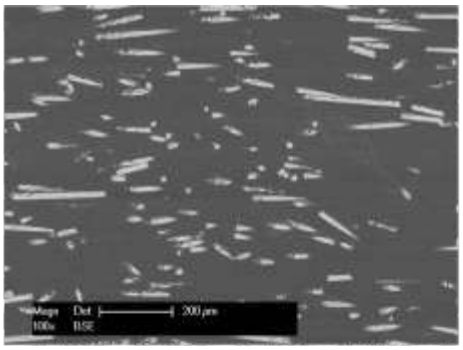

Fig 5(b). SEM for PA12 with 20 wt%GF

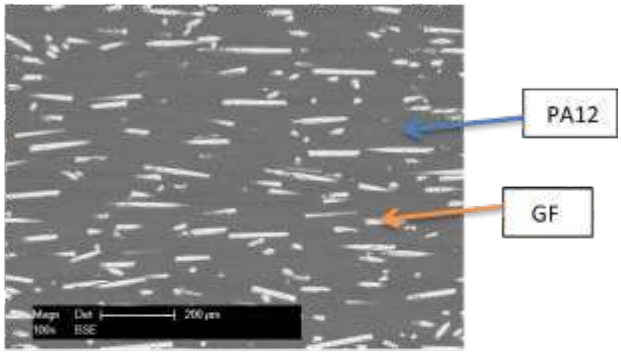

Fig 5(c). SEM for PA12 with 30 wt%GF

3.2 Tensile strength

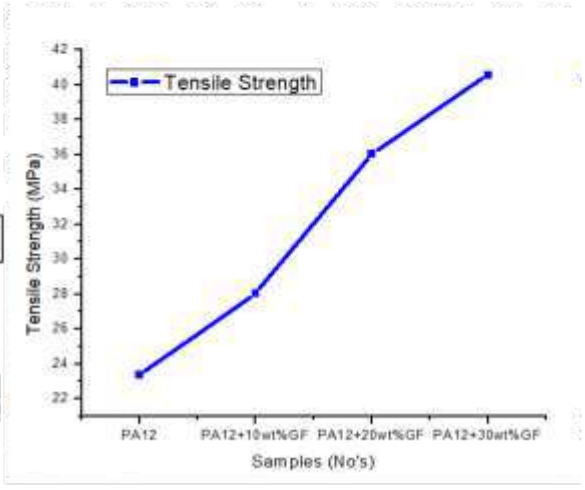

Fig 6. Tensile strength

The Tensile strength of various creations of glass fiber reinforced PA12 composites is appeared in Fig 6. It becomes evident that there is an improvement in tensile strength of virgin PA12 due to reinforcement addition. PA12 with 10%wt GF composite reveals an increased tensile strength of 28.04 MPa which is about 25% higher than that of flawless polymer blend. PA12 with 20%wt GF composite reveals an increased tensile strength of MPa which is about 45% greater than that of virgin polymer blend and PA12 with 30%wt GF composites has increased the tensile strength of 40.56 MPa which is about 80% higher than that of virgin polymer blend. Incorporation of GF with virgin polymer blend results in rapid improvement in tensile strength of the virgin polymer. Further incorporation of GF results in gradual improvement in tensile strength of neat polymer blend. This proves that different compositions of PA12-GF offers higher resistance to deformation because of reinforcement of glass fiber content, henceforth thus builds the stiffness of the PA12-GF composite under axial loading.

3.3 Percentage of elongation at break

The elongation at break of the different compositions of the PA12-GF blends demonstrates in Fig 7. Fracture strain is the ratio of changed length to the original length after breakage of the specimen. Virgin PA12 has the elongation up to 20.8% whereas PA12 with 10.1%wt GF has the elongation up to 10% which is about 50% less than that of pure PA12 blend.PA12 with 20%wt GF composite and PA12 with 30%wt GF has the elongation up to 6.3% and 4.7% respectively which is about 67% and 78% less than that of neat polymer blend. This indicates that incorporation of glass fiber with unadulterated polymer has reduced the elasticity of the pure polymer blend quickly. Further filler loading results in gradual decrease in the elasticity of the unadulterated polymer blend.

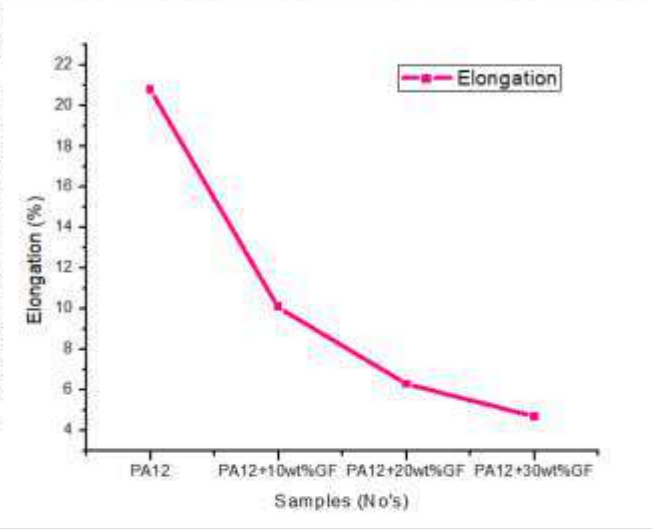

Fig 7. Elongation at break

3.4 Young's modulus

Young's modulus measures the stiffness of the solid material. It characterizes the connection amongst anxiety in a material in the direct versatility administration of a uniaxial deformation. Young's modulus has been calculated from obtained results and shown in Fig 6. As we discussed earlier, incorporation of glass fiber with pure PA12 blend improved the tensile strength of the pure polymer blend. Improvement in tensile strength influencing the Young's modulus of the PA12-GF composites. PA12 with 10%wt GF reveals an increased Young's modulus of 2056 MPa which is about 48% greater than that of virgin PA12. Similarly PA12 with 20%wt GF and PA12 with 30%wt GF composites has the Young's modulus of 2948

MPa and 4026 MPa respectively which is about 110% and 190% higher than that of neat polymer blend. Reinforcement of glass fiber with PA12 results in impulsive change of Young's modulus. Further filler loading has improved the Young's modulus of the polymer blend gradually.

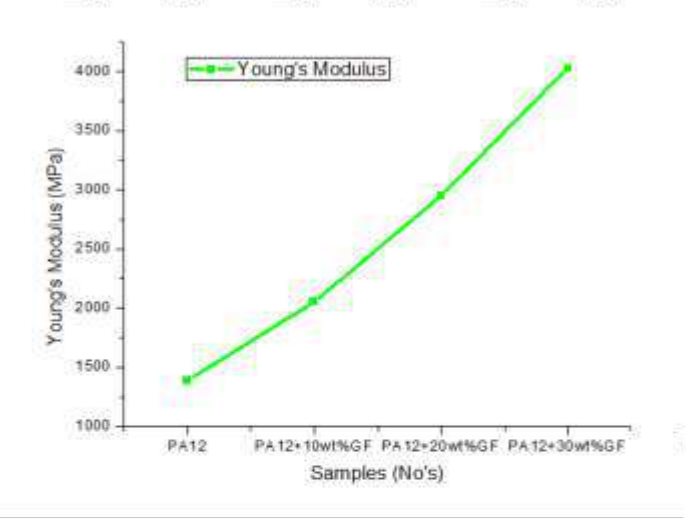

Fig 8. Young's modulus

4. CONCLUSION

It has been inferred from the present research, the printed specimen of glass fiber reinforcement polyamide matrix in FDM process has been contributed as follows.

1. Uniform distribution of the glass fiber in the polymer matrix in all the three combinations test samples of PA12 with 10wt%, 20wt% and 30wt% GF were observed in the FDM printed samples.
2. Higher properties were attained due to uniform distribution and 30wt% of GF in the matrix for printed samples.
3. After incorporation of 10wt% of glass fiber, tensile strength and Young's modulus of the polymer matrix were increased by 25% and 48% respectively. Whereas elongation is decreased by 50%.
4. Incorporation of 20wt% of glass fiber has increased the tensile strength and Young's modulus of the virgin polymer by 45% and 110% respectively. However elongation is reduced by 67%.
5. Reinforcement of 30wt% of glass fiber increased the tensile strength and Young's modulus of the pure polymer by 80% and 190% respectively. Though elongation is decreased by 78% of the neat polymer.
6. Incorporation of glass fiber in all three composition (10wt%, 20wt% and 30wt %) has positively affected the tensile strength of the pure polyamide.

Acknowledgement

On behalf of all team members of this research the corresponding author wishes to thank Mr.Sibi chakaravarthi, Former Project Member, Westphalian University of Applied Sciences and Sri Krishna College of Engineering and Technology for all support required to carry out this research.

Authors Contribution

Dr R.Soundararajan have put the idea of this work and edited the complete article. Mr.J.Jayasuryaa has appraised the results,

composed and free hand written the article. Mr.T.Mithulpranav and Mr.R.Jayasurya have conceived the experiment specimens for testing and summarized the responses.

REFERENCES

[1] Kaufui V.Wong and Aldo Hernandez, "A Review of Additive Manufacturing" Department of Mechanical and Aerospace Engineering, University of Miami, Coral Gables, FL 33146, USA

[2] F.Calignano, D.Manfredi, E.Ambrosio, S.Biamino, M.Lombardi, E.Atzeni, A.Salmi, P.Minetola, L.Iuliano, P.Fino, Overview on additive manufacturing technologies, Proc. IEEE 105 (2017) 593–612, http://dx.doi.org/10.1109/JPROC.2016.2625098.

[3] S.A.M.Tofail, E.P.Koumoulos, A.Bandyopadhyay, S.Bose, L.O'Donoghue, C.Charitidis, Additive manufacturing: scientific and technological challenges,market uptake and opportunities, Mater. Today 0 (2017) 1–16, http://dx.doi.org/10.1016/j.mattod.2017.07.001.

[4] G.W.Melenka, B.K.O.Cheung, J.S.Schofield, M.R.Dawson, J.P.Carey, Evaluation and prediction of the tensile properties of continuous fiber-reinforced 3D printed structures, Compos. Struct. 153 (2016) 866–875, http://dx.doi.org/10.1016/j.compstruct.2016.07.018.

[5] M.Alimardani, E.Toyserkani, JP.Huissoon. Three-dimensional numerical approach for geometrical prediction of multilayer laser solid freeform fabrication process. J Laser Appl 2007;19(1):14e25.

[6] A.Yakovlev, E.Trunova, D.Grevey, M.Pilloz, I.Smurov. Laser-assisted direct manufacturing of functionally graded 3D objects. Surf Coatings Technol2005;190(1):15e24.

[7] J.Kruth, P.Mercelis, J.Van Vaerenbergh, L.Froyen, M.Rombouts, Binding mechanisms in selective laser sintering and selective laser melting, Rapid Prototype. J. 11 (2005) 26–36.

[8] B.Mueller, D.Kochan, Laminated object manufacturing for rapid tooling and patternmaking in foundry industry, Comput. Ind. 39 (1999) 47–53.

[9] M.Too, K.Leong, C.Chua, Z.Du, S.F.Yang, C.M.Cheah, S.L.Ho, Investigation of 3D non-random porous structures by fused deposition modelling, Int. J. Adv.Manuf. Technol. 19 (2002) 217–223.

[10] J.Kruth, M.Leu, T.Nakagawa, Progress in additive manufacturing and rapid prototyping, CIRP Ann. Technol. 47 (1998) 525–540.

[11] S.S Crump, Manufacturing of new type curvilinear tooth profiled involute gears using 3D printing, U.S. Patent 5 121 329, 1992.

[12] W.A.Walters, In Solid Freeform Fabrication Symposium Proceedings, 1992; p 301.

[13] H.V.Divya, L.L.Naik and B.Yogesha 2016 Processing techniques of polymer

matrix composites –A review Int. J. Eng. Res. General Sci. 4 357-62

[14] M.Kawasumi, N.Hasegawa, M.Kato, A.Usuki, and A.Okada. (1997). Preparation and mechanical properties of polypropylene-clay hybrids. Macromolecules, 30(20), 6333-6338.

[15] Y.Zheng, E.K.Yanful, and A.S.Bassi,(2005).A review of plastic waste biodegradation. Critical Reviews in Biotechnology, 25(4), 243-250.

[16] D.Jiang, D.E.Smith, Anisotropic mechanical properties of oriented carbon fiberfilled polymer composites produced with fused filament fabrication, Addit. Manuf 18 (2017) 84–94, http://dx.doi.org/10.1016/j.addma.2017.08.006.

[17] J.Diaz, L.Rubio. Development to manufacture structural aeronautical parts in carbon fiber reinforced thermoplastic materials. J Mater Process Technol 2003;143–144:342–6.

[18] D.Nabi Saheb and J.P.Jog. Natural Fiber Polymer Composites: A Review, Advanced in Polymer Technology: 1999, Vol. 18, pp. 351-363.

[19] M.Ramesh, K.Palanikumar and K.Hemachandra Reddy. Mechanical property evaluation of sisal–jute–glass fiber reinforced polyester composites. Composites: Part B 48, 2013, pp. 1–9.

Hard Facing of SS316LN by Direct Metal Deposition of Ni Based Wear Resistant Alloy

Himanshu Balhara[a*], Abhishek Kumar[b], S. Madhavan[C]

[a,b,c] Department of Mechanical Engineering
SRM Institute of Science and Technology
Kattankulathur-603 203

*Corresponding Author E-mail: himanshu.balhara31@gmail.com
Contact no: +91-44-27417823
Fax: 91-44-27453903

Abstract:

In the area of hard facing Ni based alloys, Plasma Transferred Arc (PTA) was chosen for various Prototype Fast Breeder Reactor (PFBR) components. Grid plate of PFBR is a massive structure with large number of sleeves providing a foundation for the sub-assemblies. High cracking susceptibility of this process often required the development of critical procedure during actual fabrication. Sound joints with minimal heat inputs were decided as the promising answer for the above issue. At this juncture, direct metal deposition, additive manufacturing technique was identified. So, the present work pertains to studies on direct metal deposition of NiCrFeB over SS316LN for grid plate application in PFBR. The effect of Laser power on the microstructure and mechanical properties are analyzed. Results indicate that dilution is minimal with reduced distortion. Electron microscopy analysis and X-ray diffraction study on the hard facing and interface reveal the formation of various strengthening phases.

Key words: NiCrFeB, LENS, Microstructure, SS316LN, Dilution

1.Introduction

Rising concern regarding environmental issues, local pollutions and climate change is posing a threatening question on sustainability. Nuclear energy is a preferred option for base load electricity. Prototype Fast Breeder Reactor (PFBR) is a pool type Sodium Cooled Fast Reactor (SFR) and uses Mixed Oxide (MOX) fuel with 25 % plutonium oxide and 75 % depleted uranium oxide [1]. Nuclear Reactor components are exposed to extreme atmospheres during their service lifetime, including high temperatures, corrosion, and high stresses. However, the high temperature environment during the operation can lead to corrosion, oxidation, and thermal and mechanical fatigue of the grid plates and other major components of the reactor.

Therefore, the choice of structural materials broadly depends upon the fuel (metallic or ceramic) for the core and on the coolant (gas, sodium, lead) for the heat transport circuit components [1]. Austenitic Stainless steel of 300 (SS316LN) series find its way for the major application as a structural material in prototype fast breed reactors (PFBR) due to its good corrosion resistance property. Liquid sodium is used as coolant in PFBR to eliminate the protective oxide film present on the surface of stainless steel and also act as a reducing agent [2,3]. Due to high temperature acquaintance in the reactor high contact stresses are encouraged which result in self-welding of the materials and later this changes to galling the extreme form of adhesive wear.

Many experimental studies have been carried out to eliminate the wear on the reactor materials using cobalt based hard facing alloy (Stellite) but due to its radioactive contamination at high temperature it forms cobalt 60 isotopes which degrade the reactor life to the half. In order to enhance structural property, advanced materials and sophisticated designs have been developed. Ni-base surfacing

alloys (colmonoy5) exhibit inimitable combination of high temperature strength and wear resistance [4] and due to the addition of carbides and borides it enhances the abrasion property and have been widely used in the fabrication of PFBR components. This choice of hard facing material is proposed at keeping induced radioactivity to the lowest for maintenance and to resist the galling and erosion at elevated temperatures.

Plasma Transfer Arc was one the welding techniques used in hard facing of cobalt based alloys over metal substrate but the results of welding are characterized by a large temperature increase in the workpiece, re-crystallization, and weakening of the base alloy due to a wide temperature distribution over the working area.

Contrary to this method, Direct Metal Deposition (DMD) is a progressive additive manufacturing technology used to repair and rebuild damaged components, to manufacture new components, and to apply wear- and corrosion- resistant coatings. DMD produces fully dense, functional metal parts directly from CAD data by depositing metal powders pixel-by-pixel using laser melting and a patented closed-loop control system to maintain dimensional accuracy and material integrity [5,6]. Heat transfer in the DMD laser cladding that typically uses a 0.5 – 3.0 mm diameter laser beam occurs in localized areas [7]. As a result, the heat-affected zone (HAZ) and residual stresses are minimal and therefore a lower part distortion and better mechanical characteristics are attained.

LENS is actual a metal deposition technology that produces a very fine weld bead, exposing the component to very low heat than conventional methods. This results in reduced "heat-affected zone" and have more control during the repair process so that it does not damage the underlying part [8]. And, subsequently a LENS deposit is much finer and more accurate than welding techniques, far less finishing work is required

This technology allows real-time control over the composition and micron level features of coatings. Unlike other laser processing techniques, LENS is one of these sophisticated technologies, and it has many advantages in comparison with conventional technologies and many areas for application. The LENS process is, therefore, a good candidate for the hard-facing of Ni-base superalloy (Colmonoy 5) over the substrate used for fabrication of grid plates in the Nuclear Reactors i.e. SS316LN.

2. SELECTION OF MATERIALS:

The concerned materials have been selected keeping in mind the constraints and operating conditions for the upcoming reactor such as working temperature of 500^0-650^0.This work pertains to improving the surface properties of conventionally used base material as reference.

2.1 SELECTED MATERIALS:

2.1.1Base material

Based on the initial analysis it has been found that steel alloys are extensively used in sodium fast reactors owing to its favorable properties at elevated temperatures. After analysis of the challenges faced by these class of steels it was decided to clad them with Ni-based super alloy to improve upon the existing structures. For this study SS316LN was selected for laser cladding the hard-facing alloy.

Chemical Composition of Substrate Metal:

2.1.2Colmonoy Alloy

Nickel-based hard facing alloy Colmonoy-5 is preferred in nuclear power plants, due to low-induced radioactivity. Colmonoy is a Ni based super alloy developed by the Wall Colmonoy for the protection and renovation of critical industrial components. Ni-Cr-Fe-B (COLMONOY 5) hard facing alloy conforming to AWS A5.21 specification was deposited on 316LN stainless steel substrate using Laser Engineered Net Shaping (LENS) process. The welding parameters employed for the deposition process are given in Table. The thickness of the coating on this specimen was typically between 1,5- and 2,0-mm. Table 2 shows the chemical composition of the Ni-Cr-Fe-B hard face alloy. Specimens of an approximate dimension of (10mmx20mm) were cut from the hard face coated blanks, and were ground and polished up to 0,25 mm finish following the standard metallographic procedures. These were etched using aqua regia solution to

reveal the microstructures. The microstructures of the specimens were examined by optical and scanning electron microscope. The hardness of the hard face coating was determined on same specimens by a Vickers Hardness Tester using a load of 1 kgf for a dwell time of 5.0 s and Rockwell hardness using major load of 15 kgf and minor load of 3 kgf for a dwell time of 2.0 sec.

MATERIAL USED	ELEMENTS, WEIGHT%									
COLMONOY 5	Co	Ni 77.0	Cr 11.2	W	Fe 4.4	B 2.6	Si 2.0	Mo 3.1	Cu	C 0.6	O 0.403

Chemical Composition of Coating Material:

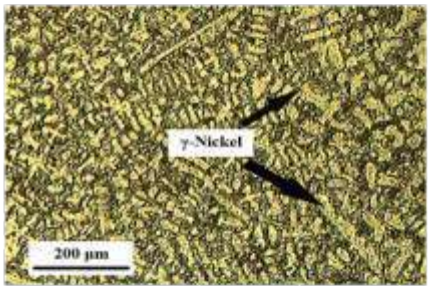

Fig (1) Microstructure of Colmonoy 5

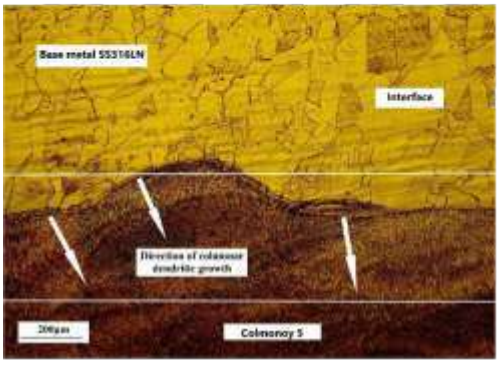

Fig (2) shows dendritic growth in dilution zone

3.Experimental Methodology

Laser cladding was performed by means of a 5 Axis DMD 105D AM machine M/s POM Inc., USA with diode laser system. The hard-facing powder was fed to the spot of cladding by a pneumatic powder feeding system. The power of the laser beam was set at 600w and shielding gas was used to provide a protective atmosphere during the laser cladding process. Cladding parameters were used, with the powder feed rate (PFR) of 4 g/min and the translation speed (TS) of laser beam was set at 600 mm/min. By modifying the deposition energy, one can tailor the strength and ductility values. For low energy input, through low power, the molten bead

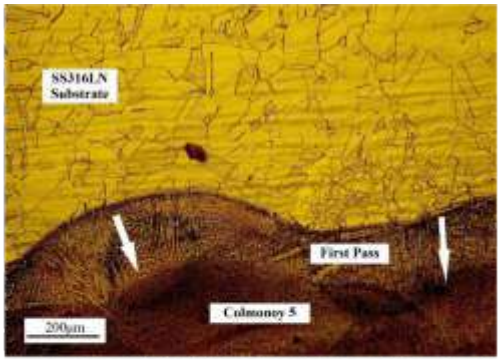

Fig (3) Microstructure of SS316LN cladded with colmonoy 5

will solidify quickly with minimum HAZ resulting in high yield and ultimate tensile strength values.

4. Metallurgical analysis

4.1. Micrographic analysis

The microstructure analysis exhibits sound deposition with no porosities and cracks. The deposition is uniform with fine equiaxed microstructure with precipitates of carbides and borides of chromium dispersed in solid solution of γ-Nickel as shown in fig (1). The microstructure near the interface and away from the interface differs to some avail. The microstructure near the interface reveals columnar dendritic growth of γ-Nickel in a direction almost perpendicular to the interface. The microstructure also reveals interdendritic precipitates of carbides and borides as shown in fig (2,3). The concentration of precipitate increases with increasing gradation from the interface surface. The dendrites were free from spike or script like features.

4.2 *Scanning Electron Micrograph*

Scanning electron micrograph shows a well fused hard face layer and substrate. Formation of dilution layer is evident. EDS mapping of AM layer shows minimal dilution of Cr and Ni. The coagulation of Ni and iron is more predominant with Cr and Mo particles pinning the boundaries. Presence of O_2 is found to be negligible. The tendency for formation of Ni_3Nb precipitate could be more than any precipitate. The grain distribution is in the order of 50-70 microns with negligible porosity. The EDS analysis also shows the composition of precipitates that cannot be precisely identified as laves phase. The dilution layer formed in between layer and clad

is very smooth and variation of Fe and Ni content fluctuates at 10% and can be seen in fig (5).

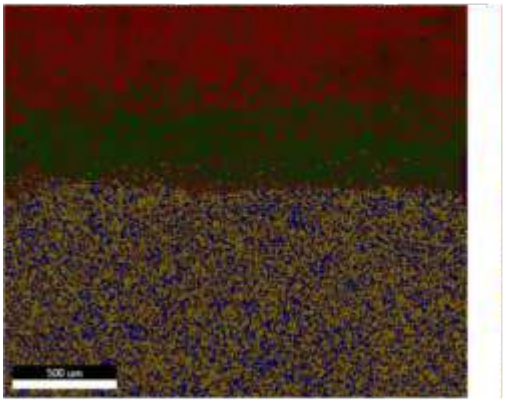

Fig (5) Area Mapping done by SEM

Fig (5) Elemental distribution shown in area mapping.

5.Microhardness Profile:

It was found that the microhardness across the layers were fairly uniform with the cladding having hardness value about 2.5 times more than the substrate. A gradation is seen through the heat effected zone. Due to mutual flow of constituents from either side the hardness of the dilution layer was maximum at the cladding side and had a decreasing trend near the substrate

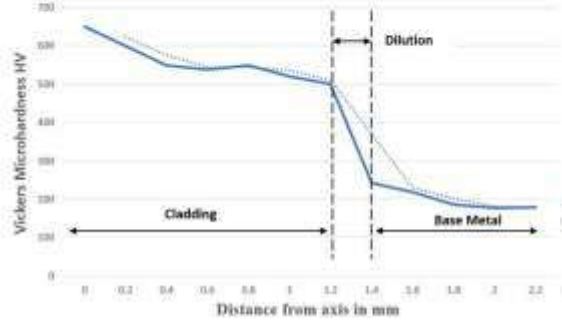

CONCLUSION:

1. The microstructures of laser cladding layer consist of Ni-rich solid solution, boride and carbide

2. It was evidenced that this alloy can be used to produce sound cladding without cracks and substantial porosities.

3.Dilution is found to be minimum when compared to other cladding processes.

References

[1] Raj, B., & Chellapandi, P. (2017). Indian Advances in Fast Breeder Nuclear Reactor Engineering. In *Energy Engineering*(pp. 39-49). Springer, Singapore.

[2] Srinivasan, R., Chellapandi, P., & Chetal, S. C. (2010). Comparison of SS 304 LN and 316 LN as choice of structural material for primary pipe in fast breeder reactors. *Transactions of the Indian Institute of Metals*, *63*(2-3), 607-610.

[3] Bhaduri, A. K., Albert, S. K., Das, C. R., & Raj, B. (2011). Hardfacing of austenitic stainless steel with nickel-base NiCr alloy. *International Journal of Microstructure and Materials Properties*, *6*(1-2), 40-53.

[4] Liu, D., Lippold, J. C., Li, J., Rohklin, S. R., Vollbrecht, J., & Grylls, R. (2014). Laser engineered net shape (LENS) technology for the repair of Ni-base superalloy turbine components. *Metallurgical and Materials Transactions A*, *45*(10), 4454-4469.

[5] Keicher, D. M., Smugeresky, J. E., Romero, J. A., Griffith, M. L., & Harwell, L. D. (1997, March). Using the laser engineered net shaping (LENS) process to produce complex components from a CAD solid model. In *Lasers as Tools for Manufacturing II* (Vol. 2993, pp. 91-97). International Society for Optics and Photonics.

[6] DUTTA, B., Singh, V., Natu, H., Choi, J., & Mazumder, J. (2009). Six-axis direct metal deposition technology enables creation. *Advanced materials & processes*, *167*(3), 29-31.

[7] Thivillon, L., Bertrand, P., Laget, B., & Smurov, I. (2009). Potential of direct metal deposition technology for manufacturing thick functionally graded coatings and parts for reactors components. *Journal of Nuclear Materials*, *385*(2), 236-241.

[8] Palčič, I., Balažic, M., Milfelner, M., & Buchmeister, B. (2009). Potential of laser engineered net shaping (LENS) technology. *Materials and Manufacturing Processes*, *24*(7-8), 750-753.

Tribological behavior of PA 12 – GF composite parts fabricated via fused deposition modeling

R.Soundararajan[a*], P.Sricharana[b], T.Shoban[b], P.V.Suchith[b]

[*a] Associate Professor, Dep of Mechanical Engg, Sri Krishna College of Engg and Tech, Coimbatore, India
[b] UG Students, Department of Mechanical Engineering, Sri Krishna College of Engg & Tech, Coimbatore, India

*Corresponding author E-Mail ID: soundararajan.mtech@gmail.com, Mobile: 9894534879

ABSTRACT

Fused deposition modeling (FDM) is one of the latest rapid prototyping techniques in which parts can be manufactured at a fast pace and are manufactured with a high accuracy. The parts were made of newly developed polyamide 12 with 10, 20, 30 weight % glass fiber (PA 12 GF) composite material by FDM process. The main moto of this research work is to carry out a study in the friction and wear behavior of composites by sliding against metal under dry sliding conditions by using a pin-on-disc tribometer. These tests were carried out on the pin on disk tribometer under varying load conditions such as 5, 10, 15 and 20 N at the run time of 5 and 10 minutes respectively. Moreover the applied load and run time on the tribological behaviors of the sliding combinations of composites under dry sliding condition that were carried out at room temperature were also investigated. The results showed that the applied load and run time significantly affects the wear rate, friction force and friction coefficient of the respective test samples. It is concluded that the newly developed composite of PA12 with 30 wt% GF shows better wear and friction behavior that can be used in automobile applications.

Key words: FDM – PA12-GF composite -Tribology behavior

1. INTRODUCTION

Rapid prototyping techniques have evolved as a major hub of producing components now-a-days due to demand. Further produced plastic parts were used in the real-time environment where the components with higher cost but low load carrying capacity, components with low exposure to heat. Despite all the advantages of the plastics, some of its drawbacks include the low hardness, a result of which the resistance of plastics to wear is very less and are often required to be replaced periodically [1].Due to the growing requirements of the industries, a good combination of the reinforcing material with the matrix can be innovated, it yields successful conditions which can withstand an assortment of strength and wear conditions [2].The wear in polymers is a phenomenon that are not affected only by a specific set of parameters, there are complex phenomenon in which numerous factors collectively affect them and thus extensive research has to be carried out to understand their properties thoroughly [1-2].Polymers have been used to manufacture gears, cams and bearings, therefore the need of the product to be long lasting and efficient requires tribological study to be carried out on them [3], In addition the common factors that attribute to wear of the materials are normal load, sliding velocity and temperature [4].It has been stated that the wear at low

speed is mainly caused due to abrasion, whereas the wear at high speed and high load conditions are mainly due to the adhesion [5].The electroplating has been identified as a valuable technique in improving the strength of these plastics[6].ABS and PA6 are two of the most important plastics that are currently being used for a wide variety of applications owing to their useful properties. A study was carried out to identify the mechanical and thermal behavior of glass fiber, $CaCO_3$hybrid reinforced ABS/PA6 based composition and it was observed that this reinforcement has strong influence done [7].

The use of inorganic material inside the matrix can improve the wear resistance of the material, but this degrades the fracture strength of the material but the right combination of such in organic materials inside the matrix can achieve the optimum parameters when the right production techniques and right composition are used[8,9]. The effect of micro and nano-particles on the tribological properties and have concluded that the wear is very less when the aluminium nanoparticles are used inside the matrix [10]. Various studies has been conducted on the effect of ZnO nanoparticles on the tribological properties of ABS composites and concluded that they significantly improve the properties of the material [11].

It has been concluded based on their study that compared to aramid and carbon fibers being used as the dispersed phase glass fibers phases produce the maximum strength [12]. Studies has suggested that at low sliding velocities, the wear was a function of the time and at high sliding velocities the wear depends on the temperature for epoxy resin filled with 68.5% silica particles sized between 20–40μm [13].

It has been identified that addition of molybdenum disulphide reduces the wear by improving the coefficient of friction of the material. The decrease in the friction coefficient has been attributed to the formation of the interfacial layers at higher temperatures despite this, the high load conditions still cause wear in the materials [14].With the addition of graphite into the matrix the coefficient of friction decreases by a very large extent as this solid lubricant aids in improving the formation of the interfacial layer which in turn aids in the reduction of the coefficient of friction of the material during abrasion[15].Fatigue and adhesion significantly contribute wear under dry sliding conditions to the due to the which occurs due to heat dissipation has been reduced[16].

Thus, the literature study suggests that there has been no works reported on the proportions of glass fibers in the PA12 polymer and this research is an attempt to address this need. Here the PA12 has been processed using fusion deposition modeling and the tribological properties of the material under different conditions of loading and runtime on the tribometer plotted against the pure PA12 polymer and the results have been submitted as such.

2. EXPERIMENTATION

2.1. Materials

The PA12 is a semi crystalline polyamide which is commonly known as nylon 6 or polycaprolactam. PA12 filaments

shows high tensile and good insulating properties that can protect heat up to 150°C with melting point range 178-180°C and density of 1.01 g/cm^3. PA12 having poor biodegradability and most of the PA12 used in the experiment are recycled one. Glass fiber (GF) is used as the reinforcement material inside the PA12 polymer matrix. Glass fiber has great mechanical properties compared to other fibers. It has density of 2.58 g/cm^3 and no true melting point, but softens up to 1200 °C, where it starts to degrade. Though it is not, as rigid as carbon fiber, it is considerably less expensive and essentially less brittle. For the present study pure PA12 and three different combinations of PA12 and GF in granule form are used.

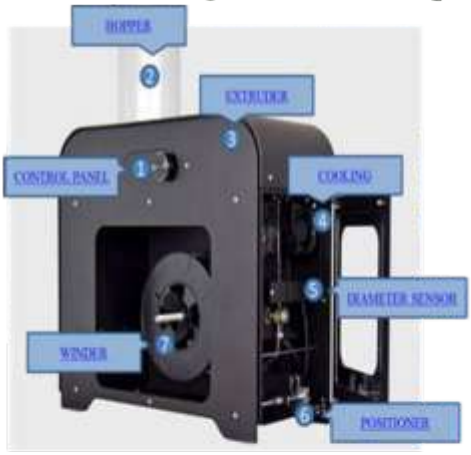

Fig 1. Filament Extruder

Fig 2. 3D Printer (FDM)

2.2. Extrusion of filaments

The PA12 and GF materials are dried at 90°C for a minimum time period of 6 hours. This is done by placing the desired weight percentage of granulates of the materials into the "Heraeus Instruments" exposed to a warmed atmosphere. The preheated material is extruded using the 3Devo-NEXT Filament Extruder with the extrusion temperature of 175°C. The Extruder has nozzle diameter of 1.75mm and length of 10m. Four different filament samples are extruded. First sample is pure PA12 and the other three samples are combinations of PA12 with 10%, 20% and 30% glass fiber respectively.

2.3. Fused deposition modeling

The test samples have been modeled with the help of SolidWorks software and saved as ".stl" format. This file is then imported into "slic3r" and the G-codes are generated. The generated G-codes are uploaded to the kühling and kühling HT500.2-3D printer. The four prepared filaments are fed into the 3D printer in order to produce the test samples with fill angle of 45°, bed temperature of 60°C, and layer height of 0.3mm and filament diameter of

1.75mm. The prepared test samples were taken for testing.

2.4. Tribometer testing

The tribological behaviors of the 3D printed test samples were tested in pin on disc wear tribometer. The prepared specimens were tested by using Ducom (TR-20LE-M108) tribometer machine to vary the influenced process parameters such as applied load 5,10,15,20 N and run time 5mins, 10mins (corresponding sliding distance of 875m and 1750m respectively), also other process parameters were kept constant such as sliding speed of 1.5 m/s, disc diameter 165 mm and disc speed of 175 rpm. The tribological behaviors such as wear rate, friction force, the coefficient of friction are taken for four test samples and the values are noted for further analysis as in Table 1.

Fig 3.Pin on disk tribometer

Fig 4. Printed Samples

Table 1.Measurement of tribological behavior

Material	Load (N)	Speed at 100 rpm (5mins run time)			Speed at 100 rpm(10mins run time)		
		Wear rate (mm^3/Nm)	Friction force(N)	Coefficient of friction	Wear rate (mm^3/Nm)	Friction force(N)	Coefficient of friction
PA12	5	1.78	0.35	0.51	1.69	0.33	0.49
	10	3.4	0.38	0.7	3.4	0.4	0.67
	15	4.7	0.41	0.74	4.5	0.53	0.7
	20	5.5	0.53	0.78	4.85	0.65	0.756
PA12+10%GF	5	1.37	0.29	0.48	1.28	0.28	0.46
	10	2.6	0.31	0.56	2.24	0.3	0.6
	15	3.1	0.35	0.64	2.78	0.36	0.66
	20	3.5	0.45	0.69	2.98	0.46	0.72
PA12+20%GF	5	1.1	0.24	0.45	1. 15	0.23	0.42
	10	2.2	0.26	0.5	1.8	0.27	0.5
	15	2.69	0.29	0.56	2.12	0.31	0.54
	20	2.87	0.41	0.62	2.3	0.38	0.59
PA12+30%GF	5	0.98	0.19	0.4	0.9	0.18	0.38
	10	1.9	0.22	0.42	1.4	0.2	0.44
	15	2.2	0.24	0.48	1.53	0.25	0.49
	20	2.35	0.34	0.53	1.66	0.28	0.53

3. RESULTS AND DISCUSSION

3.1. Wear rate

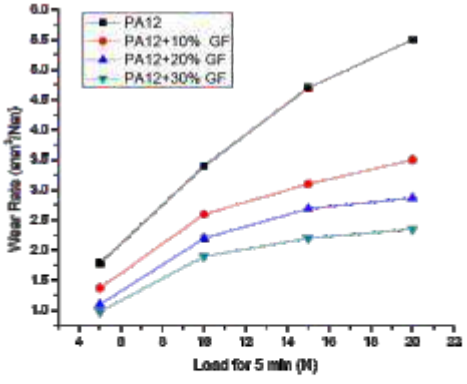

Fig 5. Wear rate for 5mins run time

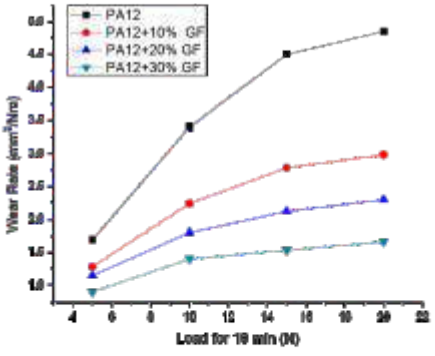

Fig 6. Wear rate for10mins run time

The wear of polymers occurs due to abrasion and adhesion mechanism. The resistance to wear for polymers improves with the support of reinforcement filler materials. By adding glass fibers in a varying weight ratio, the experimental wear rate of

the respective test samples were made highly significant. From the Fig 5 and 6, the wear rate decreases with increase in weight percentage of glass fibres due to enhancement of hardness and fatigue strength. The addition of GF increases the abrasion and sliding resistance due to its high thermal stability. For lower load conditions, the wear rate is observed to be peak for all the test samples due to the less adhesion between the surfaces. While applying higher loads, the adhesion between the surfaces gets strengthened and makes the material to wear more in sliding condition. For PA12 the value increases steadily with the increase in applied load and for other composites the wear rate increase gradually from 5 to 15 N, after that, it becomes almost stable for load of 15 to 20 N owing to sliding resistance. This sliding resistance is due to uniform wear of material while applying 5 to 15 N loads. The reinforcement of GF in PA12 matrix prevents the transition from mild to severe wear at high load condition. The loads are applied for specific time period of 5mins and 10mins.When the loads are applied for 5mins, the wear of material is lower when compared to 10mins.This happens because the fatigue stress increases for the rise in the time period. During the wear test, it is evident that there is heat dissipation from the contact surface of pin and disk due to friction which confirms impale of [17]. This further decreases the wear rate of material.

The PA12+10%GF and PA12+20%GF composites have 40.3% and 44.4% lesser value than the virgin PA12 for 20N load and 10mins time period. The wear rate of PA12+30%GF is 55.6 % lesser than the virgin PA12 for the same conditions, which is the eminent value for the taken samples. The experiment unveils that PA12+30%GF have better wear resistance than the virgin PA12and other composites.

3.2. Friction force

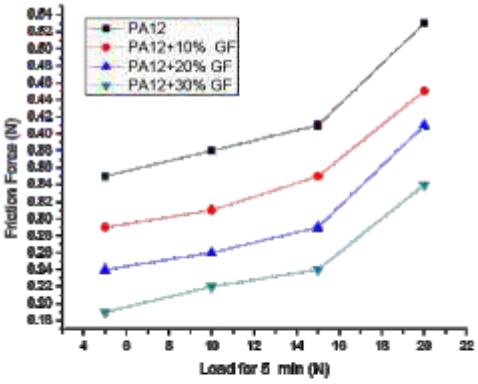

Fig 7. Friction force for 5mins run time

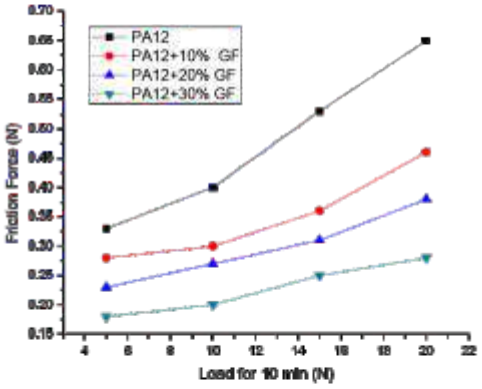

Fig 8. Friction force for10mins run time

Friction force is characterized by the resistance offered by bodies under sliding conditions. The primary tribological properties contributing to friction force are adhesion and deformation. Fig7 and 8 shows that the friction force decreases with the addition of the reinforcement material. This is because as the percentage of glass fiber increases, the surface of the material becomes smooth and it offers less resistance for

sliding. The virgin PA12 shows greater adhesion with the abrasive surface and are deformed more. On the other hand, the composites exhibit lower adhesion and low surface deformation. Due to this composites have less friction force compared to virgin PA12.

For lower load conditions, the friction force is small when compared to higher load because of low adhesion between the surfaces and lower surface deformation. The friction force increases when applying the load from 5 to 15 N, after that it attains an almost steady state condition at the load of 15 to 20 N owing to lower sliding resistance.

For 5mins time period, the friction force is lesser than for 10mins time period due to formation of strong molecular bonds between the contact surfaces. This bond formation is the result of greater contact time and it resists the sliding movement of sample. More over due to the formation of transition layers on the sliding surface, the friction force is again increased.

From the studyPA12+10%GF and PA12+20%GF have 42% and 58% lesser friction force acting on them in comparison with virgin PA12for 20N load and time period of 10 minutes. PA12+30%GF experiences 67% lesser friction force in comparison with virgin PA12 and other composites for same conditions. The experiment reveals that PA12+30%GF experiences lower friction force than the virgin PA12and other composites. This [14-20].

3.3. Coefficient of Friction(μ)

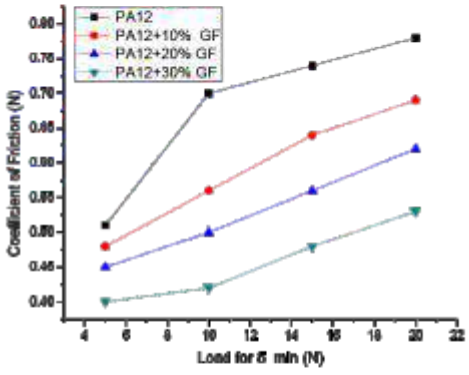

Fig 9.CoF for 5mins run time

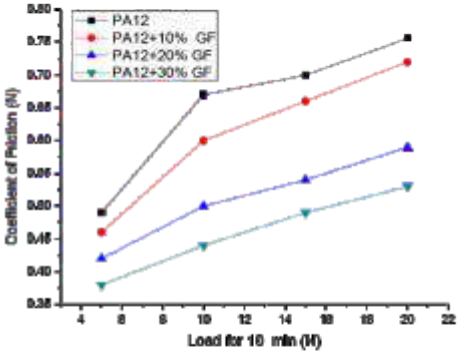

Fig 10.CoF for 10mins run time

The Friction coefficient is the ratio between the friction force and the corresponding applied load. It is a surface phenomenon and it is influenced by the nature of surface when desired conditions are applied. From Fig 9 and 10, the coefficient of friction declines with addition of GF. This is because when the asperities on the surface get diminished and it becomes smoother. For lower load conditions, the coefficient of friction value is at peak due to high initial surface roughness and this gradually decreases for higher load conditions. This is attributed to fact that the surface gets smoothened while increasing the load. By applying 5 to 15 N load, the coefficient of friction steadily decreases because of uniform elimination of surface roughness and

for 15 to 20 N load, it is slightly decreased because of less roughness value.

The coefficient of friction has a higher recorded value for 5mins due to higher resistance across the pin and the sliding material but for 10mins, it decreases as the composite surface is smoothened and much of material is worn out in the form of powder.ThePA12+10%GF and PA12+20%GF composites have 41.67% and 58.3% lesser values in comparison with virgin PA12 and other composites for 20N load and time period of 10 minutes. The PA12+30%GF67% lesser values in comparison with virgin PA12 and other composites for same condition. From the present study the PA12+30%GF composite have lower coefficient of friction value. This outcome stands with the assertion [14-20].

4. CONCLUSION

The tribological behavior of virgin PA12 and composite of PA12-GF materials in different combinations are studied at loads of 5,10,15,20 N for time period of 5 and 10 minutes at sliding velocity of 1.256 m/s using pin on disk tribometer. The summary of the above experiment is as follows

- The addition of GF increases the abrasion and sliding resistance due to its high thermal stability and so PA12+30%GF has the lower wear rate for 20N load at 10mins.
- As the percentage of glass fiber increases, the surface of the material becomes smooth and it offers less resistance for sliding and due to low adhesion and deformation property, the friction force for PA12+30%GF composite is lower than other test samples for 20N load at 10mins.
- The values of coefficient of friction of PA12+30%GF composite are lower than other test samples as the smoothness increase with addition of glass fiber which is further enhanced when the loads and time periods are increased.
- So overall tribological behavior of PA12+30%GF is better than virgin PA12 and other two composites.
- This composite can be suitable for tribological related applications in automotive industry; also it is owing to extended life span.

ACKNOWLEDGEMENT

On behalf of all teamwork of this research the corresponding author wishes to thank Sri Krishna College of Engineering and Technology for all support required to carry out this research.

AUTHOR CONTRIBUTION

Dr R.Soundararajan has put the idea of this work conceived and plan the experiments. Also investigate the result, written and edited the article. P Sricharana, T.Shoban and P.V.Suchith have carried out the experimental part and free hand written the article.

REFERENCE

1.Kalácska G, "An engineering approach to dry friction behaviour of numerous engineering plastics with respect to the mechanical properties", EXPRESS Polymer Letters, 7(2), 2013, 199-221, doi:10.3144/expresspolymlett.2013.18.

2.Briscoe B J , "Isolated contact stress deformations of polymers: the basis for interpreting polymer tribology", Tribology International, 31(1-3), 1998, 121-126, doi.org/10.1016/S0301-679X(98)00014-0 .

3.Gopala Krishna K, Divakar C, Venkatesh K, Mohan C B, Mahesh Lohith K S, "Tribological studies of polymer based

ceramic–metal composites processed at ambient temperature", Wear, 266(7-8), 2009,878-883, doi.org/10.1016/j.wear.2008.08.013.

4.Watanabe M, Karasawa M, and Matsubara K (1968),"The frictional properties of nylon. Wear", 12(3): 185-191.

5.Aigbodion V S, Hassan S B, Agunsoye J O, "Effect of bagasse ash reinforcement on dry sliding wear behaviour of polymer matrix composites", Materials and Design, 33, 2012, 322–327, doi.org/10.1016/j.matdes.2011.07.002.

6.Kulkarni M V, Elangovan K, Reddy K H, and Basappa S J, "Tribological behaviours of abs and PA12 polymer-metal sliding combinations under dry friction, water absorbed and electroplated conditions", Journal of Engineering Science and Technology, 11(1), 2016, 068-084.

7.Karsli N G, Yilmaz T, Aytac A, Ozkoc G. "Investigation of erosive wear behavior and physical properties of SGF and/or calcite reinforced ABS/PA12 composites", Composites: Part B, 44(1), 2013, 385–393, doi.org/10.1016/j.compositesb.2012.04.074.

8.Jiang L, Lam Y C, Tam K C, Chua T H, Sim G W, Ang L S, Strengthening acrylonitrile-butadiene-styrene (ABS) with nano-sized and micron-sized calcium carbonate", Polymer Journal, 46(1), 2005, 243–252, DOI: 10.1016/j.polymer.2004.11.001.

9.Difallah B B, Kharrat M, Dammak M, Monteil G, "Mechanical and tribological response of ABS polymer matrix filled with graphite powder", Materials Design, 34, 2012, 782–787, doi.org/10.1016/j.matdes.2011.07.001.

10.Mejia O O, Brostow W, Buchman E, "Wear resistance and wear mechanisms in polymer plus metal composites", Journal of Nanoscience and Nanotechnology, 10(12), 2010, 8254-9, DOI: 10.1166/jnn.2010.3026.

11.Nagaraju B, Ramji K, Prashad V S R K, "Studies on tribology properties of ZnO filled polymer nanocomposites", ARPN Journal of Engineering and Applied Science, 6(6), 2011, 75–82.

12.Zhao G, Hussainova I, Antonov M, Wang Q, Wang T and Yung D L, "Effect of temperature on sliding and erosive wear of fiber reinforced polyimide hybrids", Tribology International, 82(B), 2015, 525-533, doi.org/10.1016/j.triboint.2014.01.019.

13.Zhu P, Wang X, Wang X D, Huang P and Shi J, "Tribology performance of molybdenum disulphide reinforced thermoplastic polyimide under dry and water lubrication conditions", Industrial Lubrication and Tribology, 58(4), 2006, 195-201, DOI: 10.1108/00368790610670782.

14.Xu L, Zhu Z, Chen G and Qu C, "Effect of loading and sliding velocity on tribological behaviors of aramid fiber reinforced PA1010 composites", Industrial Lubrication and Tribology, 62(1), 2010, 46-51, DOI: 10.1108/00368791011012461.

15.Srinivas, C.L., Sarcar M M M, and Suman K N S, "Abrasive wear properties of graphite filled PA12 polymer composites", International Journal of Mechanical Engineering and Robotics Research, 1(3), 2012, 157-162.

16.Zhang S, Wang S, and Mao Y, "Mechanical and tribological properties of PTFE composites filled with POB", Advanced Materials Research, 194(196), 2011,1728-1731, doi.org/10.4028/www.scientific.net/AMR.194-196.1728.

17.Zhao G, Hussainova I, Antonov M, Wang Q, Wang T, and Yung D L, "Effect of temperature on sliding and erosive wear of fiber reinforced polyimide hybrids", Tribology International, 82, 2015,525-533, doi.org/10.1016/j.triboint.2014.01.019.

18.Garg HK and Singh R, "Comparison of wear behavior of ABS and Nylon6—Fe powder composite parts prepared with fused deposition modelling", Journal of Central South University, 22(10), 2015, 3705-3711.

19. Kamaljit Singh Boparai, Rupinder Singh, Harwinder Singh, "Wear behavior of FDM parts fabricated by composite material feed stock filament", Rapid Prototyping Journal, 22(2), 2016, 350-357, doi.org/10.1108/RPJ-06-2014-0076.

20. S.SibiChakaravarthi S, Kanchana J, Dirk Fröhling, Sonja Grothe, Gabriela Marginean,"Enhance the Material Properties of FDM Filament using PA12" International Research Journal of Automotive Technology, 1(3), 2018, 87-94.

A REVIEW ON STUDY OF POLYMERS AND RECENT DEVELOPMENTS AND FUTURE CHALLENGES IN MATERIALS FOR ADDITIVE MANUFACTURING-3D PRINTING

Dattaji K. Shinde[1], Sachin C. Kulkarni[2]
[1]Associate Professor, Production Engineering Department, V.J.T.I., Mumbai
[2] Ph.D. Research Scholar, Production Engineering Department, V.J.T.I., Mumbai

***Abstract*-3D printing or additive manufacturing (AM) is a technology that gives products to consumers and industrial markets as per their requirement in terms of dimensions and appearance. Materials that can be used in fused deposition modelling (FDM) in the form of filaments with addition of carbon nanotubes (CNTs) and graphene is a need of today. Composites with such additives can change the future of 3D printing of next generation manufacturing industry. This paper elaborates few facts and findings from a research carried out previously, enhancement in mechanical and electrical properties of newly developed material and challenge to be faced in developing a new material with better properties to be used in functional 3D printing products manufacturing.**

***Keywords:* 3D printing, additive manufacturing, graphene, carbon nanotubes, carbon black**

I. INTRODUCTION

A 3D printing produces parts or products with addition of successive layers of material on a platform by using bottom to top approach. A material can be a thermoset or thermosetting plastic with addition of certain additives such as CNTs (SWCNTs/MWCNTs) or graphene. For 3D printing most common and famous form is thermoplastic extrusion, known as fused deposition modelling (FDM)[1], where a material in the form of filament (generally 1.75mm dia.) is unwound from a spool and fed into a temperature controlled melting chamber and then extruded through a tip of nozzle as shown in Figure 1. Addition of CNTs and other structured additives improve functionality of 3D printed composite parts. Polymer composites and their development as a material for 3D printing are of greatest interest among all researchers and industry specialists.

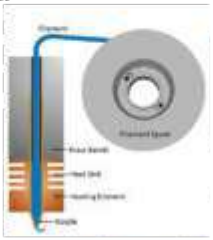

Figure 1. A picture of a extruder assembly from a FDM printer and a schematic of the extruder.

Polymer nanofibers and glass nanofibers are of considerable interest in many applications as secondary reinforcement in structural composites. [2]

A polymers commonly used for 3D printing can be listed as a Polylactic Acid (PLA) - a sustainable biodegradable polymer and Acrylonitrile Butadiene Styrene (ABS) - a strong terpolymer used in most of the 3D printed processes, are two of the most popular polymers used for FDM, and having a scope of addition of certain additives in it for the formation of new and advanced materials for the next generation and also for researchers. Apart from these two, Polyvinyl Alcohol (PVA) – a water soluble and biodegradable, Polyamides (nylons) - strong, abrasion resistant and typically used for most of the mechanical parts. All above polymers are with the potential for the inclusion of CNTs and graphene with all other structural additives to extend their multi-functional use in 3D printed composites. Interlaminar shear strength (ILSS) of fiber reinforced polymer composite is an important property for most of the structural applications. Matrix modification is an effective method used to improve the interlaminar shear strength of composite. [3]

A brief about processes in AM:

Selective Laser Sintering (SLS):

SLS uses powdered thermoplastics. A laser on the powder creates desired 3D printed object. A laser heats the powder just below its melting point and fuses the powder to create layers at specific locations. SLS uses combination of polymers and metals. Also unused powder can be recycled. Particle size of the powder affects the precision of print / 3D object. The process can be handled with addition of CNTs in powder, only heat transfer process has to be studied. [4]

Digital Light Processing (DLP):

DLP produces high resolution 3D objects. A light with controlled exposure from DLP projector or an instrument using digital micromirror device (DMD) [5] on a vat of photopolymer on a platform, hardens exposed liquid polymer. A 3D model of object in computer is sliced into 2D layers and sent to DLP printer one by one.

Stereolithography:

It is same as DLP, uses photopolymers with laser based light source. A laser beam strikes on the liquid photopolymer and polymer hardens. A recoater blade

deposits the next layer of liquid photopolymer. Printed object requires cleaning and curing in ultraviolet light. Graphene oxide [6] can be one of the additive material used alongwith polymers for 3D printing.

Many applications can be directly related to the addition of CNTs and graphene as additives for 3D printing [7,8], a sector under a rapid growth. By 2009, the 3D printing sector took over 20 years to reach $1 billion and over the following three years it reached $2 billion. Market analysis suggests it may reach upto $10 billion by 2019 [9].

Some drawbacks of 3D printing:

- A process of thermal extrusion consumes maximum electricity.
- Emission rate of ultra-fine particles is more for PLA and highest for ABS printing.[10]
- Security issue after the fabrication of 3D printing.

II. POLYMERS IN 3D PRINTING

3D printed objects need specific mechanical and design considerations. After thermal extrusion, a 3D printed part should be with proper rheological and thermal properties as it has to be extruded and solidified with maintaining layer by layer accuracy. The use of polymers in 3D printing are governed by

- Glass transition temperature (Tg)
- Melting point (MP)
- Heat capacity
- Melt viscosity at high temperatures
- Shear stress of the material

Study of structural properties will help in development of new filaments with new materials.

A nature of polymers used in 3D printing:

Amorphous polymers – non-crystalline structure, no sharp MP but have Tg

Semi-crystalline polymers - have both Tg and MP

Elastic polymers - Tg below room temperature

Rigid & brittle polymer -Tg above room temperature

Stiff/rigid backbone polymers - high Tg

Amorphous polymers decrease their strength above Tg and become soft as viscosity changes. Lower the Tg of polymer, it reaches quickly to optimal viscosity for extrusion. When polymer is heated above Tg, viscosity will change with the temperature and shear rate. Shear rate is maximum at the printing nozzle (100-200 S^{-1}). A swelling at nozzle is a radial flow of material through nozzle due to change in the viscosity which is undesirable. Addition of inelastic material (Ceramics) and carbon fillers to the polymer reduces swelling at nozzle and increases quality of 3D printing. [11]

III. THERMOPLASTIC RESURGENCE

Thermoplastic polymers are polyamide, polyolefin, polystyrene, polyester and their copolymers used in many applications from fabrics to packaging as they possess excellent mechanical properties, durability, relative ease of processing and the possibility of recycling. A thermoplastic is a polymer that softens upon heating above a temperature range and then solidifies upon cooling; this process can be repeated several times. At the molecular level, the polymer chains are associated via intermolecular Van der Waals forces that are easily broken at elevated temperatures. In contrast, thermoset polymers harden upon heating and are no longer moldable, decomposing at high temperatures. Thermoset polymers are only used with their corresponding monomers, with an initiator added, as the printed materials are cured by ultraviolet light or heat during post processing.

For 3D printing, thermoplastic polymers are the best suitable polymers as they melt and mold during the extrusion process and this has caused popularity in the production of these polymers. [12].

The most common materials used in 3D printing (FDM) are amorphous thermoplastic teracrylonitrile-butadiene-styrene(ABS),PLA,PVA,polycaprolactone (PCL) and nylon.

ABS is a terpolymer that is made from acrylonitrile, 1-3-butadiene and styrene (Figure 2). The ratio of each monomer in ABS can be selectively modified, based on the synthesis method used to yield different grades of ABS with the required mechanical, thermal and processing properties. The percentage of styrene can vary from 65–76% and acrylonitrile by 24–35%. ABS with CNTs and Graphene as Additives in 3D Printing is a light-weight, rubber-toughened thermoplastic with low temperature toughness and is stronger than polystyrene. It adopts the rubbery properties from polybutadiene, the toughness of acrylonitrile, while maintaining the reflective property of polystyrene, which can be enhanced using acetone. ABS is chemically resistant to water, aqueous acids, and alkali solutions but reacts/dissolves in carbon tetrachloride, concentrated nitric acid, concentrated sulfuric acid, esters, and acetone. For 3D printing, ABS can be produced in a variety of colors by adding pigments as raw ABS is translucent. Due to the reactive double bond in the polybutadiene region of the terpolymer, it may be oxidized in ultraviolet light, so indoor applications are preferred.

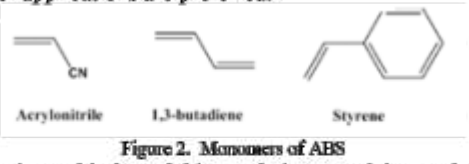

Figure 2. Monomers of ABS

PLA is a biodegradable and low toxicity polyester thermoplastic made from lactide or lactic acid monomers. [13]Both can be derived from the fermentation of carbohydrates which is a renewable resource, so PLA is considered an ecofriendly thermoplastic. PLA can be produced in amorphous and crystalline form. The most common way to produce high molecular weight PLA is by the ring opening of lactide catalyzed by a metal. PLA is a hygroscopic thermoplastic. PLA undergoes thermal degradation, scission of bonds and results in weight loss which has an effect on mechanical and rheological properties [14, 15]. It is worth noting that the extent of

degradation also depends on other factors ranging from molecular weight to particle size. Amorphous PLA is soluble in most organic solvents, while crystalline PLA is soluble at elevated temperatures.

PVA is a hydrophilic, water soluble, biodegradable thermoplastic polymer. PVA is synthesized by the hydrolysis or alcoholysis of poly (vinyl acetate) (PVAc) due to the instability of its vinyl alcohol monomer. It can be produced in two types: partially hydrolyzed or fully hydrolyzed and can reach up to 99% hydrolysis. It has been used in the medical and industrial sectors, as PVA is biocompatible due to its low toxicity and minimal cell adhesion to its surface. PVA being soluble in water makes it suitable as support material for printing complex objects by forming a support structure. Initially, PVA rafts can be printed or dual extrusion printing techniques can be used to fill voids or intricate fine details during the print. The finished object can then be immersed in water to dissolve the PVA and leave the other extruded polymer in place. Rubber elastomer filaments made up of PVA with another polymer, sold under name of "Lay-felt", are commercially available to produce micro-porous objects as end products by immersing printed objects in water.

PCL is polymerized from a caprolactone (a five member ring cyclic ester) monomer by ring opening catalyzed by stannous octoate. PCL is hydrophobic and soluble in chloroform, carbon tetrachloride, cyclohexanone, benzene, and toluene. PCL biodegrades in the presence of microorganisms. It has a low glass transition temperature of -60°C [16], which makes it less brittle than other polymers with glass transition temperatures above room temperature. As PCL has low MP, it has low processing temperatures especially when mixed with other materials to form composites.

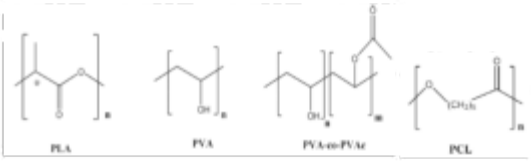

Figure 3 Structures of PLA, PVA, PVA-co-PVAc and PCL

Table 1. Comparative study of common thermoplastic polymers

Polymer	ABS	PLA	PVA	PCL
Extrusion Temp.	220 to 235°C	180 to 220°C	190 to 220°C	Very low
Degradation Temp.	400°C	210 to 240°C	-	-
Melting Point (Tm)	250°C	130 to 180°C	200°C	59 to 64°C
Glass Transition Temp.(Tg)	80 to 125°C	40 to 70°C	85°C	-60°C
Tensile Strength	30 to 55 MPa	48–52 MPa	17 to 51 MPa	10.5 to 16.1 MPa
Elastic/Tensile Modulus	897 to 2898 MPa	3500 MPa	443 to 1470 MPa	344 to 364 MPa

IV. CARBON NANOTUBES (CNTs)

Carbon nanotubes can be mixed into polymers as they possess very good mechanical, electrical, and thermal properties and can be used for 3D printing. Multiwall CNTs (MWCNTs) have structural defects which provide suitable nucleation sites that allow for strong interactions with polymers [17] and for cross-linking and functionalization [18–20]. A homogeneous dispersion of carbon nanotubes in polymeric solutions are essential if they are to be used for enhanced CNT based filaments. Aggregation of CNTs can be a problem for FDM, possibly causing blockages at the nozzle and flux instability while printing. Hence research can be made in determining the concentration of CNTs to surpass the percolation threshold (the transition between an insulating and conductive polymer) while maintaining the parameters for 3D printing.

The theoretical concentration of carbon nanotubes required to reach the electrical percolation threshold for a CNT/Polymer composite can be obtained, as a first step, by the use of the power law:

$$\sigma \propto (\varphi-\varphi_c)^n$$

Where σ is the electrical conductivity, φ is the MWCNT volume concentration in the nanocomposites, φ_c is the critical MWCNT volume concentration at electrical percolation and α is a critical exponent[6]. A comprehensive table of percolation thresholds for CNTs in polymer matrices was assembled by Bauhofer et al. [21]. It was also noted by Bauhofer that there were conflicting results concerning the dependence of the percolation threshold on the aspect ratio. The excluded volume analysis conducted by Celzard et al. showed that the percolation threshold of a fiber suspension would decrease when the aspect ratio increased[22]. Research by Bai et al. demonstrated a decreasing set of values for the percolation threshold when the CNT length increased [23]; Martin et al. [24] found an increasing percolation threshold when the CNT length increased. This problem can be reconciled by considering the type of percolation thresholds. Bai et al. possibly obtained statistical thresholds while Martin et al. acquired kinetic percolation. This is important to know as theoretical analyses reported tend to ignore the movement of filler particles and only seem to predict the dependence of the statistical percolation threshold on the filler aspect ratio.

Ultrahigh molecular weight polyethylene (UHMWPE) has been processed with MWCNTs and extruded to produce filaments [25]. However, it is not feasible to produce UHMWPE filaments by conventional extrusion due to the high Weissenberg effects [26] that would likely affect the flux during extrusion both for filament production and 3D printing. An alternative would be to use the gel-spinning technique [27] in which the polymer is dissolved and spun. The addition of MWCNTs can be problematic as they tend to aggregate during the solvent evaporation stage, but the problems were addressed by using a range of techniques including sonication, melt mixing and extrusion [25].

The compatibilization of a polymer is simply the addition of a material to immiscible blends of polymers resulting in an increase in stability. Compatibilized polyolefin rubber is an example of a composite that can be made conductive by the addition of carbon nanotubes [28] or graphene. The percolation threshold has been widely studied with carbon nanotube systems [29,30]. The study of PC, ABS and MWCNT composites confirmed that localization of MWCNTs changes from the ABS to the PC phase when the rubber content was reduced from 60 to 5% [31]. At low concentrations of rubber, MWCNTs localized in the PC phase resulting in an increase in conductivity and a low percolation threshold of around 0.5–1 wt% [29].

Ternary systems could be an important framework for developing advanced 3D printing materials. With the ternary mixture of PCL, PLA and MWCNT, it has been shown that the localization of carboxylic functionalized nanotubes can be identified at the PCL phase and at the phase interface. When the MWCNTs are not functionalized, they can only be located at the PCL phase resulting in an elevated percolation threshold. Ternary composites exhibit conductivities that are 3–4 orders higher than binary composites when the MWCNT content reaches 1 wt% [32]. Potschke et al. developed a method to mix MWCNTs into thermoplastic matrices of PC and polyamide-6 (PA6) by melt blending the PE based master batch with high MWCNT loading. This improved the CNT dispersion in PC and PA6 and also reduced the percolation threshold[33]. In general, there are many strategies that can be applied to the mixing of CNTs with polymers.

Postiglione et al. reported the assembly of conductive 3D structures using a PLA/MWCNT nanocomposites using liquid deposition modeling (LDM) with dichloromethane (DCM)[6].They reported a percolation threshold concentration of 0.67% with a conductivity of 10 S/m and the highest conductivity was obtained with 5 wt% MWCNT with 100 S/m. Postiglione found that at a composition of 35% PLA in DCM with 1 wt% MWCNT, the rheological effects prevent the extrusion through the 3D printer as a higher pressure from the extrusion assembly would be required. Nanocomposites made from 25 wt% of PLA in DCM with 1 wt% MWCNTs can be printed out at a lower shear stress with a higher shear rate ($1–50\ s^{-1}$) when compared to 30 wt% PLA in DCM with 1 wt% MWCNTs (shear rates $5–11\ s^{-1}$). Although the 25 wt% PLA/CNT mixture prints at a higher speed, a better resolution product was obtained using a 30 wt% PLA/CNT mixture at $10s^{-1}$ and a low speed of $0.1\ mm\ s^{-1}$

Grafting of single wall carbon nanotubes SWCNTs to poly(L-lactic acid) has been investigated[34] but so far MWCNTs are dominant, possibly due to their increased metallic character. However, Vatani et al. reported the fabrication of a highly stretchable sensor by dispersing 1wt% SWCNT (average diameter 1.5 nm, length 1–5 micrometer) in a matrix of a blend of two photo curable monomers (cyclic trimethylolpropane formal acrylate and acrylate ester)[35].The monomers/SWCNT composite was printed using direct writing into a polyurethanesubstrate on which the monomers were photo cured. The wires sustained strain up to 90% elongation and resistivity change increased proportionally with the strain.

Production of CNTs

Researchers are behind development of stronger and highly efficient carbon nanotube based composites material for use in 3D printing.

Production capacity of multi-walled tubes by Timesnano and Showa Denko, each producing over 2500 metric tons every year. Still demand of CNTS with conductive adhesives and fire retardant plastics. [36]. In 2015, over 400 metric tons of MWCNTs were used for conductive polymer composites with estimates reaching 1700 metric tons by the year 2020.

Carbon nanotubes have attracted researchers toward the development of prototypes and will continue to promote innovation over the next decade. The legacy of carbon nanotubes for nanotechnology may prove to be an important milestone.

Commercial CNT materials for 3D printing

3DXTech is a company that provides filaments containing carbon nanotubes. Their 3DXNano™ ESD ABS filaments (containing MWCNTs) are available with diameters of 1.75 mm and 2.85 mm for ESD applications. The filament is produced using MG-94 Premium ABS and mixed with MWCNTs and process/dispersion modifiers.

Table 2. Study of 3DXNano™ polymer

Polymer	Extrusion Temp.	FDM Platform Temp.	Surface Resistance	Tensile Strength
3DXNano™	220 to 240°C	100 to 110°C	107 to 109 Ω	42 MPa

Nanocyl are one of the worldwide leading experts in CNT based materials, producing research and industry grade carbon nanotubes. One of their product lies, PLASTICYL™, is a collection of carbon nanotubes thermoplastic concentrates for applications requiring electrical conductivity with good mechanical properties. The concentrates contain 10–20% of carbon nanotubes and are available in a diverse range of thermoplastic resins, including PC, PP, PA, PET, HDPE and others. Although these enhanced thermoplastics were not specifically aimed at the FDM sector, they have a formulation that makes them applicable, subject to the temperature range of the extruder. PLASTICYL™ can be used in many applications and a surface resistivity range of 1 to 1012 Ω

F-Electric is a PLA-based filament produced by 'Functionalize' that incorporates carbon nanotubes. F-Electric is one of the best conductive 3D filament available in the market with a 0.75 Ω-cm in volume resistivity.

Filament production

3D printing can produce a lot of waste from failed prints, supports and rafts. Recycling these materials can be highly effective in reducing the costs of printing. The process of reusing filaments is further

complicated by the need to break down the waste so that it can be successfully channeled through a feed screw to the melting chamber (surrounded by a heater) as shown in Figure 4. Extruded filaments can be collected on automated Spooler, allowing the spool to be detached and connected to a 3D printer when completed. Graphene exhibits a range of exceptional qualities including flexibility and conductivity. 3D printing filaments with graphene have the potential to enhance the manufacturing process of strong conductive composites. There are many applications of these carbon nanostructured additives in 3D printer filaments including sensors, track pads, electromagnetic and RF shielding.

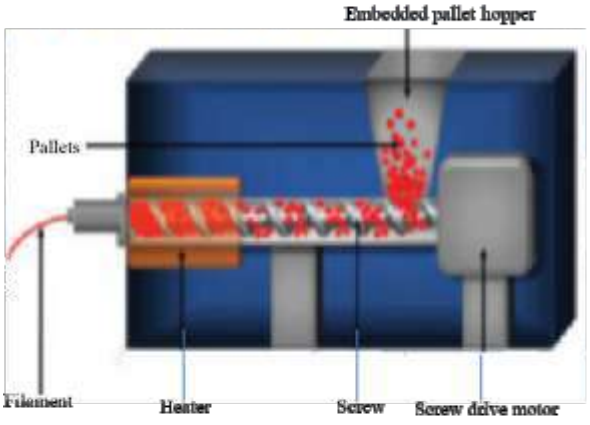

Figure 4 Diagram of a filament making

Polymer integration

The use of graphene in 3D printing started with the Canadian company Grafoid, resulting in the product MesoGraf, which is produced from raw and unprocessed graphite ore in a one-step process. Use of graphene in 3D printing will increase its conductivity and strength.

There are some limitations with current 3D printing technology, especially when attempting to produce filaments with advance functional materials such as metals, graphene and carbon nanotubes. Problems may be associated with the size of particles and temperature variations of the constituents within a polymer matrix.

Research is still ongoing into making FDM more applicable to producing advanced functional 3D printed materials. The researchers are using a combination of graphene enhanced and carbon nanotube enhanced 3D printing materials to improve the properties. Researchers are also focusing on modifying polymers with graphene [37]. Although graphene has also been referred to as a remarkable material, homogeneous mixtures of graphene and polymers are essential to get the unique properties [38]. Wei et al. stated that the major problem confronted by graphene composites was that of phase separation between graphene sheets. They addressed the problem with the use of graphene oxide (GO) to substitute graphene as the additive. GO contains oxygenated functional groups on its basal planes, which may assist graphene's dispersion in polymer phases [39].

Figure 5 Graphene infused PLA pellets and 1.75 mm filaments.

Conductive graphene filaments and pellets (Figure 5) for 3D printing contain highly conductive proprietary nanocarbon materials with PLA. Both the filaments and pellets extruded are compatible with commercially available FDM printers. The volume resistivity is listed as 1Ω-cm which provides an excellent starting point for 3D printed circuitry and capacitive touch sensors.

Research by Seung Kwon Seol of the Korea Electrotechnology Research Institute has demonstrated a process that is capable of 3D printing of pure graphene nanostructures [40]. This achievement marked the first time graphene has been printed by itself without being used as the additive. The research available in the journal 'Advanced Materials' shows potential for expansion once the challenges such as reducing the size of the extruded material and increasing the yield are addressed.

V CARBON STRUCTURED ADDITIVES

Carbon Nanotubes and Graphene are some of the popular choices as additives for 3D printing, but carbon black (CB) and carbon fibres are unique carbon structured additives that have an extensive history in manufacturing, tailoring the properties of composites for electronic applications and structural reinforcement respectively.

Carbon black

Appearance of CB is soot like but differs from soot at the molecular level. CB is produced from the incomplete combustion of heavy petroleum products such as coal tar. It is readily available and inexpensive. It is considered as one of the most popular conductive additives because of its low cost and chemical stability [41].

A conductive thermoplastic composite called 'carbomorph' which can be extruded through a consumer 3D printer.[16] In this work, Leigh et al. reported on the 3D printing of a piezo-resistive sensor from a composite of PCL with 15 wt% of CB as filler. Leigh stated that the transition from insulating to non-insulating behavior for composites with conductive filler is generally observed when the volume concentration of filler reaches a threshold of around 25% [42]. However, their decision to use 15 wt% CB was based on optimization, considering the thermal and rheological parameters required for successful printing. The thermoplastic polymer selected for the composite was the polymorph PCL. Bending the sensor resulted in a change of resistivity of 4%. The conductivity of the printed filament made from the PCL/CB composite was 11.1 S/m, which falls within the range of semiconductors.

Resistance was tested using 5 mm cubes of carbomorph by two-probe measurements with the two opposite cube

faces (painted with silver conductive paint). The resistivity of the composite, in-plane with the layers was 0.09±0.01 Ω m^{-1} and perpendicular to the layers, the resistivity was 0.12±0.01 Ω m^{-1}. This is a significant observation as the reduction in the resistivity of 25% from the perpendicular to parallel orientation is a feature that needs to be considered for the next generation of functional composites. The plane of the layers of the printed filaments provides an unperturbed conductive pathway between the electrodes, while perpendicular to the layers, the conductive pathway depends upon the connection between successive layers.

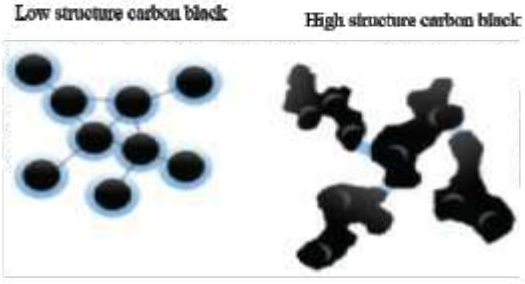

Figure 6. Low-structure and high-structure carbon black. Figure adapted from Balberg [43].

Work by Balberg into the electrical phenomena in CB polymer composites looked at the difficulties in establishing the percolation threshold for the incorporation of CB into polymers [43]. While he noted that previous studies in his reviews had explained the electrical data within the confines of inter-particle tunneling conduction[43] and/or that of classical percolation theory, the observations were far more convoluted. He noted that for different types of CB, the same volume percent of the CB phase in the composite produces different values for the resistivity [44, 45]. By investigating the characteristics, Balberg stated that the values of the (apparent) percolation threshold and the (apparent) percolation critical resistivity-exponent depended strongly on the particular type of CB. The particles could be treated in terms of how spherical-like they look, with more spherical CB particles termed 'low structure' CB, in comparison to 'high-structure' CB. Closely packed network of spheres representing the low structure in a polymer composite with nearest neighbor tunneling. The black spherical structures are the CB particles, and the blue shells represent the tunneling distance. The nearest-neighbor connections (black lines) indicate the dominant conducting elements that result in percolation-like behavior.

Figure 6 also shows a high-structure CB polymer composite. The distances between the nearest inter-particle surfaces have a narrow, non-diverging distribution of the tunneling resistor values in the network. PLA filaments with CB as an additive are commercially available. Protopasta offers filaments that have a volume resistivity of 15 Ω·cm, resulting in 3D prints that are 30 Ω·cm perpendicular to the layers and 115 Ω·cm through the layers.

Carbon fiber

Carbon fibers plays a very important role in reinforcement of composite materials because of their high tensile strength, low weight and low thermal expansion. FDM has one limitation of low transfer of strength in the printed composites, but the use of carbon fibers in 3D printing can create high strength composites. Ning et al. reported printing out parts from an ABS/carbon fiber composite with different percentages by weight. The highest tensile strength reported for a 5 wt% composite of carbon fibers in ABS, printed using FDM was 42 MPa [46]. The tensile strength dropped as the percentage of carbon fiber increased to 10 wt%. The ductilities of all composites were less than the pure ABS. The 7.5 wt% carbon fiber composite had the largest value for the Young's modulus. The reduction in the tensile strength and ductility of composites exceeding 10 wt% was due to the higher porosity of those composites.

A new start-up, MarkForged Inc., has been working on improving the integration of carbon fibers. The company has developed a new printer which uses two separate print heads. The first head dispenses a polymer such as nylon or PLA, while the other dispenses a carbon fiber tow which is a coated thermoplastic. As the carbon fiber can be introduced during any part of the print process, composites can be produced without reinforced sections. MarkForged reported that tests demonstrated that the parts produced were stronger than 6061-T6 aluminum.

Carbon fiber filaments are also offered by Proto-pasta with fibers mixed with PLA. Proto-pasta states that the abrasive nature of the filament may cause the extrusion nozzle to fail prematurely.

VI. ELECTRICAL CONDUCTIVITY OF SWCNTs & MWCNTs

Polymers are having relative dielectric constant in the range of 2–5 and very low electrical conductivity < 10-12 S/cm. Electrical properties of the polymers can be improved by embedding them with different types of filler. [47-53]

As per study of Wong et al. [54] the addition of conductive fillers such as metallic particulates/fibers, carbon black and carbon nanotubes to the polymer matrices, above a percolation threshold, increases the conductivity abruptly. [54-59] Practical realization of such polymeric composites still needed practice to make them electrically improved at small filler concentrations so that they can retain the mechanical properties of pure polymers and not suffer from brittle behavior.

The addition of fillers with a high aspect ratio showed percolation at a very low concentration,[60] e.g., 0.04 wt.% silver nanowire (aspect ratio = 85) for the polycarbonate (PC)/silver nanowire nanocomposites.[61] Carmona[55] showed the percolation dependency on the polymer matrices for a given carbon black filler.

SWCNTs and MWCNTs have been used as conducting fillers due to their high aspect ratio which results in low percolation threshold with good conductivity for the polymer nanocomposites. [62-66]

Po¨tschke et al.[67] studied and stated that the dielectric properties of melt processed PCMWCNTs nanocomposites depends upon the type of processing methods, type, size, shape and dispersion of fillers in the matrices.

Inherent conductive polymers possess inadequate mechanical properties and processability. [68] Therefore, PC based nanocomposites with good mechanical properties and dimensional stability would be potential candidates for the electronic applications.

Table 3. Comparative Study of PCSWCNTs & PCMWCNTs

TECHNIQUE	PCSWCNT	PCMWCNT
XRD	Confirms the presence of MWCNT and SWCNT	
TEM	Less impurities	More impurities
HRTEM	Assembled into bundles which consist of few tens of SWCNTs	Several graphene sheets coaxially arranged with an outer diameter of about 20 nm.
SEM	Less number of pores indicates better adhesion	more number of pores indicates poor adhesion
	CNTs are well connected together and distributed uniformly in the PC matrix.	
PROPERTY		
Electrical Conductivity	10^{-4} S/cm	
Percolation Threshold	0.5 vol. % (1 wt. %)	4 vol. % (7.8 wt. %)
Aspect ratio	Higher	Lower
Entanglement	Much higher	Much Lower
Impurity level	Much Lower	Much Higher

With increase in the vol. % of SWCNT or MWCNT above a critical vol. % (i.e. percolation threshold), the nanocomposites become electrically conductive. Study of Hornbostelet al. and Po¨tschke et al. [62, 64] states that the percolation was occurred at around 0.5 vol. % (1 wt. %) for SWCNT/PC nanocomposites, prepared by melt extrusion using untreated SWCNT and SWCNT treated with carboxyl group. Chen et al. [63] studied the MWCNT filled PC nanocomposites and found the percolation at about 5 wt. % which is less than that of present findings. The higher value of percolation is due to presence of some impurities in the MWCNT sample as per TEM image. The maximum achieved AC conductivity of both the CNT/PC nanocomposites was about 10^{-4} S/cm (as against 10^{-9} S/cm for control PC). This result indicates that addition of a small amount of CNT has improved the electrical conductivity of the nanocomposites by more than five orders of magnitude compared to PC matrix.

DISCUSSION

In the field of nanotechnology, a multi-disciplinary field of additive manufacturing covers many aspects of chemistry, physics and engineering. Areas of development in AM are advancements in the composition of the filaments/material, pellets and resins for printing; and the equipment used for filament production. 3D printing of bio-inspired materials can be considered as the best example for the same. Kang et al. recently produced life-sized body parts and tissues with living cells acting as the printing materials. The parts were stable enough to be used as viable replacements that could be tailored to individual needs rather than generic replacements [47].

Temperature range of the extruder assembly is a limitation for consumer thermoplastic extrusion. Entry level printers can work with ABS and PLA filaments with the nozzle temperatures in the range of 230–240°C. The latest generation of extruders such as the E3D V6 , where a hot end can withstand a high temperature extrusion up to 300°C to 400°C when the thermistor is exchanged for a thermocouple. For polycarbonate and nylon based filaments, elevated temperature is essential when addition of CNTs and Graphene will be done as an additive in 3D Printing. Sometimes high temperature would create few problems with mixed materials. At higher temperatures, polymers may degrade and the carbon nanostructured additives may cause unfavorable results during extrusion. Stratasys offer a proprietary product called Digital Materials which are a range of several hundred combinations of PolyJet base resins. The Objet260 Connex 3D printing platforms use the PolyJet resin and are capable of depositing three materials with a layer thickness of 16 μm. The build resolution is 600 dpi on both the X-axis and Y-axis, and 1600 dpi on the Z-axis.

The difficulty in producing mixed material filaments with carbon nanostructures and the additional problems associated with the rheology and flux during FDM extrusion are giving birth to other additive manufacturing techniques such as the PolyJet system. Carbon nanotubes, graphene and CB have been explored as additives for SLS [48–50]. Creating a homogeneous distribution of the carbon nanostructures is the main issue, but this can be achieved by simple mixing techniques. Paggi et al. reported on the process for the optimization of PA12/MWCNT nanocomposites by SLS [48]. They described a procedure for dispersing the MWCNT powder initially in chloroform using ultrasonic techniques for one hour. They added the polyamide powder to the suspension and continued mixing on a magnetic stir plate for 50 min to homogenize the solution. After a filtration process with a cellulose filter, the mixture was washed with acetone and placed in an oven at 80°C for four hours. Rotary blades were then used to homogenize the final powder. A CO_2 laser (10 watts) with a beam diameter of 250 μm was used to fuse the powder. Pulsed mode was used to operate the laser at 5 kHz and the average layer thickness produced was 200 μm.

Today's and tomorrow's market scenario of AM-

Few additive manufacturing processes show good potential for growth from 2014 to 2019. The worldwide market for 3D printing, including the services sector, will likely increase at a compound annual growth rate (CAGR) of 32.2% from 2014 to 2019. BCC Research also estimates that 'services' will reach to $7.8 billion in 2019 with a CAGR of 31.4% from 2014 to 2019 [51].

Table 3. Today's and tomorrow's market scenario of AM

AM Process	Worldwide Revenue generation	CAGR (%)
Stereolithography	$1.8 billion	27.3
PolyJet	$334 million	40.7
FDM	$1 billion	30

SLS	$504 million	32.3

The major advantage in this 3D printing market is the high level of diversification in the technology and applications. Advances in the design and function of 3D printers have catalysed the development of multi-material filaments and printing techniques that overcome some of the limitations of the durability of printed composites. 3D printing may also have a pronounced effect on more traditional manufacturing processes, affecting many aspects from the design and development of materials to the cost savings through the rapid production of custom parts. For consumers, it is the potential to be able to print replacement parts for household appliances.

SUMMARY

Polymer composites with conductive fillers/additives have the potential to be used in many areas from engineering to consumer product development, with tunable properties that include elasticity, durability, water wettability (hydrophobic/hydrophilic) and conductance.

The use of conductive filler material such as metal in polymer [52] having advantageous but there is a difficulty in the processability of the composite which may affect the quality and resolution of the 3D object. To overcome this & to reach upto a workable conductivity, the percentage weight of filler may need to increase, which causes an increase in the density and viscosity of the composite. The addition of the filler affects the rheological properties of the polymer. Metallic fillers are usually susceptible to oxidation and most of the conductive fillers used are in a 5–120 μm diameter range, which can be a challenge by itself causing blockages at the nozzle opening of most types of FDM printers, which typically have a nozzle diameter of 400 μm.

REFERENCES

[1] Gross BC, Erkal JL, Lockwood SY, Chen CP, Spence DM. Evaluation of 3D printing and its potential impact on biotechnology and the chemical sciences. Anal Chem. 2014; 86(7):3240–53.Carbon Nanotubes and Graphene as Additives in 3D Printing http://dx.doi.org/10.5772/63419247

[2]D.K.Shinde, L.Emmanwori, A.D.Kelkar - Soc. for the Advancement of Material and process,2014; Journal-4TH ISTC-WICHITA, KS oct, Compression of mechanical properties of EPON 862/W with and without teos electrospun nanofibers in nanocomposites

[3]D K Shinde, A D Kelkar - World Academy of Science, Engineering and Technology, International Science Index, 2014;Journal volume 85,Pages 53-62. Effect of TEOS electrospun nanofiber modified resin on interlaminar shear strength of glass fiber/epoxy composite

[4] Bai JM, Goodridge RD, Yuan SQ, Zhou K, Chua CK, Wei J. Thermal influence of CNT on the polyamide 12 nanocomposite for selective laser sintering. Molecules.2015; 20(10):19041–50.

[5] Shallan AI, Smejkal P, Corban M, Guijt RM, Breadmore MC. Cost-effective three dimensional printing of visibly transparent microchips within minutes. Anal Chem.2014; 86(6):3124–30

[6] Lin D, Jin S, Zhang F, Wang C, Wang Y, Zhou C, et al. 3D Stereolithography printing of graphene oxide reinforced complex architectures. Nanotechnology. 2015; 26(43):434003.

[7] Lawes S, Riese A, Sun Q, Cheng NC, Sun XL. Printing nanostructured carbon for energy storage and conversion applications. Carbon. 2015; 92:150–76.

[8] Postiglione G, Natale G, Griffini G, Levi M, Turri S. Conductive 3D microstructures by direct 3D printing of polymer/carbon nanotube nanocomposites via liquid deposition modeling. Composites A Appl Sci Manufact. 2015; 76:110–4.

[9] McWilliams A. Advanced materials for 3D printing: Technologies and global markets. BCC Res. 2014

[10] Stephens B, Azimi P, El Orch Z, Ramos T. Ultrafine particle emissions from desktop 3D printers. Atmos Environ. 2013; 79:334–9.

[11] Turner BN, Strong R, Gold SA. A review of melt extrusion additive manufacturing processes: I. Process design and modeling. Rapid Prototyp J. 2014; 20(3):192–204.

[12] Gebler M, Uiterkamp A, Visser C. A global sustainability perspective on 3D printing technologies (vol 74, p. 158, 2014). Energy Policy. 2015; 85:511.

[13] Garlotta D. A literature review of poly (lactic acid). J Polym Environ. 2001; 9(2):63–84.

[14] Al-Itry R, Lamnawar K, Maazouz A. Improvement of thermal stability, rheological and mechanical properties of PLA, PBAT and their blends by reactive extrusion with functionalized epoxy. Polym Degrad Stabil. 2012; 97(10):1898–914.

[15] Pelegrini K, Donazzolo I, Brambilla V, Grisa AMC, Piazza D, Zattera AJ, et al. Degradation of PLA and PLA in composites with triacetin and buriti fiber after 600 days in a simulated marine environment. J Appl Polym Sci. 2016;133(15):43290.

[16] Leigh SJ, Bradley RJ, Purssell CP, Billson DR, Hutchins DA. A simple, low-cost conductive composite material for 3D printing of electronic sensors. PLoS One. 2012; 7(11).248 Carbon Nanotubes - Current Progress of their Polymer Composites

[17] McCarthy B, Coleman JN, Curran SA, Dalton AB, Davey AP, Konya Z, et al. Observation of site selective binding in a polymer nanotube composite. J Mater Sci Lett. 2000; 19(24):2239–41.

[18] Gao YL, Zhai QJ, Barrett R, Dalai NS, Kroto HW, Acquah SFA. Piezoelectric enhanced cross-linked multi-walled carbon nanotube paper. Carbon. 2013; 64:544–7.

[19] Steven E, Saleh WR, Lebedev V, Acquah SFA, Laukhin V, Alamo RG, et al. Carbon nanotubes on a spider silk scaffold. Nat Commun. 2013; 4.

[20] Ventura DN, Stone RA, Chen KS, Hariri HH, Riddle KA, Fellers TJ, et al. Assembly of cross-linked multi-walled carbon nanotube mats. Carbon. 2010; 48(4):987–94.

[21] Bauhofer W, Kovacs JZ. A review and analysis of electrical percolation in carbon nanotube polymer composites. Compos Sci Technol. 2009;69(10):1486–98.

[22] Celzard A, McRae E, Deleuze C, Dufort M, Furdin G, Marêché JF. Critical concentration in percolating systems containing a high-aspect-ratio filler. Phys Rev B. 1996;53(10): 6209–14.

[23] Bai JB, Allaoui A. Effect of the length and the aggregate size of MWNTs on the improvement efficiency of the mechanical and electrical properties of nanocomposites-experimental investigation. Compos A Appl Sci Manufact. 2003;34(8):689–94.

[24] Martin CA, Sandler JKW, Shaffer MSP, Schwarz MK, Bauhofer W, Schulte K, et al.Formation of percolating networks in multi-wall carbon-nanotube–epoxy composites.Compos Sci Technol. 2004;64(15):2309–16.

[25] Mahfuz H, Khan MR, Leventouri T, Liarokapis E. Investigation of MWCNT reinforcement on the strain hardening behavior of ultrahigh molecular weight polyethylene. J Nanotechnol. 2011;2011:9.

[26] Smook J, Pennings AJ. Suspension spinning of ultrahigh molecular-weight polyethylene.Polym Bull. 1983;10(7–8):291–7.

[27] Pakhomov PM, Golikova AY, Khizhnyak SD, Shavyrina MA, Galitsin VP, Gribanov SA, et al. The structure of high-strength ultrahigh-molecular-weight polyethylene fibres fabricated by the gel-spinning method. Fibre Chem. 2006;38(3):200–6.

[28] Dever F, Baez E, Shanks RA, Brandt M. Conductive polyolefin-rubber nanocomposites with carbon nanotubes. Compos A Appl Sci Manufact. 2016;80:13–20.

[29] Besco S, Modesti M, Lorenzetti A, Donadi S, McNally T. Effect of modified clay on the morphology and electric properties of PC/ABS-MWCNT composites. J Appl Polym Sci. 2012;124(5):3617–25.

[30] Ji MZ, Deng H, Yan DX, Li XY, Duan LY, Fu Q. Selective localization of multi-walled carbon nanotubes in thermoplastic elastomer blends: An effective method for tunable resistivity-strain sensing behavior. Compos Sci Technol. 2014;92:16–26. Carbon Nanotubes and Graphene as Additives in 3D Printing http://dx.doi.org/10.5772/63419249

[31] Sun Y, Guo Z-X, Yu J. Effect of ABS rubber content on the localization of MWCNTs in PC/ABS blends and electrical resistivity of the composites. Macromol Mater Eng.2010;295(3):263–8.

[32] Wu D, Zhang Y, Zhang M, Yu W. Selective localization of multiwalled carbon nanotubes in poly(ε-caprolactone)/polylactide blend. Biomacromolecules. 2009;10(2):417–24.
[33] Pötschke P, Pegel S, Claes M, Bonduel D. A novel strategy to incorporate carbon nanotubes into thermoplastic matrices. Macromol Rapid Commun. 2008;29(3):244–51.
[34] Olalde B, Aizpurua JM, Garcia A, Bustero I, Obieta I, Jurado MJ. Single-walled carbon nanotubes and multiwalled carbon nanotubes functionalized with poly(L-lactic acid): a comparative study. J Phys Chem C. 2008;112(29):10663–7.
[35] Vatani M, Lu Y, Lee K-S, Kim H-C, Choi J-W. Direct-write stretchable sensors using single-walled carbon nanotube/polymer matrix. J Electr Packag. 2013;135(1):011009.
[36] Davenport M. Twists and shouts: A nanotube story. Chem Eng News. 2015;93(23):10–5.
[37] Barletta M, Puopolo M, Tagliaferri V, Vesco S. Graphene-modified poly(lactic acid) for packaging: Material formulation, processing and performance. J Appl Polym Sci. 2016 ;133(2).
[38] Huang X, Qi XY, Boey F, Zhang H. Graphene-based composites. Chem Soc Rev.2012;41(2):666–86.
[39] Wei XJ, Li D, Jiang W, Gu ZM, Wang XJ, Zhang ZX, et al. 3D printable graphene composite. Sci Rep. 2015 ;5.
[40] Kim JH, Chang WS, Kim D, Yang JR, Han JT, Lee GW, et al. 3D printing of reduced graphene oxide nanowires. Adv Mater. 2015;27(1):157–61.
[41] Soares BG, Touchalenmane F, Calheiros LF, Barra GMO. Effect of double percolation on the electrical properties and electromagnetic interference shielding effectiveness of carbon-black-loaded polystyrene/ethylene vinyl acetate copolymer blends. J Appl Polym Sci. 2016 ;133(7).
[42] Rebouil JP, Moussalli G. About some DC conduction processes in carbon-black filled polymers. Int J Polym Mater. 1976;5(1–2):133–46.f
[43] Balberg I. A comprehensive picture of the electrical phenomena in carbon black–polymer composites. Carbon. 2002;40(2):139–43.
[43] Balberg I. Tunneling and nonuniversal conductivity in composite-materials. Phys Rev Lett. 1987;59(12):1305–8.250 Carbon Nanotubes - Current Progress of their Polymer Composites
[44] Rubin Z, Sunshine SA, Heaney MB, Bloom I, Balberg I. Critical behavior of the electrical transport properties in a tunneling-percolation system. Phys Rev B. 1999;59(19):12196–9.
[45] Sichel EK, Gittleman JI, Sheng P. Transport properties of the composite-material carbon-poly(vinyl chloride). Phys Rev B. 1978;18(10):5712–6.
[46] Ning F, Cong W, Qiu J, Wei J, Wang S. Additive manufacturing of carbon fiber reinforced thermoplastic composites using fused deposition modeling. Compos B Eng. 2015;80:369–78.
[47] J.R. Yoon, J.W. Han, K.M. Lee, and H.Y. Lee, Trans. Electr. Electron. Mater. 10, 116 (2009).
[48] J. Xu and C.P. Wong, J. Electron. Mater. 35, 1087 (2006).
[49] V. Singh, A.R. Kulkarni, and T.R. Rama Mohan, J. Appl.Polym. Sci. 90, 3602 (2003).
[50] A. Qureshi, A. Mergen, M.S. Erog˘ lu, N.L. Singh, and A.Gu¨ lu¨og˘ lu, J. Macromol. Sci., Pure Appl. Chem. 45, 462(2008).
[51] Y.J. Li, M. Xu, and J.Q. Feng, Appl. Phys. Lett. 89, 072902(2006).
[52] E.S. Lim, J.C. Lee, J.J. Kim, E.T. Park, Y.K. Chung, and H.Y. Lee, Integr. Ferroelectr. 74, 53 (2005).
[53] L. Dai, Conducting Polymers (London: Springer, 2004), p. 41.
[54] J. Xu, M. Wong, and C.P. Wong, IEEE Electron. ComponentTechnol. Conf. (2004). doi:10.1109/ECTC.2004.1319391.
[55] F. Carmona, Phys. A 157, 461 (1989).
[56] A. Boudenne, L. Ibos, M. Fois, J.C. Majesté, and E. Ge´hin,Compos. A 36, 1545 (2005).
[57] Y.P. Mamunya, V.V. Davydenko, P. Pissis, and E.V.Lebedev, Eur. Polym. J. 38, 1887 (2002).
[58] A.S. Luyt, J.A. Molefi, and H. Krump, Polym. Degrad.Stab. 91, 1629 (2006).
[59] I. Balberg, Phy. Rev. Lett. 59, 1305 (1987).
[60] A.E. Eken, E.J. Tozzi, D.J. Klingenberg, and W.J. Bauhofer,J. Appl. Phy. 109, 084342 (2011).
[61] I. Moreno, N. Navascues, S. Irusta, and J. Santamari´a, IOP Conf. Ser.: Mater. Sci. Eng. 40, 012001 (2012).
[62] P. Po¨tschke, G.M. Abdel, I. Alig, S. Dudkin, and D. Lellinger,Polymer 45, 8863 (2004).
[63] L. Chen, X.J. Pang, and Z.L. Yu, Mater. Sci. Eng., A 457,287 (2007).
[64] B. Hornbostel, P. Po¨tschke, J. Kotz, and S. Roth, Phys.Status Solidi B 243, 3445 (2006).
[65] P. Po¨tschke, T.D. Fornes, and D.R. Paul, Polymer 43, 3247(2002).
[66] P. Po¨tschke, B. Hornbostel, S. Roth, U. Vohrer, S. M.Dudkin,and I. Alig. AIP Conference Proceedings (2005). doi:10.1063/1.2103938.
[67] P. Po¨tschke, S.M. Dudkin, and I. Alig. Polymer 44, 5023(2003).
[68] R.K. Goyal and A. Kadam, Adv. Mater. Lett. 1, 143 (2010).
[47] Kang H-W, Lee SJ, Ko IK, Kengla C, Yoo JJ, Atala A. A 3D bioprinting system to produce human-scale tissue constructs with structural integrity. Nat Biotech. 2016;34(3):312–9.
[48] Paggi RA, Beal VE, Salmoria GV. Process optimization for PA12/MWCNT nanocomposite manufacturing by selective laser sintering. Int J Adv Manuf Technol. 2013;66(9–12):1977–85.
[49] Athreya SR, Kalaitzidou K, Das S. Microstructure, thermomechanical properties, and electrical conductivity of carbon black-filled nylon-12 nanocomposites prepared by selective laser sintering. Polym Eng Sci. 2012;52(1):12–20.
[50] Makuch A, Trzaska M, Skalski K, Bujkowski M. PA-G composite powder for innovative additive techniques. Compos Theory Pract. 2015;15(3):152–7.
[51] Varotto A. Global markets for 3D printing. BCC Res. 2015. Report No.: IAS102A.
[52] Liu H, Webster TJ. Enhanced biological and mechanical properties of well-dispersed nanophase ceramics in polymer composites: From 2D to 3D printed structures. Mater Sci Eng C. 2011;31(2):77–89.
[53] Penkova AV, Acquah SFA, Dmitrenko ME, Sokolova MP, Mikhailova ME, Polyakov ES, et al. Improvement of pervaporation PVA membranes by the controlled incorporation of fullerenol nanoparticles. Mater Des. 2016;96:416–23.
Carbon Nanotubes and Graphene as Additives in 3D Printing http://dx.doi.org/10.5772/63419251

How does the Thermal Degradation influence the spreadability, packing dynamics, and electrostatic behaviour of metallic powder?

Naveen Mani Tripathi,
GranuTools,
Rue Jean-Lambert Defrene,
4340, Awans, Belgium
naveen.tripathi@granutools.com

Filip Francqui
GranuTools,
Rue Jean-Lambert Defrêne,
4340, Awans, Belgium
filip.francqui@granutools.com

Geoffroy Lumay
University of Liège,
Allée du 6 Aout, 4000,
Liège, Belgium
geoffroy.lumay@granutools.com

Abstract- **To answer the need of the Additive Manufacturing (AM) raw material characterization few relevant methods are available in the market. There is a need that the flow field of the powder should be comparable in the process of measurement cell. With this information in mind, GranuTools has developed a workflow for powder characterization. Our main goal is to have one instrument per geometry that mimics the process. In this paper, we have shown how this range of instruments can be used to follow the quality evolution of a powder after several processes. First, the standard aluminium alloys are selected and placed under different thermal stresses. The powders spreadability (GranuDrum Instrument), the packing dynamics (GranuPack Instrument) and the electrostatic behavior (GranuCharge Instrument) were then analyzed. This analysis presents that it is possible to monitor thermal degradation by analyzing the ability of the powder to build-up electrical charge. Indeed, on one hand, a low Cohesive Index is observed for a powder easy to spread and a fast packing dynamics yield a mechanical piece with a lower porosity. However, on the other hand, the powders with high cohesive index at ambient temperature are showing better spreadability and high compaction after thermal degradation, which is highly desirable for the AM.**

Keywords- ***Additive Manufacturing, spreadability, packing dynamics, electrostatic***

I. INTRODUCTION

In Additive Manufacturing (AM) processes, adding one by one superfine layer at a time creates a three-dimensional object. Therefore, the term AM implies adding material to create the object[1,2]. In contrast, if an object is created by classical means, it is often necessary to remove material through milling, machining, etc. However, despite AM is more economic than classical machining. In most cases, only a small proportion of powder that is laid down in a build process is welded into a component. The rest is then unfused and consequently available for reuse. Nonetheless, powders properties should be the first considerations are they govern machine parameters[3]. Indeed, if we consider the unfused powder as contaminated and not adapted for reuse, the cost of AM will not be economic enough. Powder deterioration results in two phenomena:

a) **Products chemistry modification:** Indeed, the main concern is to create solid structures comprised of the pure alloys. Therefore, we must avoid any kind of powder contamination such as oxides or nitrides.
b) **Change in mechanical properties (such as shape/morphology, Particle Size Distribution (PSD)):** In fact, those parameters are related to another key-parameters, which are powders flowability and spreadability. In other words, any modifications in the powder characteristics may result in a product that cannot be evenly distributed across the bed.

Material processed through AM, experience complex thermal process cycle. Therefore, there is a need to better understanding the link between the flow behaviour and processing of the powders and to reduce the variance in properties from machine to machine across materials and machine type [4,5].

II. CONTRIBUTION

Regarding raw materials (or powders) characterisation, few relevant measurement methods are available in the market to answer the needs of AM. Indeed, the stress state and the flow field of the powder should be comparable in the measurement cell and in the process[6]. Different recent publications have evidenced that the classical flowmeters are unable to give pertinent information about powder spreadability in powder-bed-based AM. In addition, the shear cell testers, the classical rheometers, and the existence of a compressive load are incompatible with the free surface flow used in AM devices. AM has a positive impact on the environment by reducing carbon footprints and energy consumption. Therefore, the further work needs to be done. With this information in mind, GranuTools has developed a workflow for powder characterisation for AM[8, 9]. Our main goal is to have one instrument per geometry that mimics accurately and precisely the process.

This research is used to understand and follow the evolution of the quality of a powder after several printing processes. First, several standard aluminium alloys (AlSi10Mg) were

selected and placed for different durations at different thermal stresses (from 100 to 200°C). The powders spreadability (GranuDrum Instrument)[8-10], the packing dynamics (GranuPack Instrument)[11-13] and the electrostatic behaviour (GranuCharge Instrument)[14, 15] were then used to analyse them. It has been proven that it is possible to monitor thermal degradation by analysing the ability of the powder to build-up electrical charge. High electric charge causes bad flowability of powders. Therefore, it is quite important to closely observe the build up charge and the method to control it. Cohesion and packing dynamics measurements are well suited to follow powder quality. Indeed, on one hand, a low Cohesive Index is observed for a powder easy to spread. On the other hand, a powder with a fast packing dynamics will yield a mechanical piece with a lower porosity in comparison with a product harder to pack.

III. MATERIAL METHODS

A. Selected Powders

Three different aluminium alloys powders (AlSi10Mg) (called as sample A, B, and C) and one Stainless Steel 316L (SS 316L) sample with different particle size distribution were selected. The samples grain size distribution were measured by Laser diffraction analysis/ISO 13320, these are the supplier data. The high-resolution image and the available material properties are listed in the following figure 1 and Table 1 respectively.

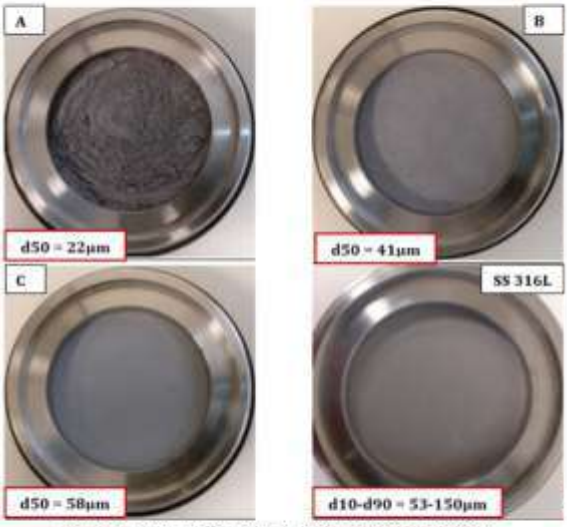

Figure 1. Images of Samples A, B, C and SS 316L powders

S. No.	Materials		d_{50} (µm)	ρ (g/ml)
1	Aluminium alloys powders (AlSi10Mg)	Sample-1	22	1.334
2		Sample-2	41	1.382
3		Sample-3	58	1.380
4	Stainless steel 316L		101	4.544

TABLE 1: MATERIAL PROPERTIES

It is important to note that these powders were stocked in our lab during several months. Therefore, their properties may be slightly different than those communicated by the manufacturers.

B. Methods

According to Snow, topics related to the AM, such as thermal distortion and residual stress and process modeling efforts are received recent attention. However, studies related to the powder feedstock requirements (spreadability) for powder bed fusion and directed energy deposition (electric charges) systems, etc. remain scarce. Recently researchers have begun to investigate the influence of powder characteristics on the AM process. In addition, the standard characterization techniques used in the industry, fail to capture powder characteristics relevant to the AM[16]. Therefore, our first consideration is the powders properties, since they govern machine parameters.

For this purpose, three parameters will be investigated in this research:

i. Powders spreadability
ii. Packing dynamic
iii. Electrostatics.

These parameters also correlate the bulk powder characterizations, such as the powder rheometry, and angle of repose, which gives the indication of spreadability. In addition, utilizing the effect of heat treatment, again these properties (the rheology, spreadability, and triboelectric properties) of the powders are compared.

i. Powders spreadability is the homogeneity and "smoothness" of the powder bed after the recoater operation. This parameter is essential because a smooth surface is easier to print and gives better parts. This parameter will be investigated using the rotating drum instrument (GranuDrum) with the Cohesive Index measurement[8].

ii. Packing dynamic is the second key parameter, because, a powder with fast packing, means a product will low porosity. Since, pores represent weaknesses within the material, they can act as crack initiation sites. This behaviour is measured with the packing dynamics analyser (GranuPack) using the Hausner ratio (Hr).

iii. The powder tribe-electrometer measures the ability of a powder to create electrostatic charges during a flow in contact with a selected material. The presence of electric charges in a powder induces cohesive forces leading to the formation of agglomerates. Moreover, the result/measurement of powder tribe-electrometer is highly sensitive to grains surface state (oxidation, contaminants and roughness). Then, the ageing of a recycling powder can, be quantified precisely (± 0.5nC).

B.1 Spreadability measurement

GranuDrum is an automated powder flowability-measuring instrument, which is based on the method of rotating drum

principle[8-10]. A horizontal cylinder with transparent sidewalls called drum is half filled with the sample of powder. The drum rotates around its axis at an angular velocity ranging from 2 rpm to 60 rpm. A Charge Coupled Device (CCD) camera takes snapshots (30 to 100 images separated by 1s) for each angular velocity. The air/powder interface is detected on each snapshot with an edge detection algorithm. Afterwards, the average interface position and the fluctuations around this average position are computed. Then, for each rotating speed, the flowing angle (also known in the literature as 'dynamic angle of repose') α_f is computed from the average interface position and the dynamic cohesive index σ_f is measured from the interface fluctuations. The morphology of the material affects the angle of repose. Smooth and round particles can't pile up (form low angle of repose) as compared to the small and interlocking particles. The angle of repose ranges from 0° to 90°.

In general, a low value of the flowing angle α_f corresponds to a good flowability. The flowing angle is influenced by a wide set of parameters: the friction between the grains, the shape of the grains, the cohesive forces (van der Waals, electrostatic and capillary forces) between the grains. The dynamic cohesive index σ_f is only related to the cohesive forces between the grains. A cohesive powder leads to an intermitted flow, while a non-cohesive powder leads to a regular flow. Therefore, a dynamic cohesive index closes to zero corresponds to a non-cohesive powder. When the powder cohesiveness increases, the cohesive index increases accordingly.

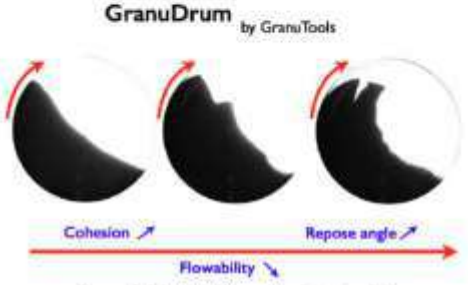

Figure 2. Material flow pattern in GranuDrum

In addition to the measurement of both the cohesive index σ_f and the flowing angle α_f as a function of the rotating speed, the rotating drum allows to measure the first avalanche angle and the powder aeration during the flow.

It is clear from the above figure 2, that moving from left to right, the cohesion increases and therefore the flowability reduces. Taking into consideration the individual figure, we can see that as the cohesion increases the pattern of the inclined surface is tends to be irregular and resulting high angle of repose this is because of high van der wall forces within the particles.

B.2 Packing dynamics measurements

Bulk density, tapped density and the Hausner ratio measurement (commonly named "tap-tap test") are very popular for packing dynamics measurement because of both the simplicity and the rapidity. Hausner ratio is basically correlated with the flowability of powders and granular materials. Moreover, the density and the ability of a powder to increase its density are important parameters for storage, transportation, caking, etc. The recommended procedure is defined in the pharmacopeia. This simple test has three major drawbacks, which are as follows:

- **i.** The result of the measurement depends on the operator. Indeed, the filling method influences the initial powder volume.
- **ii.** The volume measurements by naked eyes are also observer dependent and induce strong errors on the results.
- **iii.** Finally, with this simple method, we completely miss the compaction dynamics between the initial and the final measurements.

The packing dynamics analyser instrument is an automated and improved tapped density measurement method based on the recent fundamental research results[8-10]. The behaviour of the powder submitted to successive taps is analysed with an automatized device.

The Hausner ratio (Hr), the initial density $\rho(0)$ and the final density after n taps $\rho(n)$ are measured precisely. The tap number is commonly fixed at n=500. Moreover, extrapolation of the maximum density $\rho(\infty)$ are extracted from the compaction curves and additional indexes can be used. The powder is placed in a metallic tube with a rigorous automated initialization process. Afterwards, a light hollow cylinder is placed on the top of the powder bed to keep the powder/air interface flat during the compaction process. The tube containing the powder sample rose up to a fixed height of ΔZ and performs free falls. The free fall height is generally fixed to ΔZ = 0.001m (1mm) or ΔZ = 0.003m (3mm). The height h of the powder bed is measured automatically after each tap.

From height (h), volume (V) of the pile is computed. As the powder mass (m) is known, the density (ρ) is evaluated and plotted after each tap. The density is the ratio between the mass (m) and the powder bed volume (V). With the GranuPack method, the results are reproducible with a small quantity of powder (typically $3x10^{-5}$ m^3 (35 ml)). The Hausner ratio is related to the compaction ratio and is calculated by the following equation:

$$Hr = \frac{\rho(500)}{\rho(0)}$$

Where, $\rho(0)$ is the initial bulk density and $\rho(500)$ the tapped density computed obtained after 500 taps.

B.3 Electrostatic measurements

Electrostatic charges are created inside a powder during a flow[14, 15]. This apparition of electric charges is due to the triboelectric effect, which is a charge exchange at the contact between two solids. Accumulation of charge on the particle may cause repel and attraction of the particles and resulting the bad flowability. During the flow of a powder inside a device (printer, mixer, silo, conveyor, ...), the triboelectric effect takes place at the contact with in the grains and between the grains and the device. Therefore, the

characteristics of the powder and the nature of the material used to build the device are important parameters.
The GranuCharge instrument measures automatically and precisely the quantity of the electrostatic charge created inside a powder during a flow in contact with a selected material. The powder sample flows inside a vibrating V-tube and fall in a Faraday cup connected to an electrometer.

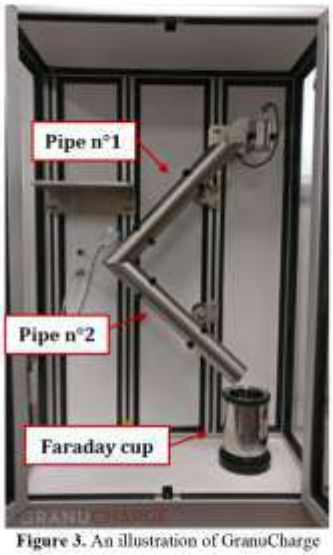

Figure 3. An illustration of GranuCharge

The electrometer measures the charge acquired by the powder during the flow inside the V-tube. In order to obtain reproducible results, a rotating or a vibrating device is used to feed the V-tube regularly.
The triboelectric effect is a result in one object gaining electrons on its surface, and therefore becoming negatively charged, and another object losing electrons, thus, becoming positively charged. Which material becomes negative and which becomes positive depend on the relative tendencies of the materials involved to gain or lose electrons. Some materials have a greater tendency to gain electrons than others, in the same manner that others tend to lose electrons easier. To represent these trends, the triboelectric series was developed (Table 2).

TABLE 2: TRIBOELECTRIC TREND OF DIFFERENT MATERIALS

Cationic materials	
Air	+
Human Hands, Skin	
Glass	
Human Hair	
Nylon	
Silk	
Aluminium	
Cotton	Mostly neutral
Steel	-
Wood	
Amber	
Nickel	
Copper / Silver	
Gold / Platinum	
Polyester / Polystyrene	
Cellophane Tape	
Polyvinylidene chlonde	
Polyurethane	
Polyethylene	
Polypropylene	
Polyvinylchloride	
Silicon	
Anionic materials	

Table 2 lists materials with tendency to charge positively and others with tendency to charge negatively. In the middle of the table, there are listed materials that do not show tendency to behave either way. However, this table only gives information about materials charging behaviour tendency.
With this reason the particular powder tribe electrometer was developed, which gives precise numerical values about powders charging behaviour.

IV. Experimental Results

In order to investigate thermal degradation, several experiments were carried out. The virgin samples were analysed at the same room humidity/temperature, i.e. 35.0±1.5%RH and 21.0±1.0°C with GranuPack, GranuDrum and GranuCharge.
Since, we have advantage to measure the flowability of high temperature material with rotating drum instrument. Therefore, we took advantage of this facility to check the flow behaviour at high temperature. The samples were placed during one or two hours at 200°C and were immediately analysed using GranuDrum (samples will be designed as "hot"). The powders were afterwards placed in a container until it reaches ambient temperature and were finally analyzed (cold powder) using GranuDrum, GranuPack and GranuCharge.

A. Spreadability

A.1 Experimental Protocol

Before experiment, air relative humidity (RH, %) and temperature (°C) are recorded. Once these steps are completed, the powder is poured inside the rotating drum

cell, and then experiment is started. The cohesive index is linked to the fluctuations of the interface (powder/air) position, and it only represents the three contact forces (Van der Waals, Capillary, and Electrostatic). Therefore, the cohesive index quantifies powder spreadability.

A.2 Results

Figure 4 summarizes the results obtained with GranuDrum. Figure 4 (a-d), represents the trend of cohesive index with respect to the rotating drum speed (rpm). In each figure, three to four states of individual powder are compared, which are listed as follows:

i. Flow behaviour at normal temperature and relative humidity.
ii. Flow behaviour of hot powder (heated at 200°C for 2 hrs.).
iii. Flow behaviour of cold powder, after heat treatment (heated at 200°C for 2 hrs. and then allowed to cool at room temperature for next 2 hrs. (Annealing)).
iv. Flow behaviour of hot powder, after heat treatment (heated at 200°C for 2 hrs. and then allowed to cool at room temperature for next 1 hr. (Annealing)).

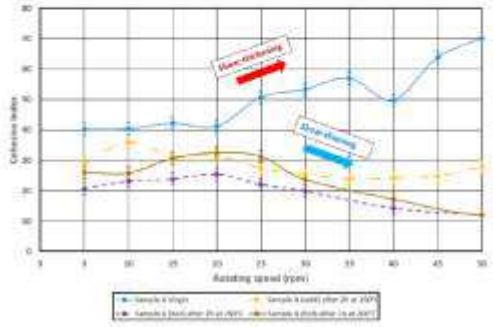

(a)

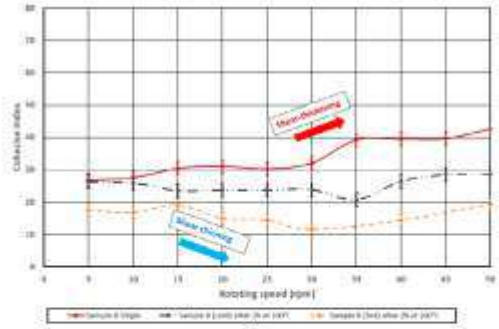

(b)

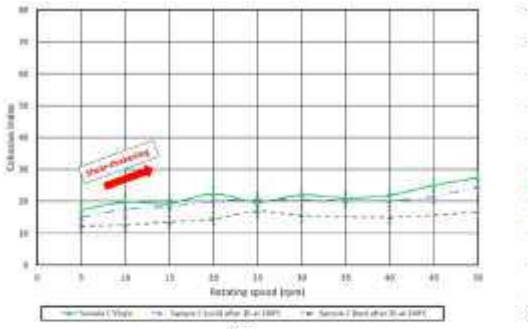

(c)

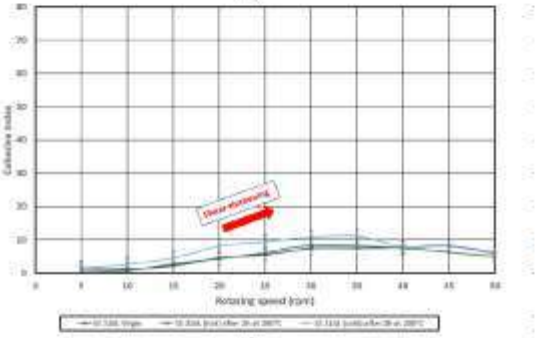

(d)

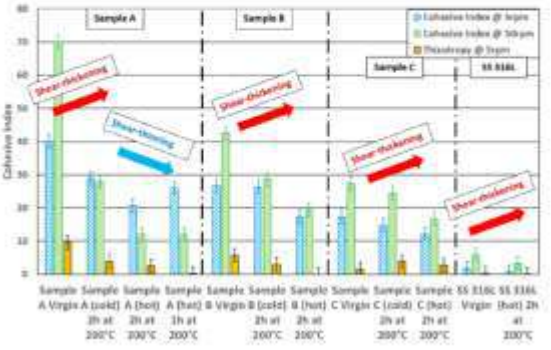

(e)

Figure 4. Trend of Cohesive Index with respect to drum rotating speed (rpm) for different materials **(a)** Sample A **(b)** Sample B **(c)** Sample C **(d)** SS316L **(e)** Comparison of Cohesive Index (5 and 50 rpm) and Thixotropy (5 rpm) of all tested materials

First of all, judging by the low value of Thixotropy parameter (cohesive index), it is possible to conclude that which product is not sensitive to the agglomeration and which one is not. From figure 4 (a), it is clear that at normal temperature and relative humidity (RH) the cohesive index is highest as compared to the other three curves and also compared to the other three powders as well (powder at normal temperature) from rest of the figures (Figure 4 (b-d). All four samples (Figure 4 (a-d)) are showing the similar average trend of cohesive index at normal temperature, which is increasing with increase of rotating drum speed (rpm). This trend is more dominant (high value of cohesive index) for finest powder (highest possibility of van der Waals forces: shear thickening), which is obvious (Figure 4 (a)). With increase of powders particle size the rate of increase of cohesive index is reducing (shear thinning) with

increase of rotating drum speed (Figure 4(a-d)). Particularly in figure 4 (c) and (d), it is very close to the specific constant value of cohesive index, that means the rotating speed is not influencing the cohesive index. Therefore, we can conclude that at normal temperature and relative humidity, probability to form the agglomerate is highest in finest particle and even its rate of change rapidly increases with increase of rotating drum speed.

Now, to compare the effect of thermal degradation, different heat treatment processes are opted on each of the material. It is clear from figure 4 (a) that the powder at 200°C kept for 2 hrs. has lowest cohesive index and it decreases with increase of drum rotating speed because there will be no humidity and chance to form the agglomerates will be negligible. Similar trend was observed in the other figures as well. Therefore, we can say that the cohesive indexes of processed materials are lowest and have less influence as the particle size increases.

Further cases in figure 4 (a-d) are showing that heated powders are kept to be cold for next 2 hrs. Therefore, this will has chance to absorb some amount of humidity and resulting increase in cohesive index as compared to the hot powders. Similar, phenomenon is observed when hot powder was kept to be cool for next one hr.

It is also clear from Figure 4 that the trend of cohesive index is not particular with respect to the drum rotating speed. Therefore, for the comparison of all tested materials two specific cases of rotating speeds are selected for the cohesive index and one speed for the Thixotropy comparison are selected to prepare a bar chart for each material (Figure 4 (e)).

From Figure 4 (e), for sample A (and slightly sample B) the thermal stress completely change the powder rheological behaviour, with a modification from shear thickening to shear thinning. Globally, every powder achieves a better spreadability (i.e. a lower Cohesive Index) when heated up and after being cooled down. Sample C and SS 316L are not highly affected by temperature and only show a shear-thickening behaviour. The effect of temperature seems also to be dependent on particles specific area. Indeed, the smaller the particles the more important the temperature influences.

Additionally, the more the material thermal conductivity, the more the effect on temperature on it (i.e. $\lambda_{Al\ 225°C}$ = $250 W.m{-}1.K{-}1$) and $\lambda_{SS\ 316L\ 225°C}$=$19 W.m{-}1.K{-}1$)

Finally, working at high temperature seems to be a good choice with Aluminium alloys powders, because their spreadability increases. Even the cooled down sample achieve a better spreadability in comparison with the virgin powders.

B. Packing Dynamics

B.1 Experimental protocol

For each experiment with the packing dynamics analyzer (GranuPack), 500 taps were applied to the sample with taps frequency of 1Hz and the measurement cell free-fall was 1 mm (∝ tap energy). The powder mass is recorded before each experiment. The sample is poured inside the measurement cell by following the software instructions (i.e. without user dependency). Measurements were repeated two times for evaluating reproducibility and the average value and standard deviation were considered. Once the packing dynamics analysis is done, the initial bulk density (ρ(0)), the final bulk density (at a number of taps, n = 500 ; i.e. ρ(500)), the Hausner ratio (Hr), and the Carr index (Cr) parameters are recorded.

B.2 Results

Figure 5 represents the full compaction curves (bulk densities versus number of taps) and figure 6 represents the Hausner ratio, free and tapped bulk density (n=500) of each material respectively.

Figure 5 (a) and (b) represent the comparative study of the bulk densities (free and tapped) of all virgin samples (Sample A, B, C and SS316L) and also after their heat treatments. Error bars are displayed on every curve and they were calculated using the average value and the standard deviation calculated with the help of repeatability tests. It is clear from the graph that the finest powder (sample A) has lowest free bulk density and coarse powder (SS 316L) has largest free bulk density. In terms of tapped bulk densities for virgin powders, we can see that sample A, B and C achieve approximately the same values if error bars are taken into account (1.380g/ml). The SS 316L product is without surprise the heaviest one (ρ(0) = 4.554g/ml). Regarding the tapped densities, SS 316L is still the heaviest powder (ρ(n) = 5.044g/ml), sample A comes in second position (ρ(n) = 1.668g/ml) followed by sample B (ρ(n) = 1.645g/ml).

Finally, sample C has the lowest one (ρ(n) = 1.581g/ml).

Figure 6 represents the comparison of virgin and processed samples of all tested powders with respect to the Hausner ratio, free bulk density (ρ(0)), and tapped bulk density (ρ(n=500)). If the powder is heated up, its Hausner ratio decreases. Nonetheless, this trend only occurs for sample B, C and SS 316L. Indeed, for sample A, due to error bars size, it is impossible to conclude. Similarly, the free and tapped bulk densities are increasing after heating the powders. This is because of the high compaction the volume is reduced and the density increases.

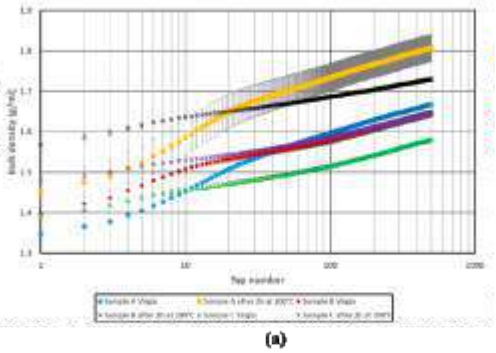

(a)

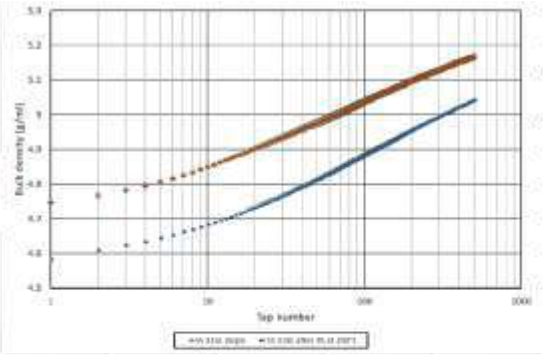

(b)

Sample Name	ρ(0) [g/ml]	σ ρ(0)	ρ(n) [g/ml]	σ ρ(n)	ε(%)	σ ε(%)	Hr	σ Hr	CI	σ CI	ρ(ᵐ) [g/ml]	σ ρ(ᵐ)
Sample A	1.334	0.008	1.668	0.008	18.0	0.5	1.250	0.008	20.0	0.5	1.701	0.001
Sample A after 2h at 200°C	1.439	0.036	1.808	0.033	14.8	1.5	1.257	0.008	20.4	0.5	1.836	0.029
Sample B	1.302	0.003	1.645	0.008	11.4	1.0	1.191	0.009	16.0	0.6	1.738	0.008
Sample B after 2h at 200°C	1.552	0.031	1.730	0.004	13.8	4.1	1.225	0.033	10.3	0.9	1.794	0.006
Sample C	1.380	0.004	1.681	0.002	19.1	2.5	1.146	0.002	12.7	0.1	1.673	0.001
Sample C after 2h at 200°C	1.468	0.008	1.645	0.006	10.4	9.6	1.121	0.010	10.8	0.8	1.729	0.031
SS 316L	4.544	0.005	5.044	0.000	41.0	1.5	1.130	0.000	9.9	0.1	5.283	0.005
SS 316L after 2h at 200°C	4.717	0.003	5.362	0.002	34.1	1.8	1.095	0.003	8.7	0.1	5.362	0.001

(c)

Figure 5: Bulk density as a function of tap performed by the GranuPack (logarithmic scale) (a) Sample A, B and C (b) SS 316L (c) GranuPack results for bulk densities, flowability and compaction dynamics

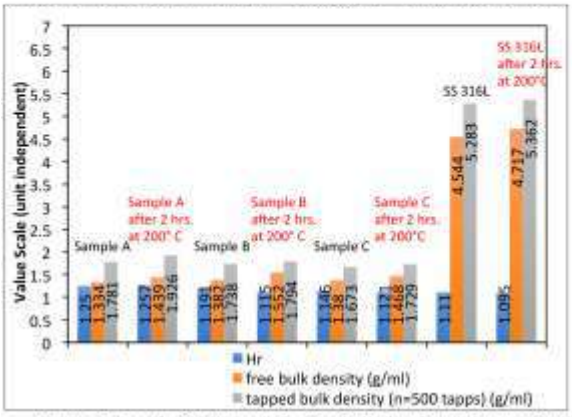

Figure 6: Trend of Hausner ratio, free bulk density, and tapped bulk density for all tested powders (virgin and processed at 200°C)

Finally, it can be concluded that working at high temperature has better packing dynamics, which is similar to spreadability. Only sample A is exhibiting the lower packing dynamics after heat up. This is because of high error bars. Hausner ratio is decreasing with high temperature work and also with increase in particle size because it results high tapped bulk density (n=500). In this way, it also confirms that the thermal degradation is beneficial for the AM.

C. Electrostatics

C.1 Experimental protocol

For each experiment with the GranuCharge, the vibrating feeder was used (Figure 7). SS 316L pipes were selected:

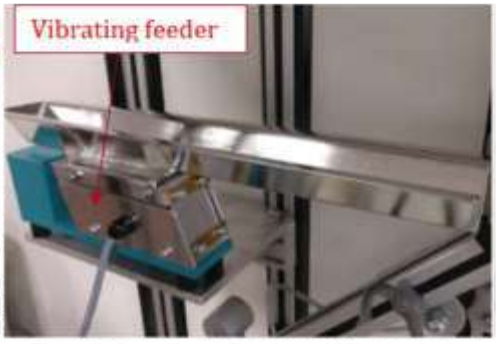

Figure 7: GranuCharge: Rotating and Vibrating feeder

The quantity of product used for each measure was approximately 40ml and the powder was not recycled after a measurement. Measurements are repeated three times for evaluating reproducibility. Before experiment, powder mass (m_p, in g), air relative humidity (RH, %), and temperature (°C) are recorded.
At the beginning of the test, the initial powder charge density (q0, in µC/kg) is measured by introducing powder inside the Faraday cup.
At the end of experiment, powder mass is recorded. Final charge density is then calculated at the end of experiment (q_f, µC/kg) and, finally:

Δq ($\Delta q = q_f - q_0$).

C.2 Results

Table 3 and Figure 8 represent GranuCharge raw data (σ is the standard deviation calculated with the repeatability tests) and the results presented as a histogram (only q_0 and Δq are presented) respectively:

TABLE 3: GRANUCHARGE RAW RESULTS

Powder Name	<q0> (nC/g)	σ <q0>	<qf> (nC/g)	σ <qf>	<Δq> (nC/g)	σ <Δq>
Sample A	0.136	0.063	0.092	0.005	-0.044	0.058
Sample A 2h at 200°C	0.031	0.026	0.322	0.103	0.292	0.078
Sample B	0.220	0.041	-0.144	0.001	-0.364	0.040
Sample B 2h at 200°C	0.174	0.000	0.383	0.062	0.209	0.062
Sample C	0.244	0.040	-0.182	0.005	-0.426	0.040
Sample C 2h at 200°C	0.541	0.000	-0.207	0.000	-0.747	0.000
SS316L	-0.045	0.004	-0.060	0.002	-0.015	0.006
SS 316L 2h at 200°C	-0.091	0.005	-0.058	0.003	0.033	0.008

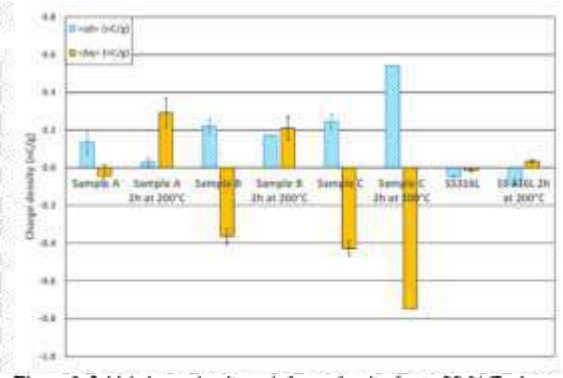

Figure 8: Initial charge density and charge density due to SS 316L pipes

First of all, regarding virgin Aluminium alloys powders initial charges; it is impossible to conclude due to error bars size. SS 316L has the lowest amount of initial charges; this is maybe due to the fact this product has the highest PSD.
However, after a flow in contact with SS 316L pipes, sample A acquire a lowest amount of charges, in comparison with powder B and C, which highlight similar trends. Additionally, if a SS 316L powder is rubbed against a SS 316L pipe, a charge density close to zero is observed (triboelectric series).
After a thermal stress of 200°C for 2 hours, powders behaviour becomes highly interesting. Indeed, for sample A and B, initial charges decrease and final charge change from negative to positive. Nonetheless, product B is still more charged than A. For sample C, the trend is conserved (positive initial charge and final charge after a flow), but the amount of charges is increased after the thermal degradation. Finally, SS 316L powder has a slightly highest amount of initial charges, and its charge density variation becomes positive (but remains low, i.e. 0.033nC/g).

V. CONCLUSION

In this research, the effect of thermal degradation on the collective behaviour of several Aluminium alloys (AlSi10Mg) and SS 316L powder is investigated. The virgin powders were studied under several conditions: ambient air, heated up to 200°C for two hrs., and heated up to 200°C and again cooled in ambient condition for next 1 and 2 hrs.
Three different instruments were used to measure and understand the rheology and powder flow dynamics: the GranuDrum for spreadability assessment, the GranuPack for packing dynamic analysis, and the GranuCharge to evaluate powder triboelectricity in contact with SS 316L pipes.
We had advantage to check the flowability of the processed powders at high temperature as well. It is found that working with a powder at high temperature improves the product spreadability; this effect seems to be more important for powders with high specific area and for a material with a high thermal conductivity. The GranuPack confirms these results, where materials after thermal stress process improve the Hausner ratio for every powder (except sample A, due to error bars size). Finally, looking at the initial charge, it was interesting, because some products were highly impacted by the thermal degradation process, since their charge sign was changed. The differences between the Aluminium alloys and SS 316L powder was also easy to highlight, since SS 316L sample was not highly charged after a flow in contact with SS 316L pipes.

6. Nomenclature

Letter	Description	Units
CI	Cohesive Index	(-)
DOR	Dynamic Angle of Repose	°
Cr	Carr Index	(-)
Hr	Hausner ratio	(-)
m_p	Powder mass	G
T	Temperature	°C
RH	Relative Humidity	%
$\rho(0)$	Initial bulk density	g/mL
$\rho(n)$	Bulk density after n taps	g/mL
$\rho(\infty)$	Optical tapped density	g/mL
q_0	Initial charge density	nC/g
q_f	Final charge density	nC/g
Δq	Charge density variation	nC/g
τ	Modelling compaction dynamic parameter	(-)

VI. REFERENCES

[1] S. Mellor, L. Hao and D. Zhang, "Additive manufacturing: A framework for implementation", *Int. J. of Production Economics*, 2014, vol. 149, pp. 194-201.

[2] S. Ford and M. Despeisse, "Additive manufacturing and sustainability: an exploratory study of the advantages and challenges", *J. of Cleaner Production*, 2016 137, 1573-1587 (2016).

[3] V. V. Popov, A. Katz-Demyanetz, A. Garkun and M. Bamberger, "The effect of powder recycling on the mechanical properties and microstructure of electron beam melted Ti-6Al-4 specimens", *Additive Manufacturing*, 2018, vol. 22, pp. 834.

[4] E. Herderick, "Additive Manufacturing of Metals: A Review", *Proceedings of MS & TŐ11*, 2011 pp. 1413.

[5] D. Herzog, V. Seyda, E. Wycisk, C. Emmelmann, "Additive Manufacturing of Metals", *Acta Materialia*, 2016. Vol. 117, pp. 371-392.

[6] J.A. Muñiz-Lerma, A. Nommeots-Nomm, K.E. Waters and M. Brochu, "A comprehensive approach to powder feedstock characterization for powder bed fusion additive manufacturing: A case study on AlSi7Mg", *Materials*, 2018, vol. 11, pp. 2386.

[7] W.E. Frazier, "Metal additive manufacturing: a review", *Journal of Materials Engineering and Performance*, 2014, vol. 23, no. 6, pp. 1917-1928.

[8] G. Yablokova, M. Speirs, J. Van Humbeeck, J.-P. Kruth, J. Schrooten, R. Cloots, F. Boschini, G. Lumay, J. Luyten, "Rheological behavior of β-Ti and NiTi powders produced by atomization for SLM production of open porous orthopedic implants", 2015, *Powder Technology*, vol. 283, pp. 199–209.

[9] G. Lumay, F. Boschini, K. Traina, S. Bontempi, J.-C. Remy, R. Cloots, and N. Vandewalle, "Measuring the flowing properties of powders and grains", 2012, *Powder Technology* vol. 224, pp. 19-27.

[10] A. Schrijnemakers, S. André, G. Lumay, N. Vandewalle, F. Boschini, R. Cloots and B. Vertruyen, "Mullite coatings on ceramic substrates: Stabilisation of Al2O3–SiO2 suspensions for spray drying of composite granules suitable for reactive plasma spraying", *Journal of the European Ceramic Society*, 2009, vol. 29, pp. 2169–2175.

[11] K. Traina, R. Cloots, S. Bontempi, G. Lumay, N. Vandewalle and F. Boschini, "Flow abilities of powders and granular materials evidenced from dynamical tap density measurement", 2013, *Powder Technology*, vol. 235, pp. 842-852.

[12] G. Lumay, S. Dorbolo and N. Vandewalle, "Compaction dynamics of a magnetized powder", *Physical Review E, 2009,* vol. 80, no. 4, pp. 041302.

[13] N. Vandewalle, G. Lumay, O. Gerasimov and F. Ludewig, "The influence of grain shape, friction and cohesion on granular compaction dynamics", *The European Physical Journal E*, 2007, vol. 22, no. 3, pp. 241-248.

[14] A. Rescaglio, J. Schockmel, F. Francqui, N. Vandewalle, and G. Lumay, "How tribo-electric charges modify powder flowability", *Annual Transactions of The Nordic Rheology Society*, 2016, vol. 25, pp. 17-21.

[15] A. Rescaglio, J. Schockmel, N. Vandewalle and G. Lumay, "Combined effect of moisture and electrostatic charges on powder flow", *EPJ Web of Conferences*, 2017, vol. 140, pp. 13009.

[16] Z. Snow, "Understanding powder spreadability in powder bed fusion addive manufacturing", 2018, M.Sc. Thesis, The Pennsytvania State University, PA, USA.

Developing Robust 3D Printed Parts for Automotive Application using Design for Additive Manufacturing and Optimization Techniques

Saravanakumar Shanmugam
General Motors Technical Centre India
5th Floor, Creator, ITPB, Whitefield,
Bangalore – 560066, INDIA
{saravanakumar.me &desai.sharan21}@gmail.com

Abhijith Naik, Sujan Tand Sharanabasappa Desai
General Motors Technical Centre India
5th Floor, Creator, ITPB, Whitefield,
Bangalore – 560066, INDIA
{abhijithster&sujusherry2009} @gmail.com

Abstract **- Additive Manufacturing (AM) is catching increased attention in the recent past due to its critical contributions in the 4th Industry revolution, commonly known as Industry 4.0. AM has come a long way from manufacturing proto parts to functionally capable parts with various enhancements to suit variety of applications. AM is proven to be the effective way to manufacture parts faster and economical than conventionally manufactured parts especially in low volume productions. This agility makes AM the most suited manufacturing technique for better integration between different industries and domains as the need for better collaboration increases. It's increased flexibility to manufacture functional parts is pushing the industry to go for 3D printed parts. As the skill requirements to design the components for AM is different than conventional manufacturing, product designers are facing increased challenges to design for AM. Printing and post processing methodologies have close connection with quality of parts. This research article analyzes various aspects right from the importance of Design for AM (DfAM), material consumption and quality of the parts. This article also talks about the importance of print and part design optimization methodologies.**

Keywords **-** ***DfAM, Optimization, Industry 4.0, Additive Manufacturing (AM), 3D Printing.***

I. Introduction

The Fourth Industrial Revolution commonly known as Industry 4.0 is making a significant impact in both business and society by creating various opportunities for lifetime. New ideas and potential that were previously unimaginable are becoming reality due the introduction of technologies such as AI, Robotics and Additive Manufacturing (AM) [1]. AM in particular is the cornerstone of the current industrial phase with digitization of the manufacturing, parallel with Automation, Internet of Things, Big data etc (Figure 1.). It is also argued in the literature that the digitization of manufacturing process realized by AM can bring about a new era with a huge potential to revolutionize the manufacturing process [2]. AM is also seen as a potential game changer in maintenance, repair and overhauling areas. Initially introduced as a rapid prototyping process, AM techniques are now used for end-of-use products [3]. Emergence of AM has made the leading manufacturing companies to rethink on how they conduct the manufacturing activities. It enables the production of high value, complex and customized products. AM also leads to reduction of time-to-market and the cost of manufacturing.

Fig. 1 Industry 4.0 technologies

The term 'additive manufacturing' covers a broad range of production technologies that fabricate products layer-by-layer, enabling three-dimensional objects to be 'printed' on demand. Some of the most widely adopted AM technologies are Fused Deposition Modelling (FDM), Stereolithography (SLA), Selective Laser Melting (SLM), Selective Laser Sintering (SLS) and Digital Light Processing (DLP), but there are a variety of other AM processes too, including Polyjet, Electron Beam Melting (EBM) and Laminated Object Manufacture (LOM). In terms of materials, a variety of polymers, metals, ceramics and composites can be used for AM. The use of these materials is dependent on the type of AM process used.

Alongside the advances that have been made in AM in the industrial market, a variety of consumer grade '3D printers' have proliferated in the market. Most of these home 3D printers (e.g. RepRap, Makerbot, Ultimaker) are based on the Fused Deposition Modelling (FDM) technology originally developed by the US firm Stratasys. Their commercialization was made possible following the expiry of the first patents protecting this technology, an open source movement that saw hobbyist activities around the technology and crowdfunding through platforms such as Kickstarter and Indiegogo. These machines offer the promise that individual consumers will be able to design and produce personalized products at their convenience. The design freedoms offered by AM allow product and component redesign. Using additive techniques, several parts made of the various material can be replaced by one integrated assembly, which will reduce or eliminate cost,

time and quality problems resulting from assembling operations. Assembly cost is minimized or even cut out through part consolidation[4].

A. *Overview of the Printing Process*

The general principle of layer manufacturing indicates that the steps or procedures employed by the AM machines is almost identical. In general, the following typical steps are followed by all AM machines depicted in Figure 2. The AM based production of parts start from a software model that fully describe the external geometry developed in a CAD solid modeling software. The geometry data as a 3D solid or surface representation, is passed from the CAD environment to the AM machine in STL or object (OBJ) file formats. These file formats are today included in most solid modeling tools and are commonly used interface formats with AM machines.

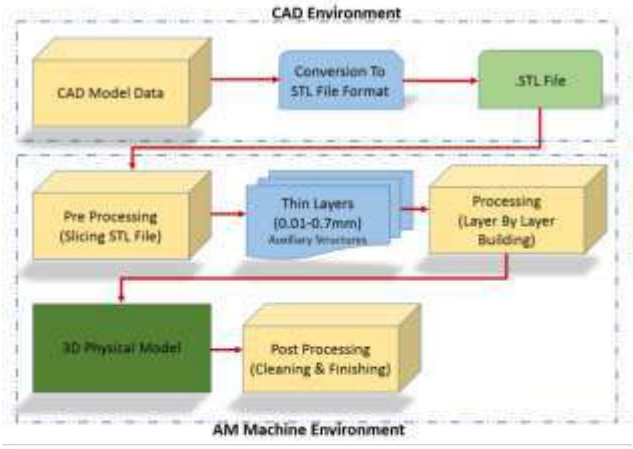

Fig. 2 Typical steps followed by AM machines

The STL file format is derived from the initial commercial RP technology Stereolithography. STL also stands for Standard Tessellation Language and is currently used as an industry standard format to export geometry data to 3D printers. It represents the 3D model using information about the co-ordinates and outward surface normal of triangles. The output to the AM machines environment is a boundary representation of the 3D object that is approximated by a mesh of triangles, where the STL file can be output as either binary or ASCII (text) format. OBJ file format is also used as an exchange format by many software programs as an alternative to STL file format particularly when information about colors or materials is desirable because the STL fileformat lacks the ability to define and transfer data about materials or microstructure volumetrically. The file format has both ASCII format (.obj) and binary format (.mod).

B. *Fused Deposition Modelling Technology*

FDM technology is one of the technologies developed to transform layer manufacturing from prototyping to functional parts directly from digital model in CAD systems. FDM machine prints the part using diverse thermoplastic materials such as ABS and nylon by deposition-based process where a heating jet deposits the melted plastic material layer-by-layerin a similar way as an inkjet printer. The nozzles of the print head are controlled by a motor and extrudes plastic filament that is rapidly cooled by surrounding low temperature air (Figure 3.). Though the fabricated part uses only one material, the FDM machines can extrude two materials: themodel material and the support structure material. The last mentioned is particularly needed when it is required to provide support structure for horizontally overhanging features of the component.

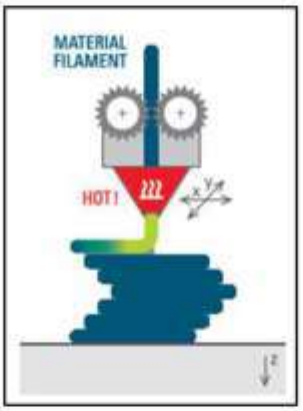

Fig. 3 FDM Process

The printing accuracy (both dimensional and geometrical) and surface finish, in general, can improve with reduced layer thickness while material deposition. However, lower layer thickness has adverse effects on the fabrication time leading to high production costs[2].Several roadblocks still pose a challenge to manufacture a successful functional part which are further elaborated in the upcoming chapters.

II. AM Implementation Challenges

Manufacturing is about converting raw materials, components, or parts into finished goods/articles that meet customer's expectations [5]. While several AM techniques are taking the centerstage as preferred manufacturing techniques, several challenges must be overcome to implement it in Industry 4.0, many of which are discussed below:

- Small-scale production; not designed for mass production, as traditional manufacturing methods perform faster at lower cost and yield better material quality[6].
- Limited skillset; Knowhow on AM processes, parameters and materials is still limited to very few designers and not yet well understood. Hence a challenge to incorporate DfAM techniques.
- Perception that Additive Manufacturing is only for prototyping and not for functional part needs to be removed[6].
- Designing a component to be produced by a 3D printer needs a rethinking of the design approach used.

Understanding on AM processes, materials and parameters is limited to very few designers.

- Proper standards to control quality is yet to be well established.
- Imperfections: Inferior mechanical properties due to defects and anisotropy; rough surface finish, variation in material properties and dimensions of printed polymer parts; dependence on processes used[6].
- Also, shelf life of the materials and its storage methods are not well defined which may lead to degradation of its mechanical properties
- Post Processing: Many printing techniques require extensive post processing, which may be due to the stair stepping effect that arises from incrementally placing one layer on top of another, or because finishing layers are needed. They are labour intensive[4].
- Cost: High quality printers and AM materials are expensive, slow speed of deposition (there are physical limits on increasing these speeds), need for postprocessing, higher costs for large production. Most of these limitations are due to the fact that AM is still a developing technology[6].
- Challenges in IP Protection:Connected systems and easy availability of 3D printable digital data (CAD) have posed a challenge to protect the IP rights and regulate the usage of CAD data to print the functional part. Absence of IP standards and regulation have posed a serious threat to counterfeiting of designs and may lead to brand dilutions as well[7].

III. DFAM

Design for additive manufacturing is a topic that involves unpacking the design freedom that AM provides and its vast potential. Here, all aspects like Design, materials, machines, process parameters, part properties, and quality are intertwined. Capability and capacity of AM can only be realized by leveraging the design freedom that AM provides. DfAM involves skills necessary to create designs that both leverage the unique design space of AM, yet importantly are manufacturable.

To truly understand Design for Additive Manufacturing (DfAM), one must increase value within the constraints of a selected AM process, or more often the end-to-end workflow for manufacturing. Both engineering knowledge and digital tools should be utilized to create a high-performance design while selection and configuration of the AM process should be well thought over to maximize its benefits and accommodate its challenges and limitations. At first there should be shift of designer's mindset, from traditional design for conventional manufacturing and assembly (DfMA), to design for additive manufacturing (DfAM). It is essential to understand the "job to be done" by the product, and to consider user and customer input during the design process. Hence, the design space of AM provides a more effective means to create products that are truly customer-focused.

In DfAM, efficient usage of material is achieved versus light weighing a component from a conventional machining process where material wastage is very high. With AM, we are only adding material where it needs to be which contributes to higher material efficiency with lattice structure or topology optimized design. Examples shown in Figure. 4 and Figure. 5 illustrates the significance of DfAM in part printing strategy for efficient use of support and model materials.

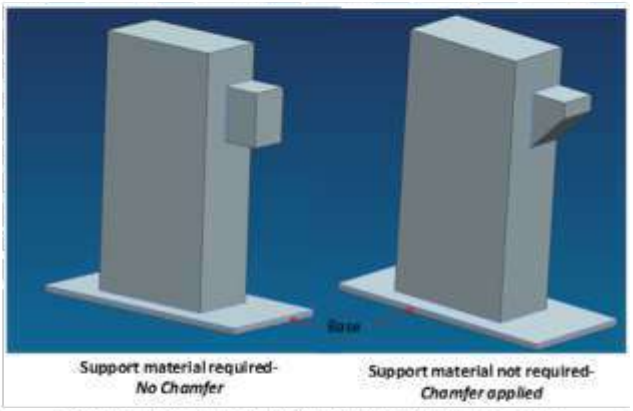

Fig.4 Apply 45-degree chamfer to build model without support

As model material itself can support the layer build, the support material can be eliminated by providing a minimum of 45-degree chamfer (provided the functionality allows) as shown in Figure. 4 and Figure. 5. As discussed, the model material can self-support itself, provided the angle is greater than a minimum value of 45 degrees,also known as self-supporting angle.

Fig. 5 Apply 45-degree chamfer to build model without support

IV. Material Consumption and Cost

A. Material Consumption

For the AM process, various designs of products only require different CAD files. This disconnects the diversity of product design from the material investment of production tooling. The ability of AM to manufacture parts of complex geometries also minimizes the need to break up the design into small pieces. The final products are produced with minimum excess material.

From an economic standpoint, the reduction in the amount of raw material usage is usually offset by the cost of

the materials. PS(Polystyrene) is a considerably low-cost material, making the high percentage of waste affordable. For AM on the other hand, the currently available materials are far more expensive than PS, especially the photopolymer used in the SLA(Stereolithography) devices. However, SLA represents only one among many AM technologies and the materials used are as diverse as the technologies. Many AM technologies use similar or even the same materials as other traditional manufacturing methods, including many different metals, nylon and ABS. These technologies also have a high efficiency
in material usage as demonstrated with the SLA technology. For the technologies that use same or similar materials as in the more traditional manufacturing methods, a clear reduction of wasted materials is expected.

B.Setup Cost

The setup time and the associated cost between AM and injection molding are a unique scenario. The cost to produce and prepare a mold for injection molding process may range from 3-8 days depending on the complexity. The initial setup time required for injection molding can largely limit the capability of manufacturing in a short lead time. Whereas, AM requires very less or even close to zero tooling and minimal labor.

C.Energy Cost

There is a variation in the cost of energy consumed per method. For AM, the amount of energy consumed is significantly less than injection molding because of the minimal area required for heating and the subsequent losses. The mass of the printed object is the largest factor in determining the energy cost for additive, whereas the total run time is the largest factor with injection molding.

D.Wastage Cost

Waste is typically an unavoidable aspect of any manufacturing operation, and AM have very low waste percentage. Over the past years, the research team collected data on the typical waste percentage of additive parts. Overall, the team found that the average waste percentage of AM using FDM technology is around 12.8 % of total mass. Although AM have low material wastage, injection molding also has significantly lower waste percentiles. Typically, in injection molding, the waste percentile is around 18 % by mass. This number also varies greatly because of mass and can be controlled with mold design and part orientation.

E.Labor Cost

AM and injection molding manufacturing used for this analysis demonstrated similar and low labor costs of operation. Most injection molding machines run continuously without direct labor, once it is setup. The same is true with most AM as well. For most additive processes, the machine can be setup in less than an hour, whereas injection molding requires significant setup time.

To overcome cost factor in AM, there are higher savings in cost per unit if maximum number of parts are printed simultaneously within the workspace. If only some small quantities are demanded by the customer, different jobs should be combined with each other to fully utilize the work-space/Machine.Additionally, small quantities should be printed on smaller machines to reduce the hourly rate for machines.

Product performance defined by its functional requirements and its benefit to the customer can also alter the balance of production cost and sale price, and therefore total profit. If a product redesign improves performance, the customer may be willing to pay a price that outpaces the increased pro-duction cost of the new design[8].

On the automotive production floor, jigs and fixtures play a major role in the manufacturing line. Jigs, custom-made tools used to guide and hold another work piece during an operation, devices used to hold a piece in a fixed location during an industrial or assembly process, are used to produce reliable products and repeatedly with high production rate.With fast and near labor-free production, 3D printing (additive manufacturing) offers a powerful solution for producing jigs and fixtures. 3D printing manufacturing aids can reduce lead times, provide cost savings, improve performance and add efficiencies to the production floor. The benefit of 3D printing is shorter lead times; some parts can be produced in a matter of hours. Prototyping a jig or fixture to test its performance is sometimes critical and can be accomplished with 3D printing faster than conventional manufacturing. 3D printed jigs and fixtures are built from a digital file rather than hard tooling, allowing designers to produce aids on-demand and as needed. The CAD file can be updated and redesigned at any time, then reprinted and delivered in days. With advantages such as quick turnarounds, part consolidation and near labor-less production, 3D printing jigs and fixtures delivers an overall cheaper venture. The process also reduces material waste and helps you avoid costly expenses associated with inventory and storage. The advantage of AM is to reduce number of parts and assembliesfrom DfAMdesign and print as one part. An example to explain the concept of part consolidation is shown in Figure. 6[13].

Fig. 6 Logo fixture 3D printed as single part for automotive assembly line[13].

V. Role of Optimization in Part Design and Printing

Conventional methods of manufacturing have many constraints. Designers are used to observe a part and getting convinced that the part may succeed in injection molding or not, as the design space required to manufacture the same is limited. Another driving constraint is the manufacturability, for instance what the part must look like to be cost effectively injection molded. AM can give that larger design space by creating fewer assembly parts and drive the design based on function and performance.

Good knowledge of AM processes enables designing of parts with more effective outcomes. But if the additive manufacturing workflow is infused with computational tools like Topology Optimization in addition to user's knowledge and intuition, the design space can be enlarged vastly. These computational tools produce designs that are not necessarily the same every time but are good enough within certain defined boundary conditions.

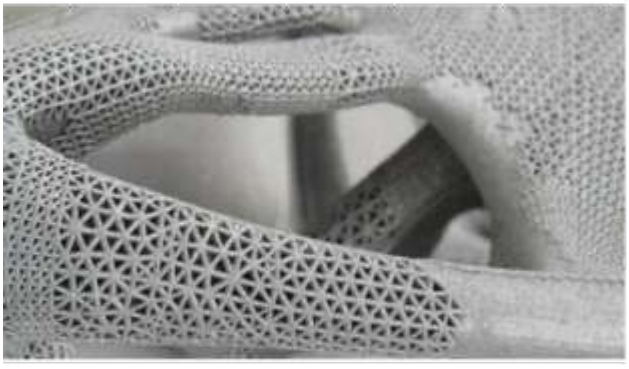

Fig.7 Topology Optimization using Lattice structure[9].

A classic example of a topology optimized part with lattice structure optimization is shown in Figure 7. where the material usage is optimized with respect to the given loading and boundary conditions. With a topology optimized part combined with AM, we're only putting material where we need it and we get much more efficient usage of that material versus light weighing a component from a subtractive/machining process. Some tools are tailored to give a variety of designs, a spectrum of outcomes with different levels of performance. And those could be ranked in terms of their cost to produce and their strength or their performance based on the application. Designers can even end up with beautiful, sometimes crazy looking part geometries which are very much functional. It may have an organic shape with an internal lattice geometry. The size and shape of the lattice may change locally, because the software used in design adapted the lattice according to the expected stress.

VI. Discussion

DfAM motivates designers and engineers to look at problems with "fresh eyes" or with a "Learning mind." While past knowledge and expertise has often been the value we add in our work, it may well become one of the biggest contributors to generate new AM innovations. In this regard, it is instructional to look back at prior methods of Design for Manufacture and Assembly (DfMA), which have ultimately shaped the way we think about Design for Additive Manufacturing (DfAM).

To help designersimplement DfAM and successfully print a part with proper process parameters, lessons learnt, and best practices have been identified based on experiments and past printing experiences. These rules include part shape, dimensions, manufacturing orientation, post processing parameters etc. Case studies presented in the upcoming chapters explain the significance of process parameters and DfAM in printing AM parts.

A. Case study 1

Figure 8. shows a quality defect (crack propagation) in 3D printed assembly aid used in automotive manufacturing plant. There were no visible defects observed when part was taken out of build sheet. However, a hairline crack was observed when it was post processed in a soap solution at 85°C to remove the soluble support material. Investigations proved that the temperature gradient between the part and the soap solution contributed to the crack due to thermal expansion. By reducing the temperature gradient between the soap solution and the part, the crack propagation was eliminated.

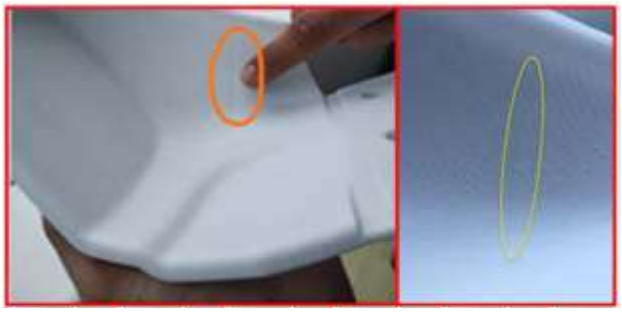

Fig. 8 Hairline crack developed after post-processing, caused due to high temperature gradient between part and soap solution

B. Case study 2

Classic example of an undesired support strategy where a basic support was used only to hold the part is shown in Figure 9. Here, an end effector/gripper for a collaborative robot (COBOT) where the part was 150mm long and had a 44mm diameter base with a stepped design was printed. Printer had failed to print the full part successfully because of the wrong support strategy. The part, while in the print process, went off from the build sheet resulted in skewing away from the dimensional accuracy. For a part with a long dimension like this, support strategy should be such that it should cover/support the entire part while printing. Hence build orientation gains importance as one of the prime strategies to be considered before printing.

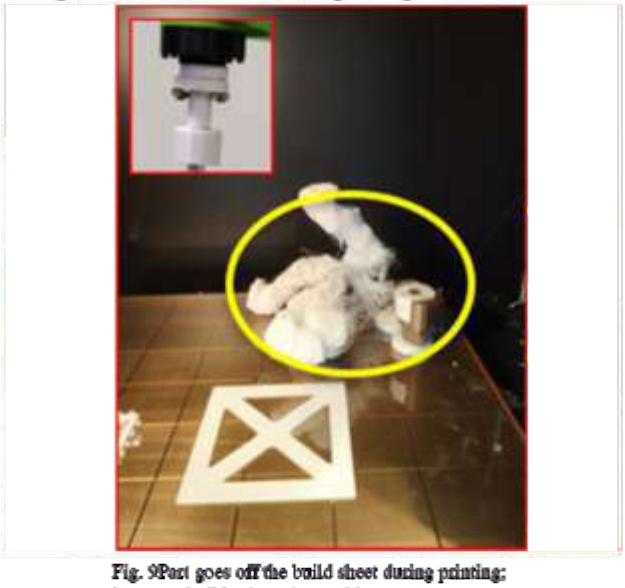

Fig. 9Part goes off the build sheet during printing; cause:incorrect build orientation and incorrect support strategy

C. Case study 3.

Figure 10. shows a classic example of a poor print quality and surface finish of the part. It was observed that the support material did not reach the top surface of the part due to wrong build orientation. Also, the model material's high moisture absorption while in storage has resulted in non-uniform material deposition during the printing process.

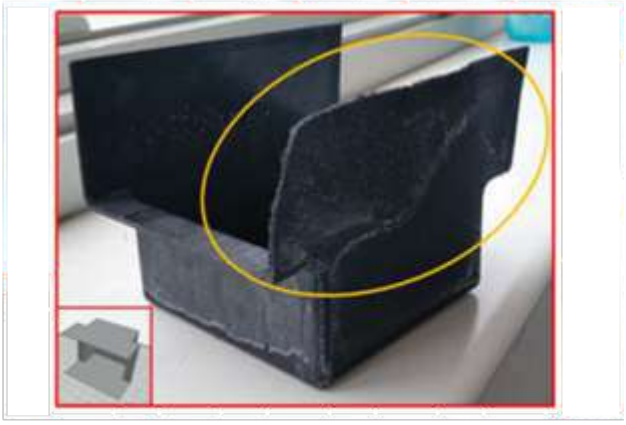

Fig. 10 Poor dimensional quality and surface finish of 3D printed part caused due to multiple reasons:
a) incorrect build orientation b) insufficient support b) high moisturecontentin model material, resulting into non-uniform material deposition

D. Case study 4

To explain the factors to be considered for developing a robust part, a 3D printed Logo case study has been presented. Various software tools are available in the market for print and part optimization. In this example, GrabCAD software was used for print optimization. A lattice structure print optimization technique was applied to print the Logo based on the form, fit and functional requirements.

The initial part design and its print orientation in GrabCAD is shown in Figure. 11. The estimated consumption of support material was 4.3 cubic inches. The estimated print time was 4.35 hours. It was the integrated part design where the Logo and the mount was printed as a single part. With the help of GrabCAD software, the orientation and support strategy were decided for printing.

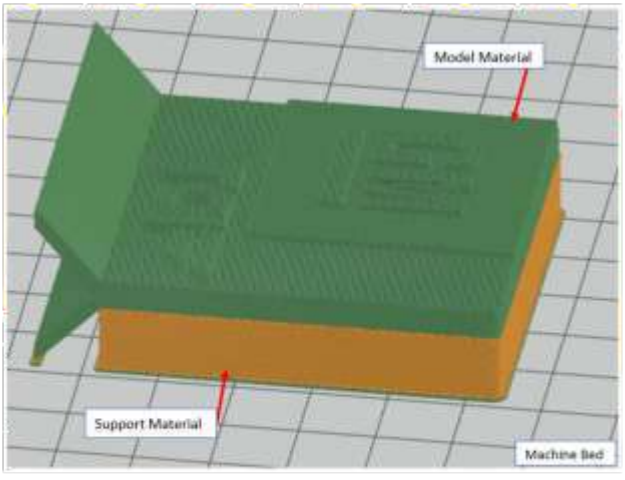

Fig. 11GrabCAD image of Initial Design

Further, DfAM techniques were brainstormed to reduce the support material consumption, a revised part design

(Figure 12.) was proposed in place of initial design. The mount and the Logo were split, and with horizontal print strategy shown in Figure 12., a considerable improvement in material utilization was seen. The estimated support material consumption was 1.3 cubic inches while the estimated print time came down to 3.3 hours.

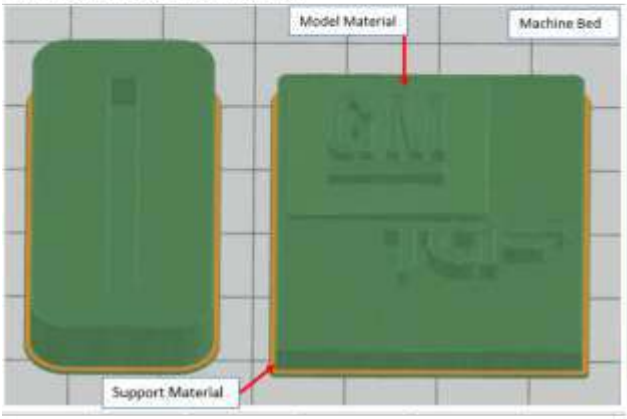

Fig. 12GrabCAD image of Revised Design

The revised design was successfully printed (Figure 13.) using FDM Fortus 400MC Stratasys machine with Polycarbonate (PC10) model material and SR100 support material. Actual consumption of 1.3 cubic inches of support and 9.8 cubic inches of model material were utilized for printing this Logo. The model was successfully printed in 3.20 hours.

Fig. 13 Final Part before Post Processing

Post processing plays a significant role to achieve the required finish. The support material was removed by hand without the involvement of any hand tools as the support material was used only at the base of the part. 3M 413Q 220 Wet to dry grade emery was used to obtain the final quality (Figure 14).

Fig. 14 Final Part after Post Processing

This case study explains the significance of DfAM and how it can contribute to save material consumption, printing time and robust part print. The material consumption and the time predicted by GrabCAD is closely matching with the actual material consumed and the printing time. With the revised design, with minimal support material requirement the part was printed faster than the initial design without compromising the intended purpose.

VII. Conclusion

In this article, the role of AM in the Industry 4.0 era and potential challenges to adapt AM technology in the current manufacturing scenario was discussed in detail. The importance of DfAM and how it plays a significant role in terms of material consumption and component cost were also discussed. Introduction to part optimization and the usage of GrabCAD software for print optimization was explained with specific case studies. AM is emerging as a potential game changer in the modern manufacturing sector while it also includes many implementation challenges to realize its full potential. It is concluded that changing the way designers think to design parts for AM, effective usage of Optimization software for print/design optimization and effective post-processing techniques would help overcome the challenges to develop a robust part that can fulfill its intended purpose.

References

[1] Dion Weisler (2019), Accelerating a more sustainable industrial revolution with digital manufacturing[Online]. Available : https://www.weforum.org/agenda/2019/01/3d-printing-fourth-industrial-revolution-sustainable/

[2] Lenu, Hirpa G., "On Opportunities and Limitations of Additive Manufacturing Technology for Industry 4.0 Era," *Advanced Manufacturing and Automation VIII*, Springer, pp. 106–113, Dec. 2018.

[3] Sossou, Germain., Demoly, Frédéric., Montavon, Ghislain., Gomes, Samuel., "An additive manufacturing-oriented design approach to mechanical assemblies,"*Journal of Computational Design and Engineering*, Vol.5, pp. 3-18, Nov. 2017.

[4] Ford, Simon., Despeisse, Melanie., "Additive manufacturing and sustainability: anexploratorystudy of the advantages and challenges,"*J. Cleaner Production*, Vol. 137, pp. 1573-1587, 2015.
[5] (2019) Business Dictionary.[Online]. Available: http://www.businessdictionary.com/definition/manufacturing.html
[6] Iwona Jasiuk, Diab W. Abueidda, Christopher Kozuch, Siyuan Pang, Frances Y. Su, And Joanna Mekitrick, "An Overview on Additive Manufacturing of Polymers", *JOM*, Vol70, *pp* 1047-4838, Jan. 2018
[7] Chan, Hing Kai., Griffin, James., Jia Jia Lim, Fengli Zeng, Anthony S.F. Chiu, "The impact of 3D Printing Technology on the supply chain: Manufacturing and legal perspectives,"*International Journal of Production Economics*, Vol 205, pp. 156–162, 2018
[8] Franchetti, Matthew., & Kress, Connor., "An economic analysis comparing the cost feasibility of replacing injection molding processes with emerging additive manufacturing techniques,"*Int J Adv Manufacturing Technology*, Vol 88, pp. 2573–2579, 2017
[9] Renishaw (2019) Metal 3D Printing.[Online]. Available: https://www.renishaw.com/en/metal-3d-printing--32084
[10] (2018) Business Dictionary.[Online]. Available: http://www.businessdictionary.com/definition/manufacturing.html
[11]Resource Consumption of Additive Manufacturing Technology, 2012 https://www.diva-portal.org/smash/get/diva2:831234/FULLTEXT01.pdf
[12]Vaneker, T.H.J., "The role of Design for Additive Manufacturing in the successful economical introduction of AM,"*Procedia CIRP*, Vol. 60, pp. 181 – 186, 2017
[13](2019), 3D printed Jigs & fixtures: A powerful solution for productionfloor[Online]. Available : https://www.stratasysdirect.com/applications/jigs-fixtures/3d-printed-jigs-fixtures-powerful-solution-production-floor

Review: Scope and Challenges of 3D printing of Footwear

Devicharan R[a*], Pranjalikanchi[b],Falguni Nagla[b]

[a]Assistant Professor Senior Scale, Department of Media Technology, Manipal Institute of Technology, Manipal Academy of Higher Education, Manipal, India.

[b]B.Tech student, Department of Media Technology, Manipal Institute of Technology, Manipal Academy of Higher Education, Manipal, India.

*Corresponding author E-Mail ID:devicharan.r@manipal.edu,Mobile:9620220394

ABSTRACT

The Additively Manufacturing technique was mainly used for 'rapid prototyping' of designs and with continuous research and development, AM can now not only satisfy the rapid prototyping needs, but can assist with the requirement of end-use products as well. Fashion dates back centuries, housing a variety of cultures and their traditions. As time passed, this sector has evolved and today, it requires a constant need for change and development. With 3D printing, this constant need for change can be satisfied in many intriguing ways. The traditional methods of manufacturing footwear are cherished as they promise accuracy. With developments in manufacturing techniques, the same accurate designs, manually created by an artist can now be 3D printed, saving a considerable amount of time and money. This technology does not pose any sense of designing limitations, nor does it require a form of intensive technology training. With a thorough understanding of FDM method and the available materials, one can understand how this technology can bring about a drastic change in the footwear industry.(2)

Key words: FDM, Footwear 3D Printing, TPU

1.INTRODUCTION

The craft of creating footwear have been around for centuries, and for a long time it was all done by hand. Process of shoe manufacturing started with Charles Goodyear making a breakthrough finally after decades of experimentation, dating back to 1844. The discovered process was called "vulcanization" where rubber was heated to mix Sulphur with it – to create the perfect mixture of rubber especially for manufacturing shoe soles and is used till date. He patented the method where he used a combination of mixing, curing and heating, a process still used today.

Show soles were earlier made of wood or canvas, and as time passed, Rubber composites were used. These compounds are put into a hopper that mixes it according to the formula they are producing it for and then melted and squeezed between large rollers of a banbury press in the form of a large sheet. It is then folded over onto a large pallet and shipped to shoe sole producers, who feed strips of it into an extruder which melts it again and forms it into the required shape of shoe soles, using metal outsole molds. Firstly, these molds cost a fortune and would easily wear out. This mass manufacturing process does not feed the necessity of customization. If at all, someone required designing the sole as per their foot design, manufacturers would use clay impressions of their foot to make soles matching them. Given these clay impressions were the only way, they were not reliable enough.

With the application of 3D printing, a lot of the limitations offered by the conventional methods are eradicated, mainly the ability to personalize. 3D printing also increases the efficiency, helps optimize the incorporated lattice structures, is economical and environment friendly.

2.METHODOLOGY

To understand the application of FDM to make shoe soles, one needs to understand the technology thoroughly.

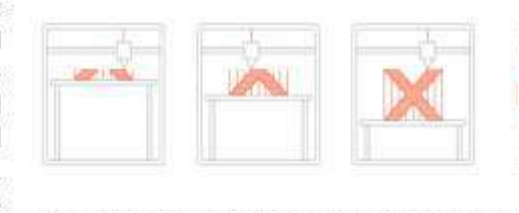

Fig 1. Fused Deposition Modelling Process

The technology of Fused Deposition Modeling was developed by S. Scott Crump in the late 1980s and was commercialized in 1990 by a company named Stratasys. In this process the object is built layer –by – layer from the bottom up by heating and extruding thermoplastic filament. The first step is to create 2D slice of the object with the help of AutoCad or any design software. The software also determines path to extrude the thermoplastic material and support material if needed. Then the material is fed into the temperature controlled extruder head, where it is converted into semi liquid state. The thermoplastic material is heated just beyond its Glass Transition temperature (Tg). The head extrudes fine filament of thickness in the range 0.254 mm and deposits in layers on a fixtureless base. Where a support or buffering is needed, the 3D printer deposits a removable material that acts as scaffolding. When layer is finished, it moves in the Z direction to the next layer. The layering process is done vey precisely and bonded and solidified. Once the process is complete, the support material is removed and the object is finished. Mainly polymeric materials such as Acrylonitrile Butadiene Styrene, Polylactic acid, Polycarbonate, Polyamide, Polystyrene etc. are used in FDM 3D printers. This technology is widely used in various industries such as aerospace, automotive, medical etc. apart from that it attracts a large number of professionals such as engineers, designers, educators and they can make any prototype or product for their requirements.

On comparing this method to the other AM technologies, it happens to be the most economical and is capable of providing the consumer with the desirable end product. To achieve the stage of personalizing shoes using 3D printing, it is better if the technology is affordable and so are the raw materials, making the final product affordable by the common man. The methods using resin based polymers could also be used for this purpose in the future once their application and service costs can be made affordable.

New, improved and enhanced FDM raw materials constantly keep entering the market making the right material selection extremely difficult. Although PLA(poly lactic acid) and ABS (acrylonitrile butadiene styrene) thermoplastics have always been the go-to materials, they are not sufficient to cater to all the different types of applications. These two materials have more or less dominated the market but pose shortcomings such as low elongation at break point and their structural properties could not suffice(is enough for) for applications such as printing molds for food articles.

Mechanical performance, Visual quality, and Process are the three main factors a material is typically graded on. To acquire an in-depth understanding of each material, the polymers properties have been further broken down. The final

choice depends on the consumers requirement.

TPU(thermoplastic polyurethane) displays the highest elongation at break point. The following properties are showcased by TPU making it the most desirable material for printing of shoe soles.(1).

1.Resistance to external tampering

Note- tampering means interfere with something to cause damage.

This particular feature of this polymer ensures a long life of the product with no compromise on its aesthetics. A property like resistance to abrasion is highly critical for applications like Interior Automobile parts, special purpose cables, and other probably applications giving the best results when compares to other thermoplastic filaments.

In technical terms, the final amount of resistance to scratch/abrasion is calculated by accurately measuring the loss in the weight of the specimen in a typical standard wear test as depicted below -

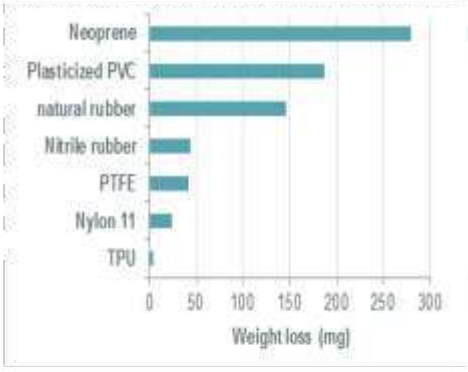

Fig 2.Depictionof Weight loss

The results seen in the above chart clearly depicts the much superior abrasion of the TPU polymer when compares to other substances such a PVC and rubbers.(5).

2. Aid to Ergonomics

The developments in the filament fabrications have made it achievable to produce a "plasticizer-free" TPU which provides with an incredible amount of toughness.

These new and improved solutions provide with a good quality of surface finish, along with a better adhesiveness(helps to stick together) to the surrounding layers as well as an improved resistance to abrasion when compare to other sustaining industrial materials like ABS and Nylon.

3.Resistance to Ultra Violet light

The polymer TPU makes sure of the fastness of colors to the desirable parts. It shows a much higher resistance to UV radiation and hence, a much higher stability of the color. All of these properties combined with the pre-existing good mechanical properties.

These polymers have the perfect characteristics and versatility to best suit applications such as for electronics and footwear.

4.Highly Breathable TPU (thermo plastic polyurethane)

Optimum comfort ensured by this polymer, due to its highly breathable property. This property satisfies a variety of applications.

The conventional TPU can be combined with the "breathable" TPU to perfectly satisfy the requirement for that specific application.

5.Combination of High Transparency with Abrasion Resistance

The "crystal-clear TPU" is the polymer that provides with a very good hardness. This specific property perfectly suits the application of extruding the very material into see-through films and tubes and can substitute the parts which were traditionally made with injection molding

methods and now can by directly made using this TPU transparent filament.

6.More Advantages –

Displays the highest amount of flexibility
High resistance to most solvents
Flexibility uncompromised at a range of temperatures
Retaining of properties at very low temperatures
Resistance to "High-energy" radiance

3.RESULTS

It was encountered during the designing phase of the shoe sole, CAD software needs new features to properly satisfy the industries demands of personalization and an increase in the quality of the shoe sole. We decided on following a "specific design methodology" that helped us tackle the challenge much easily. This method included CAD modeling tools which drastically reduced time taken for designing and also increased the functionality and quality of the shoe sole as per the requirement of the client. These particular tools involved the design of the foremost sole body, along with the outsole and the other functional elements as the side sole treads. Moreover, it involved "polysurface parameterization" to artistically produce intricate 3D models and possible geometrical deformations which would help to make the final changes to the sole models to suit the requirements better.
Our methodology also used mathematical models to understand the soles resistance to slipping and also helped acquire the friction coefficient which was later incorporated into the design to enhance the shoe soles functionality. This helped understand the basic design flaws in the earlier stages, allowing the designers to remake the flawed parts of the sole. This methodology also satisfies the manufacturing of the usual shoe sole designing process and can be applied in various phases of the production process. Moreover, implementing this methodology at such an early stage results in little to no problems in the lifespan of the production.

With such a thorough knowledge on FDM technology along with understanding TPU in depth, it can be concluded that this material definitely suits best for printing of shoe soles. There may be new polymers introduced in the later future but for now, TPU suffices all the requirements.

REFERENCES

1.Eerdekens,Maarten; Staes,Filip;Pillington,Thomas;Deschamps, Kevin," A novel magnet based 3D printed marker wand as basis for repeated in-shoe multi segment foot analysis: a proof of concept", Foot and ankle research, pages:1-6, 2017.

2.Davia-aracil,Miguel;Jimeno-morenilla,Antonio;Salas,Faustino," A new methodological approach for shoe sole design and validation", Pages: 3495 -3516, 2016.

3. Jin-Rae Cho1,2, Seung-Bum Park3,*, Sung-Hyun Ryu1, Sung-Ho Kim1 and Shi-Bok L," Landing impact analysis of sports shoes using 3-D coupled foot-shoe finite element model", mechanical science and technology,2009.

4. T.mass,C.paradigm," mass customization and footwear".

5. Cho, Jin-rae; Park,Seung-bum, Ryu,Sung-hyun; Kim,Sung-ho; Lee,Shi-bok," Landing impact analysis of sports shoes using 3-D coupled foot-shoe finite element model", Volume 23 , Pages:2583-2591, 2009.

6. Nielsen,Kjeld," Open Innovation, Co-Creation and Mass Customisation: What Role for 3D Printing Platforms?", Proceedings of the 7th World Conference on Mass Customization, Personalization, and Co-creation (mcpc 2014),Issue Mcpc, Pages- 359-376, 2014.

7.Kwon,Yu;lee,young a ;kim,sook jin," Case study on 3D printing education in fashion design coursework",fashion and textiles,4:26,2017.

8. Lee, Young A; Koo, Sumin Helen,"Introduction to special collection on 3D 0 and wearable technology in fashion",fashion and textiles, volume 5, Issue 1 , Pages 3-6, 2018.

9.micallef,j," What's Possible with 3D Printing?Enter a new era of design with 3D printing",Beginning design foe 3D printing,Aug 19, 2015.

10.Lushan San and Li Zhao,"Envisioning the era of 3D printing: a conceptual model for the fashion industry",fashion and textiles ,volume 4, issue 1, 2017.

Parametric optimization of Dual material Polycarbonate and Acrylonitrile Butadiene Styrene (PC-ABS) using Fused Deposition Modelling (FDM) technique

Hetal Purohit
Mechanical Engineering Dept
Lokmanya Tilak College of Engineering
Mumbai, India
hetalswndia@gmail.com

Prof. J.J.Dange
Mechanical Engineering Dept
Lokmanya Tilak College of Engineering
Mumbai, India
Jayesh.dange111@gmail.com

***Abstract*— The additive manufacturing (AM) is the new age manufacturing technology. Fused deposition modelling (FDM) is a type of AM process in which a thermoplastic is extruded out of heated nozzle. The nozzle moves as per G-codes in X-Y plane to form the desired geometry in three dimensions, on a heated bed (in some cases) which moves in Z-direction. These are cartesian machines, whereas in delta machines the bed is stationary only the nozzle moves in all the three dimensions. There are some FDM printers which use dual material extrusion technology to make parts out of two different materials or sometimes two colors of same material. This study involves dual material FDM to make specimens in Polycarbonate and Acrylonitrile Butadiene Styrene for tensile test. The specimens are modelled as per ASTM D-638 Type-I standard in CAD modelling software Autodesk Fusion 360. They are fabricated on an FDM 3D printer Delta HC 250. The aim is to optimize the input parameters for mechanical properties using Taguchi Method. The results show that for maximum ultimate tensile strength and elongation at break 0.1mm layer height, 30% infill and 70:30 ratio of PC-ABS is optimum.**

Keywords*— *Additive manufacturing, Fused deposition modelling, Dual material extrusion, Polycarbonate, Taguchi method

I. Introduction

Additive Manufacturing (AM), also known as Rapid Prototyping (RPT) or 3D Printing is around for almost four decades but still looks brand new. In Indian scenario this technology is in nascent stage and it is still used for prototyping and envisioning rather than as main stream production process. The myths about the capabilities of this comparatively novel technology are hard to shake. Nevertheless, AM is gaining momentum. It is expected to grow to its full potential in coming years with rate at which it is expanding. According to 6Wresearch, India 3D Printer Market is projected to record $79 Million by 2021 [1]. In spite of the 3D printers being expensive, the researches and advancement in the technology, government aid for the start-ups under skill India initiative, patents being released and raw material availability, promise a steady growth in AM sector.

II. Literature Review

This section aims at summarizing the relevant literature reviewed for the selection of various parameters and specimen dimensions and understanding the problem. Strength is always an issue with 3D printed parts. So, majority of researches ([2] [3] [4] [5] [6]) aimed at studying mechanical properties of 3D printed parts.

Heechang Kim et al. [2] in their study performed tensile test on both single and dual materials, PLA and ABS material. They varied the percentage composition of both materials and found that when they vertically sandwich two materials there are problems with adhesion. Difference in tensile strength doesn't have much significance as compared to pure ABS and PLA materials. They also studied the effect of structural arrangement on tensile properties for 50% ratio and found that the horizontal sandwich structure provides considerable difference in strengths. The horizontal arrangement provides better strength than vertical boundaries. Hence in present study, the specimen used has sandwiched PC and ABS material layers horizontally rather than vertically.

Jason T Cantrell et al [4] measured modulus, offset yield stress, elongation at break, strain energy density and strength at yield (using Iosipescu specimens for shear employing digital image correlation (DIC)) for shear as well as for tension. Effect of build and raster orientation has been observed on anisotropy of ABS and PC specimen. They studied these properties separately for both material which helps in understanding the individual strength of PC and ABS parts. For ABS specimens no significant difference was observed in young's modulus or poisson's ratio for different build and raster orientations. For PC on edge and +45/-45 flat orientation has similar tensile properties. This study has taken +45/-45 flat orientation for studying tensile properties of combined PC-ABS specimen.

Taguchi method is used for optimisation of various process parameters of FDM for different thermoplastic materials in many of the earlier researches ([7], [5], [8], [9], [10], [3], [11], [12] and have been referred to understand the application to present study. B.M. Tymrak et al. [13] and I.M. Chac'on [14] performed the test on specimens manufactured by low cost 3D printers and the parts were found to have acceptable mechanical properties.

Few recent researches have been carried out on 3D printing composite materials. Zhenzhen Quan et al. [15] studied the effect of printing direction on compressive properties of ABS specimens, Carbon Fibre (CF)/ABS specimens and 3D braid preform composite. M. Mansour et al. [16] studied the effect of reinforcing polyethylene terephthalate glycol (PETG) with 20% carbon fibre and found higher

compressive strain and hardness than pure material. Wenfeng Hao et al. [17] used a modified 3D printer to manufacture CF reinforced thermosetting composites and found better mechanical properties than usual thermoplastic composites and 3D printed short CF reinforced composites. G.D. Goh et al. [18] performed mechanical tests on carbon fibre (CF) and glass fibre (GF) reinforced thermoplastic (nylon based) to study tensile, flexural and quasi-static indentation process and found pre-impregnated thermoplastics to be having higher tensile and flexural that pure thermoplastic filament.

As found in the previous researches, mentioned above, composites have higher mechanical properties. Our aim here is to find out how varying the material percentage of PC and ABS, infill and layer height would affect the tensile strength and manufacturing time of the specimens for XY, +45/-45 flat orientations while 3D printing with a non-industrial grade 3D printer

III. Experimental Details

A. Methodology

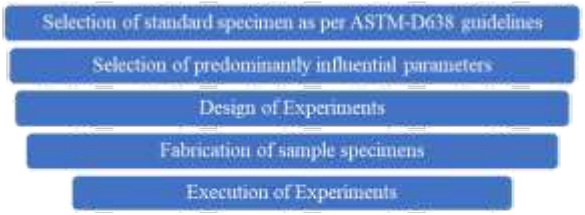

Fig. 1 Methodology of Research

B. Standard Specimen Preparation

The specimen selected for tensile testing is ASTM D638 Type I and the orientation selected for the specimens is +45/-45 raster angle flat orientation. The dimensions of the specimen are as given below in Fig. 2.

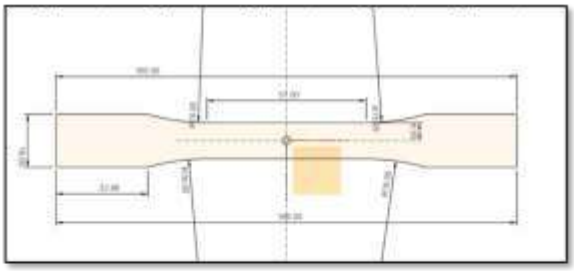

Fig. 2 Dimensions of specimen ASTM D638 Type I (All dimensions in mm)

C. Selection of predominantly influential parameters

Design of Experiment (DOE) is a methodology for quality improvement [19] [20]. The concept was developed Sir R.A. Fiscchcr and Dr. Genechi Taguchi, a Japanese statistician added three orthogonal arrays (OAs) to his work. For this study, three parameters (Percentage composition, Infill percentage and layer height) are selected to study their effect on the tensile properties of the specimen and manufacturing time. TABLE I shows factors and their levels.

TABLE I PARAMETERS FOR DOE

S.No	Factors	Symbol	Level 1	Level 2
1	Infill Percentage	A	30%	100%
2	Percentage of PC and ABS respectively	B	50% - 50%	70% - 30%
3	Layer Height	C	0.2mm	0.1mm

D. Design of Experiments

a) Layout of specimen

In 70-30% specimen, the PC layer is sandwiched between three separate ABS layers as shown in Fig. 3. The thickness of the specimen is 7mm. For 50-50% PC-ABS specimens, total thickness is divided into half. Alternate layers of PC-ABS are taken to avoid layer separation as shown in picture Fig. 4. Since PC has warping tendencies, ABS layers are kept on the bottom to avoid warpage.

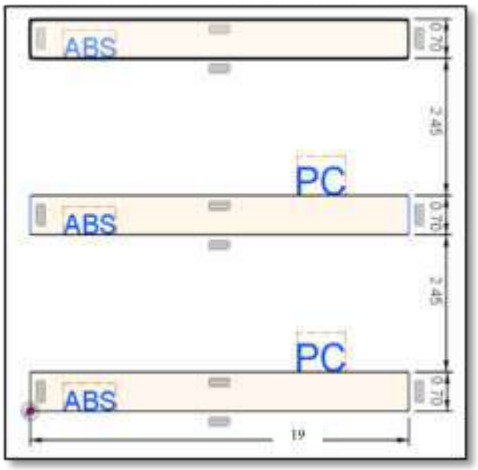

Fig. 3 PC-ABS 70-30% sample schematic cross section (All dimensions in mm)

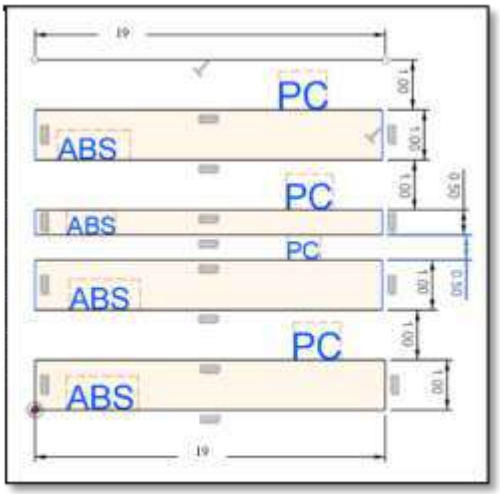

Fig. 4 PC-ABS 50-50% sample schematic cross section (All dimensions in mm)

b) Selection of Orthogonal Array

The selection of suitable orthogonal array is done for three factors two level problem.

1. No. of factors- F= 3 and No. of levels- n=2 and i= interaction =0
2. Degree of freedom- Dof= F(n-1)+ i(n-1)(n-1)+1
   Dof= 3(2-1) + 0 (2-1) (2-1) +1 = 4
3. No. of treatment conditions= No. of rows of orthogonal Array>= Dof
   Selecting OA4 [21] corresponding to Dof= 4.

The orthogonal array OA4 for the experiment is shown in TABLE II.

TABLE II OA4 FOR EXPERIMENTAL SETUP

Treatment Condition (TC)	Factors		
	A	*B*	*C*
1	30	50:50	0.2
2	30	70:30	0.1
3	100	50:50	0.1
4	100	70:30	0.2

Three set of samples are fabricated to study the response on manufacturing time and tensile properties of the blended specimen.

E. Fabrication of specimens

Specimens were fabricated on 3D printer Delta HC-250. The machine is a delta 3D printer and comes with a heated chamber, vacuum heated bed and bed size of 240mm X 240mm X 300mm.

F. Execution of experiments

Three sets of four samples each were tested on a Universal Testing Machine (capacity up to 400kN) manufactured by FEI, India at Fan Services, India testing facility. The manufacturing time was noted from simplify 3D software for printing the dual material PC-ABS specimens.

IV. Results and Discussions

TABLE III shows average results of the tensile testing for three parameters at two level.

TABLE III EXPERIMENTAL RESULTS AS PER OA4

TC	Infill	Ratio	Layer Height	Ult. Tensile Strength at Break (N/mm2)	Tensile Strength at Yield (N/mm2)	Elongation at Break (%)	Elongation at Yield (%)	Tensile Modulus (N/mm2)	Time (min)
1	30	50:50	0.2	10.98	9.91	4.07	2.4	270.67	87
2	30	70:30	0.1	44.27	40.04	8.07	3.7	564.33	139
3	100	50:50	0.1	40.94	39.42	5.3	4	799.33	171
4	100	70:30	0.2	10.60	10.15	3.13	2.8	345.33	84

Highest ultimate tensile strength, tensile strength at yield and elongation at break is found for treatment condition 2. Whereas treatment condition 3 gives greater tensile modulus and elongation at yield. Least manufacturing time is taken by treatment condition 4.

A. S/N Ratio and Main effect Plot

The figures below (Fig. 5 - Fig. 10) depict the main effect plot of data means and S/N ratio for all six response variables. Main effects plots show how each factor affects the response characteristic and are represented by a line [22]. A main effect exists when different levels of a factor affect the characteristic differently.

S/N ratio is the output that measures variations from the desired output when there are noise factors present. There are six types of S/N ratios: 1. Nominal-the-best 2. Target-the best 3. Smaller-the-better 4. Larger-the-better 5. Classified attribute 6. Dynamic. The Minitab software is used to draw results from the response variable. Larger-the-better approach is applied to ultimate tensile strength, tensile strength at yield, elongation at break, elongation at yield, tensile modulus and smaller the better approach to manufacturing time.

The layer height has the heights effect on response variables as seen from the mean effect plots as compared to other factors. Layer height 0,1mm has greater effect on S/N ratios of all responses but time.

B. Ultimate Tensile Strength

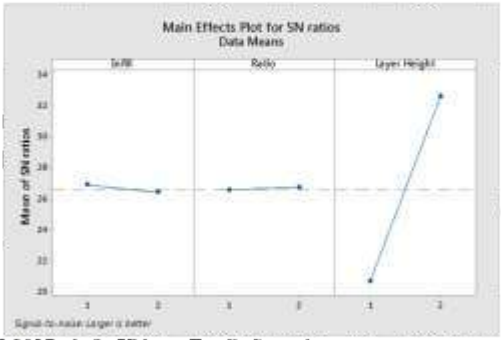

Fig. 5 S/N Ratio for Ultimate Tensile Strength

C. Tensile Strength at yield

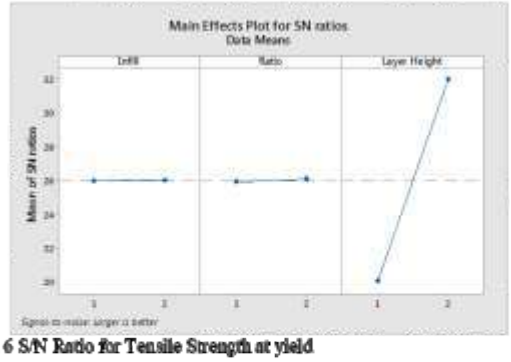

Fig. 6 S/N Ratio for Tensile Strength at yield

D. Elongation at Break

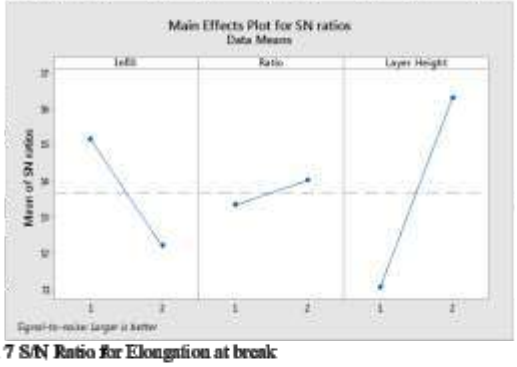

Fig. 7 S/N Ratio for Elongation at break

E. Elongation at Yield

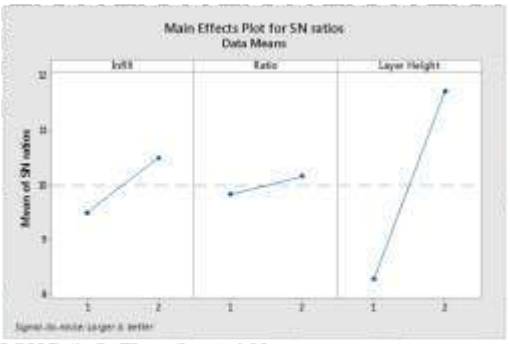

Fig. 8 S/N Ratio for Elongation at yield

F. Tensile Modulus

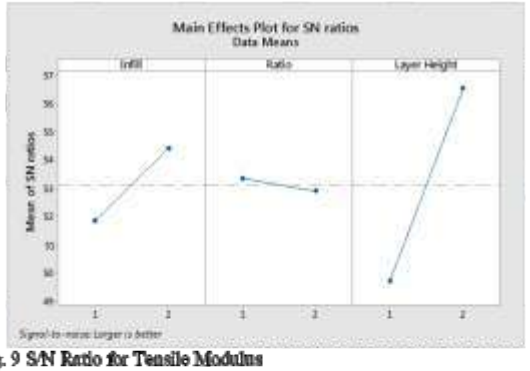

Fig. 9 S/N Ratio for Tensile Modulus

G. Manufacturing Time

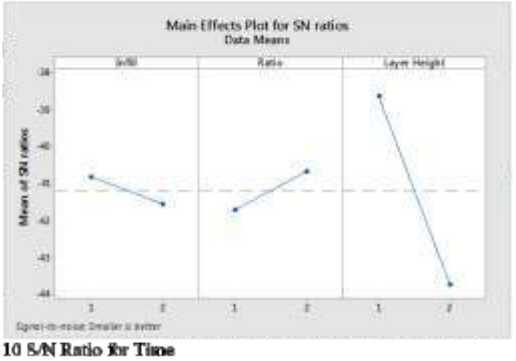

Fig. 10 S/N Ratio for Time

V. Conclusion

The parameters for fused deposition modelling of PC-ABS specimens for two levels of ratio, infill and layer height were optimized using Taguchi's orthogonal array (OA4). It was found that

- For maximum ultimate tensile strength, tensile strength at yield, elongation at break - 0,1mm layer height, 70:30 ratio and 30% infill are optimum.
- For maximum elongation at yield and tensile modulus - 0,1mm layer height, 50:50 ratio and 100% infill are optimum.
- For minimum time - 0,2mm layer height, 70:30 ratio and 100% infill are optimum.

Depending on the requirement of strength or time saving the respective parameters can be used.
By observing the mean effect plots for means and for S-N ratios, for all six response variables, it can be concluded that:

- Layer Height is the key control factor over infill and ratio.
- For 0.1mm layer height, the mean of all response variables is higher than for 0.2mm layer height.
- Similarily, 0.1mm layer height has greater effect on S-N ratios than 0.2mm layer height, except for manufacturing time.
- For manufacturing time, 0.2mm layer height has higher effect.

The cost benefit for such exercise is minimal for parts as small as the specimens that we have used. But when parts that are larger in size, they can be designed specifically for dual material for strength consideration and the cost benefit can be worked out and can be explored in future studies. There is a possibility of widening the research by involving more process parameters like printing speed, number of perimeters, raster angle etc. to get a detailed optimized setup for such applications. Further studies on Impact strength analysis for the PC-ABS blended specimens can be made.

References

[1] 6Wresearch, "India 3D Printer Market (2015-2021)," 6Wresearch, April 2015.

[2] E. P. S. K. B. P. N. K. a. S. L. Heechang Kim, "Experimental Study on Mechanical Properties of Single- and Dual-Material 3D Printed Products," Procedia Manufacturing , vol. 10, p. 887 – 897, 2017.

[3] M. Z. S. L. L. S. J. P. &. Y. H. Xinhua Liu, "Mechanical property parametric appraisal of fused deposition modeling parts based on the gray Taguchi method," The International Journal of Advanced Manufacturing Technology, vol. 89, no. 5-8, p. 2387–2397, 2017.

[4] S. R. D. D. R. G. L. D. J. A. A. Y. A. J. Jason T Cantrell, "Experimental characterization of the mechanical properties of 3D-printed ABS and polycarbonate parts," Rapid Prototyping Journal, vol. 23, no. 4, pp. 811-824, 2017.

[5] B. C. Vishwas M, "Studies on Optimizing Process Parameters of Fused Deposition Modelling Technology for ABS," Materials Today: Proceedings, vol. 4, no. 10, pp. 10994-11003, 2016.

[6] A. A. A. G. S.-M. G. G.-G. M. A. P. Josep M. Puigoriol-Forcada, "Flexural Fatigue Properties of Polycarbonate Fused-deposition Modelling Specimens," Materials & Design, vol. 155, pp. 414-421, 2018.

[7] R. C. Vijay.B.Nidagundi, "Studies on Parametric Optimization for Fused Deposition Modelling Process," Materials Today: Proceedings, vol. 2, p. 1691 – 1699, 2015.

[8] A. Q. B. A. A. G. Ala'aldin Alafaghani, "Experimental Optimization of Fused Deposition Modelling Processing Parameters: a Design-for-Manufacturing Approach," Procedia Manufacturing, vol. 10, p. 791 – 803, 2017.

[9] G. T. M. C. L. K. C. J. C. &. M. M. Krishna P. Motaparti, "Experimental investigation of effects of build parameters on flexural properties in fused deposition modelling parts," Virtual and Physical Prototyping, 2017.

[10] E. L. D. K. Kyle Raney, "Experimental characterization of the tensile strength of ABS parts manufactured by fused deposition modeling process," Materials Today: Proceedings, vol. 4, p. 7956–7961, 2017.

[11] M. F. R. S. M. A. F. R. G. a. A. P. M. S. Uddin, "Evaluating Mechanical Properties and Failure Mechanisms of Fused Deposition Modeling Acrylonitrile Butadiene Styrene Parts," Journal of Manufacturing Science and Engineering, vol. 139, 2017.

[12] G. W. Y. T. Y. F. Z. Guoying Dong, "Optimizing process parameters of fused deposition modeling by Taguchi method for the fabrication of lattice structures," Additive Manufacturing, vol. 19, pp. 62-72, 2018.

[13] M. K. J. P. B.M. Tymrak, "Mechanical properties of components fabricated with open-source 3-D printers under realistic environmental conditions," Materials and Design, vol. 58, pp. 242-246, 2014.

[14] M. C. E. G.-P. P. N. J.M. Chae´on, "Additive manufacturing of PLA structures using fused deposition modelling: effect of process parameters on mechanical properties and their optimal selection," Materials & Design , vol. 124, pp. 143-157, 2017.

[15] J. S. J. Y. X. Q. C. C. M. M. T.-W. C. Zhenzhen Quan, "Printing direction dependence of mechanical behavior of additively manufactured 3D preforms and composites," Composite Structures, vol. 184, pp. 917-923, 2018.

[16] K. T. D. T. &. A. A. M. Mansour, "Mechanical and Dynamic Behavior of Fused Filament Fabrication 3D Printed Polyethylene Terephthalate Glycol Reinforced with Carbon Fibers," Polymer-Plastics Technology and Engineering , vol. 57, no. 16, pp. 1-11, 2018.

[17] Y. L. H. Z. H. C. D. F. Wenfeng Hao, "Preparation and characterization of 3D printed continuous carbon fiber reinforced thermosetting composites," Polymer Testing, vol. 65, pp. 29-34, 2018.

[18] V. D. A. N. S. A. S. S. J. W. Y. G.D. Goh, "Characterization of mechanical properties and fracture mode of additively manufactured carbon fiber and glass fiber reinforced thermoplastics," Materials and Design, pp. 79-89, 2018.

[19] J. A. a. F. J. Antony, "Teaching the Taguchi method to industrial engineers," Work Study, vol. 50, no. 4, pp. 141-149, 2001.

[20] S. W. K. F. a. H. R. Jiju Antony, "Process optimisation using Taguchi methods of experimental design," Work Study, vol. 50, no. 2, pp. 51-58, 2001.

[21] D. H. Besterfield, Total Quality Management, (Revised Edition), Pearson Education India, 2011.

[22] J. Antony, "A Systematic Methodology for Design of Experiments," in Design of Experiments for Engineers and Scientists (Second Edition), Scotland, Elsevier Ltd., 2014, pp. 33-50.

[23] R. W. D. Walter Castro Smith, "Structural characteristics of fused deposition modeling polycarbonate material," Polymer Testing, vol. 32, no. 8, pp. 1306-1312, 2013.

[24] D. H. Besterfield, Total Quality Management, (Revised Edition), Pearson Education India, 2011.

Additive Manufacturing Society of India (AMSI)

Additive Manufacturing Society of India

"AMSI educates and promotes the latest developments and applications in Additive Manufacturing Technologies" Additive Manufacturing Society of India (AMSI) is the professional body with the objective to promote 3D printing & Additive Manufacturing Technologies. AMSI helps the design, research and development organisations, manufacturing professionals and academics in 3D Printing, Additive Manufacturing and allied technologies.

AMSI plays a major role in promoting 3D printing & Additive Manufacturing technologies and has great network and MOU's with global additive manufacturing organisations.

Additive Manufacturing Society of India Membership

Membership Benefits

- Networking and interaction opportunities with global Additive Manufacturing experts
- Provision with ample business opportunities and to enhance business relationships for industries
- Free Subscription to AMSI journals & News Letter
- Membership Certificate entitlement to use 'M AMSI'
- Provision for members to update their knowledge through workshops, conferences, publications and online courses

#42, BSK 3rd Stage, 3rd Phase, 3rd Block, 9th Cross, Bangalore- 560 085, INDIA
Tel Fax : +91 80 26729437 / 32422663
Mobile : +91 94837 17449
E-mail : contact@amsi.org.in, Website : www.amsi.org.in

Social Media Neworks: